



DISSERTATION - EE186202

INTELLIGENT PROTECTION APPARATUS TO MINIMIZE THE FALSE TRIP ISSUE IN MEDIUM VOLTAGE INDUSTRIAL POWER SYSTEM

Vincentius Raki Mahindara
071118 600 10013

Supervisors:

Prof. Ir. Mauridhi Hery Purnomo, M.Eng., Ph.D.

Dr. Eng. Ardyono Priyadi, ST., M.Eng.

Dr. Ir. Margo Pujiantara, MT.

DOCTORAL PROGRAM
DEPARTMENT OF ELECTRICAL ENGINEERING
FACULTY OF INTELLIGENT ELECTRICAL AND INFORMATICS TECHNOLOGY
INSTITUT TEKNOLOGI SEPULUH NOPEMBER
SURABAYA
2021

This page is left intentionally blank.

STATEMENT OF APPROVAL

DISSERTATION

Intelligent Protection Apparatus to Minimize the False Trip Issue in Medium Voltage Industrial Power System

This dissertation is prepared to fulfill the requirements for obtaining the degree of:
Doktor (Dr.)

at
Institut Teknologi Sepuluh Nopember




By
Vincentius Raki Mahindara
071118 600 10013

Examination Date: 13 July 2021
Graduation Period: September 2021

Approved by:

Supervisors:

1. Prof. Dr. Ir. M. Hery Purnomo, M.Eng.
NIP: 19580916 198601 1 001
2. Dr. Ardyono Priyadi, ST., M.Eng.
NIP: 19730927 199803 1 004
3. Dr. Ir. Margo Pujiantara, MT.
NIP: 19660318 199010 1 001


.....

.....

.....

Examiners:

1. Prof. Eduard Muljadi, M.S., Ph.D.
NIP:
2. Dedet Candra Riawan, ST., M.Eng., Ph.D.
NIP: 19731119 200003 1 001.
3. Dr. Dimas Anton Asfani, ST., MT.
NIP: 19810905 200501 1 002

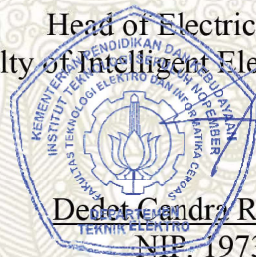
July 25, 2021

.....
21/07/21

.....

.....

Head of Electrical Engineering Department
Faculty of Intelligent Electrical and Informatics Technology



Dedet Candra Riawan, ST., M.Eng., Ph.D.
NIP: 19731119 200003 1 001

This page is left intentionally blank.

STATEMENT OF ORIGINALITY

I hereby certify that any and all parts of my dissertation with title

**“Intelligent Protection Apparatus to Minimize the False Trip Issue in
Medium Voltage Industrial Power System”**

is actually an independent intellectual work, is accomplished without the use of materials that are not allowed, and is not the work of others whom I consider as my own work.

All references cited and referenced have been written completely in the bibliography. If it turns out that I violate this statement, I am willing to accept any penalty in accordance with applicable regulations.

Surabaya, June 2021

Vincentius Raki Mahindara

This page is left intentionally blank.

ACKNOWLEDGMENTS

I would like to acknowledge the enormous help given to me in creating this dissertation. For their patience, support, guidance, and life-lessons, I would like to thank my supervisors from Institut Teknologi Sepuluh Nopember, Surabaya, Indonesia: Prof. Mauridhi Hery Purnomo, Dr. Ardyono Priyadi, and Dr. Margo Pujiantara.

A special thanks to Prof. Eduard Muljadi and Prof. Robert Marks Nelms for the opportunity of joining their research group at Auburn University, Auburn, Alabama, USA. My appreciation also extends to Prof. David Celeita (Institución Universitaria Politécnico Gran Colombiano, Bogota D.C, Colombia) for the inspiration and support. Thank you to Prof. Anang Tjahjono, who gave me a lot of insight and idea under intense discussion.

I want to thank all my friend and colleagues who made my time in the Master and PhD stage fun and enjoyable. Special thanks to Talitha Puspita, who helped me a lot since the very beginning of this scholarship (Yeah, we finally made it!). Appreciation goes to Fabian Danandjaya for all the laugh and logical advice. Thanks to all laboratory member in LIPIST (*salam pengukuran!*). Thanks to my fellow PMDSU colleagues (Deny, Alexander, Khairul, Wendy, Frengki, Lukman, Arif, and many others). My appreciation also goes to Bapak Agustinus Bimo, Ibu Wiwik, Ibu Diana, Ibu Yuhana, Ibu Rosiani, Bapak Andi, Bapak Wahyu, and many others who provides me with a lot of advice and PhD stage' tips and trick. For the research support from Nugraha Agung (Pupuk Kujang Cikampek) and Mahmoud. For the immense help during my stay in Auburn: Dr. Jinho Kim, Mayur, Eche, Tanner, Patrick, Xue Fei, Sangwon, Austin, and all resident in Broun Hall 157 (without you, my life in Auburn would have been much harder!).

Mostly and as always, my thanks to P. P. Joko Susilo, Lusiana Kardina, Maria Virginiaputri, and Gita Alethea, who often believes in me more than I do myself. I really thank you all for the endless support, care, and prays.

This page is left intentionally blank.

FUNDING SOURCES

This work was financially supported by Institut Teknologi Sepuluh Nopember on behalf of Indonesian Ministry of Education, Culture, Research, and Technology (*Kementerian Pendidikan, Kebudayaan, Riset, dan Teknologi*) under scholarship “Pendidikan Magister Menuju Doktor untuk Sarjana Unggul (PMDSU)” (2017-2021), the sandwich program scholarship “Enhancing International Publication” (2019-2020), and multi-year research grants (2018-2020).

This page is left intentionally blank.

ABSTRACT

Nowadays, the industry is facing an increasing number of appealing challenges. The most critical part is to compete in the market by figuring and shaping the new technology revolution. Along with the Fourth Industrial Revolution, the future power delivery orientation has shifted from generating and distributing electricity to continuously delivering with a high-reliability index.

A dependable electrical system requires a flexible maneuver in the distribution network and a credible protection system. The development of the network scheme and inclusion of the renewable energy resources can be used to efficiently reduce losses in the feeder and provide a contingency scenario, while reducing the sensitivity and accuracy of the conventional protection system.

Therefore, a breakthrough is required to develop electrical protection devices or even systems. Future apparatus must be intelligent enough to work in any network topology and classify events based on a multi-parameter perspective. To do that, boundaries with multi-variable considerations should be determined. Then, these boundaries should be included in the optimization process of coordinating protective equipment to minimize the electricity outage and avoid the false trip issue.

This work investigates the above-mentioned challenges and offers practical solutions to consequently improve the power system reliability and resiliency. An improved method to recognize load characteristics is included during the optimization process of protection relay settings. To attain the minimum tripping time of the protection relay, the combination of the relay curve and load characteristics is introduced. Moreover, the relation of voltage, current, and frequency is investigated to understand power system events and design a novel protection relay architecture. The proposed solutions are tested and verified on various systems, including an Institute of Electrical and Electronics Engineers (IEEE) test system and a real plant application. The proposed solution is expected to evade the false trip problem and adapt to electrical conditions that might happen in medium-voltage industrial power system networks and support the development of the Fourth Industrial Revolution.

Keywords: Electrical power, False Trip, Fault classification, Fault mitigation, Microgrid, Multi-function relay, Optimization method, Protection relay, Relay coordination, Smart grid.

This page is left intentionally blank.

CONTENTS

COVER PAGE.....	i
STATEMENT OF APPROVAL.....	iii
STATEMENT OF ORIGINALITY.....	v
ACKNOWLEDGMENTS.....	vii
FUNDING SOURCES.....	ix
ABSTRACT.....	xi
CONTENTS.....	xiii
LIST OF FIGURES.....	xv
LIST OF TABLES.....	xix
NOMENCLATURE.....	xxi
CHAPTER 1 INTRODUCTION.....	1
1.1 Background.....	1
1.2 Problem Statement.....	3
1.3 Objectives and Benefits.....	4
1.4 Roadmap.....	4
1.5 Contributions.....	8
1.6 List of Publications.....	11
1.7 Scope and Limitations.....	12
1.8 Dissertation Outline.....	12
CHAPTER 2 RECOGNIZING THE ELECTRICAL BOUNDARY FOR PROTECTION RELAY SETTINGS.....	15
2.1 Problem Definition.....	15
2.2 Electric Machine Model from the Protection System Perspective.....	17
2.3 Basic Inverse-Time (ANSI 51) OCR Operation and Coordination.....	20
2.4 OCR Optimization with the Boundary Evaluation and SFA.....	23
2.5 Results and Analysis.....	29
2.6 Discussion.....	36
CHAPTER 3 OPTIMIZING THE COORDINATION FUNCTION WITH ENHANCED MULTI-FUNCTION OVERCURRENT PROTECTION.....	37
3.1 Problem Definition.....	37
3.2 Formulation of OCR Coordination.....	39
3.3 Optimization of the Definite-Time (ANSI 50) and Inverse-Time (ANSI 51) OCRs.....	41
3.4 Consideration of Protection Limitations and Activation of the Definite- Time (ANSI 50) Function.....	44
3.5 Program Demonstration and Testing.....	45

3.6 Result Analysis.....	53
3.7 Discussion	58
CHAPTER 4 CHALLENGE OF THE PROTECTION SYSTEM IN A DISTRIBUTION NETWORK WITH A HIGH PENETRATION OF IBRs.....	
4.1 Problem Definition.....	61
4.2 SC Behavior of DGs.....	62
4.3 Observation of the SC Behavior in a Microgrid.....	63
4.4 Effects of DG Penetration on the SC Behavior.....	67
4.5 Modernized Protection Coordination Philosophy and Strategy	68
4.6 Discussion	73
CHAPTER 5 ADAPTIVE PROTECTION IN MICROGRIDS WITH THE VOLTAGE–CURRENT PARAMETER	
5.1 Problem Definition.....	75
5.2 Abnormal Events in Microgrids.....	76
5.3 Voltage-Aided OCR.....	79
5.4 Simulation Setup	84
5.5 Results and Analysis	88
5.6 Discussion	93
CHAPTER 6 INTELLIGENT PROTECTION RELAY WITH IDENTIFICATION AND CLASSIFICATION CAPABILITY	
6.1 Problem Definition.....	95
6.2 Event-Based Classification Based on CNNs.....	96
6.3 Anomalies in Industrial Medium-Voltage Power System Networks	99
6.4 Proposed IPA Architecture and Working Principles.....	101
6.5 Simulation Performance	104
6.6 Results and Discussion.....	112
CHAPTER 7 CONCLUSIONS	
7.1 Concluding Remarks	115
7.2 Suggestions for Future Research.....	116
REFERENCES	117
APPENDIX 1. IEEE 242-2001 TEST CASE.....	127
APPENDIX 2. CURRICULUM VITAE.....	131

LIST OF FIGURES

Figure 1.1. Fishbone diagram of the study.	5
Figure 1.2. Summary of the contributions for each subtopic in this study.....	10
Figure 2.1. Different curve types affecting the OCR response.....	22
Figure 2.2. Illustration of the optimized curve type of SI, VI, LTI, EI, and UI compared to the MS behavior on the same time operation target.....	23
Figure 2.3. Illustration of the allowable OCR operation range with consideration of the electric machine boundary in a TCC of the (a) induction motor, (b) transformer, and (c) generator.	25
Figure 2.4. Flowcharts of the proposed method in each domain program.	28
Figure 2.5. Simplified SLD of PT Pupuk Kujang Cikampek for the validation of the proposed method (SFA) and boundary evaluation.....	30
Figure 2.6. TCC of OCRs in case study A after the optimization process.	31
Figure 2.7. Convergence curve comparison (FA vs. AMFA) in case study A....	31
Figure 2.8. TCC of the OCRs in case study B after the optimization process. ...	32
Figure 2.9. Convergence curve comparison (FA vs. AMFA) in case study B....	33
Figure 2.10. TCC of the OCRs in case study C after the optimization process. ...	34
Figure 2.11. Convergence curve comparison (FA vs. AMFA) in case study C....	34
Figure 3.1. Overcurrent protection challenges and approaches in practice.....	37
Figure 3.2. SLD and time–current curves for two OCRs (OCR A and OCR B) with a coordination function to anticipate different fault locations (F1 and F2). OCR A only anticipates F1, whereas OCR B anticipates F2 and F1.....	40
Figure 3.3. SLD used as the test bench according to the IEEE Std. 242.....	47
Figure 3.4. Flowchart of the method to perform OCR optimization and time–current evaluation.....	49
Figure 3.5. Time–current curve of A1 using manual calculation (conventional method).....	54
Figure 3.6. Time–current curve of A1 using manual calculation (conventional method) with subjective correction in curve-evaluation technique. .	55
Figure 3.7. Time–current curve of A1, A2, and A3 using Scheme A optimization. a and b are the time responses of A1 and A2 during a fault in 4.16 F0-1, respectively. a = 0.107 s. b = 0.301 s. c and d are the time responses of A2 and A3 during a fault in 4.16 F1, respectively. c = 0.294 s. d = 0.305 s. e is the time response of A3 during a fault in 13.8 F-01. e = 0.229 s.	56
Figure 3.8. Time–current curve of A1, A2, and A3 using the Scheme B optimization. a and b are the time responses of A1 and A2 during a	

	fault in 4.16 F0-1, respectively. a = 0.141 s. b = 0.344 s. c and d are the time responses of A2 and A3 during a fault in 4.16 F1, respectively. c = 0.336 s. d = 0.345 s. e is the time response of A3 during a fault in 13.8 F-01. e = 0.26 s.	57
Figure 3.9.	Time–current curve of A1, A2, and A3 using the Scheme C optimization. a and b are the time responses of A1 and A2 during a fault in 4.16 F0-1, respectively. a = 0.1 s. b = 0.301 s. c and d are the time responses of A2 and A3 during a fault in 4.16 F1, respectively. c = 0.1 s. d = 0.309 s. e is the time response of A3 during a fault in 13.8 F-01. e = 0.1 s.	59
Figure 3.10.	The result comparison of conventional method, conventional method with correction, and the proposed method for obtaining setting of relay A1.	60
Figure 4.1.	SLD of the IEEE 13 bus with DG penetration.	65
Figure 4.2.	Model of the DG used in the simulation.....	65
Figure 4.3.	Example of the protection model used on feeder Bus 632 to Bus 671..	66
Figure 4.4.	Total SC current under various case studies.....	67
Figure 4.5.	Sunburst diagram of the SC contributions for (a) Case A (grid only), (b) Case B (DG–SG penetration), and (c) Case C (DG–IBR penetration).	70
Figure 4.6.	Voltage observation on Bus 632 in various SC locations.....	71
Figure 4.7.	Current observation between Bus 632 and Bus 671 in various SC locations. The positive polarity means that the current flow is from Bus 632 to Bus 671. By contrast, the negative polarity means that the current flow is backward.	71
Figure 4.8.	3D diagram of the current (x-axis), voltage (y-axis), and time response (z-axis) for the protection coordination on CB 632-671 under various events.	74
Figure 5.1.	SLD for a distribution network with the DG penetration. During the fault, the fault current from DG ($I_{F(DG)}$) has an opposite direction from that of the grid fault current.	77
Figure 5.2.	Time–current curve showing the impact of varying fault current magnitudes to the relay time response.....	78
Figure 5.3.	<i>VCM</i> response to the drop under some combinations of coefficients na , nb , and nc in Equation (5.9).....	83
Figure 5.4.	General assembly of the proposed relay connection.	83
Figure 5.5.	Block diagram of the proposed relay architecture. The blue line shows the analog input from the voltage and current measurements.	84
Figure 5.6.	IEEE 13 bus distribution network with the DG penetration at the end point feeder.	85

Figure 5.7. Comparison between the conventional method and proposed method: (a) RMS current oscillography at R6r during the fault at F1 compared to the relay pickup current. (b) Tripping chart of R6r. (c) Comparison of the voltage oscillography at Bus 671.	92
Figure 6.1. Reliable and sustainable power system as a result of an appropriate protection system and proper power system operations.....	96
Figure 6.2. Typical CNN block scheme.	97
Figure 6.3. Convolutional process representation [93].....	98
Figure 6.4. Filters and maps represented as neurons in a convolutional layer [93].	99
Figure 6.5. Sequence of events in the power system in terms of the voltage, frequency, and current flows.....	100
Figure 6.6. State of the art: Comparison of the block diagram on the (a) existing available relay on the market and (b) the proposed IPA.	102
Figure 6.7. Working principle flowchart of (a) the conventional relay and (b) proposed IPA.....	103
Figure 6.8. SLD used for the simulation and data gathering.....	104
Figure 6.9. Visualization of the data required to be trained in CNN.....	105
Figure 6.10. Practical measurement data from the simulation.	106
Figure 6.11. Current reading on each relay with varying events in the 11 kV bus: LG fault, LLL fault, DG outage, and MS.....	107
Figure 6.12. Voltage (a) and frequency (b) readings on each relay with varying events in the 11 kV bus: LG fault, LLL fault, DG outage, and MS.....	108
Figure 6.13. LSTM block.	110
Figure 6.14. Feeding process to LSTM layers.....	111
Figure 6.15. Keras sequential model.	112
Figure 6.16. Trial results of the CNN in recognizing the symptoms of power system operations: (a) 200 epochs and (b) 275 epochs.	113
Figure 6.17. Heatmap dataset.	114

This page is left intentionally blank.

LIST OF TABLES

Table 1.1.	Research works in the field of optimization method for electrical protection systems	6
Table 1.2.	Research works in the field of fault mitigation due to the high DG penetration.	7
Table 1.3.	Research works in the field of multi-function tripping scheme	8
Table 2.1.	Stator damage points based on a Fuji electric motor (specifications: 1320 KW, 2300 V, 50 Hz, 8 poles, 405 A, and SN: 1701J504N).....	18
Table 2.2.	Category II transformer short-time thermal load capability based on IEEE Std C57.109-2018 [55]	19
Table 2.3.	Gas turbine generator short-time thermal capabilityn(specifications: ABB-AMS 900 LE, 14.85 MVA, 50 Hz, 0.8 PF, 13.8 kV, 621 A, and 1500 RPM)	20
Table 2.4.	Parameters of an inverse-time OCR.....	21
Table 2.5.	Optimization results using the proposed method (SFA) and boundary evaluation	35
Table 3.1.	Fault current in various locations on the IEEE Std. 242 test case measured by each OCR.....	48
Table 3.2.	Optimization scenario	50
Table 3.3.	Optimized results of the OCR settings.....	51
Table 3.4.	Time operations and errors of the OCR using the optimized settings	52
Table 3.5.	<i>TDS</i> value for each curve type by using manual calculation for OCR A1	53
Table 4.1.	Maximum (sub-transient) SCs of the various DG types	64
Table 4.2.	Minimum (steady state) SCs of the various DG types	64
Table 4.3.	Case study used in the experiment	67
Table 5.1.	Voltage in each relay during the fault	86
Table 5.2.	Current flows in each relay during the fault.....	87
Table 5.3.	Parameters used in the simulation.	88
Table 5.4.	Optimized relay settings among the methods	89
Table 5.5.	Relay operating times among methods in various fault points	90
Table 5.6.	Total operation time based on the objective function and effectiveness among methods.	91
Table 6.1.	CNN-based architecture	111

This page is left intentionally blank.

NOMENCLATURE

Abbreviations:

AI	Artificial Intelligence
AMFA	Adaptive Modified Firefly Algorithm
ANSI	American National Standards Institute
CB	Circuit Breaker
CNN	Convolutional Neural Network
CTI	Clearing Time Interval
DG	Distributed Generator
DOCR	Directional Overcurrent Relay
DOL	Direct Online
EI	Extremely Inverse
FA	Firefly Algorithm
FLA	Full Load Ampere
GTG	Gas Turbine Generator
IBR	Inverter Based Resource
IEC	International Electrotechnical Commission
IEEE	Institute of Electrical and Electronics Engineers
IPA	Intelligent Protective Apparatus
LRC	Locked Rotor Current
LSTM	Long Short Term Memory
LTI	Long Time Inverse
MS	Motor Starting
NERC	North American Electric Reliability Corporation
OCR	Overcurrent Relay
OF	Objective Function
PCC	Point of Common Coupling
RES	Renewable Energy Resource
RES	Renewable Energy Resource
SC	Short Circuit
SFA	Serial Firefly Algorithm
SG	Synchronous Generator
SI	Standard Inverse
SLD	Single Line Diagram
TCC	Time Current Characteristic
TDS	Time Dial Setting for OCR
TMS	Time Multiplier Setting
UI	Ultra Inverse
VCM	Voltage current multiplier
VI	Very Inverse
WTG	Wind Turbine Generator

Symbols and notations

$AsymLRC$	Asymmetrical locked rotor current
crv	Possible curve type selection for each OCR.
CTI_{max}	Maximum CTI .
CTI_{min}	Minimum CTI .
G	Sensed current by OCR
G_s	Preset current threshold value
$G_s(U)$	Function of current threshold associated with voltage bus
$I_{x,y}$	Sensed current by OCR x during fault in location y .
I_L	Lower boundary current point.
I_U	Upper boundary current point.
I_p	Current threshold for OCR
I_{p_x}	Predefined pickup current of inverse-time (ANSI Code 51) OCR x .
I_{p_d}	Predefined pickup current of definite-time (ANSI Code 50) OCR.
$I_{p_d array}$	List of possible I_{p_d} .
$I_{p_d min}$	Minimum I_{p_d} .
I_{sc}	Short circuit current.
$I_{sc bu}$	Current value for OCR to trip as backup protection.
$I_{sc pr}$	Current value for OCR to trip as primary protection.
k_s	Locked rotor current factor
M	Ratio between sensed current and threshold value
$PICK$	Pickup state
$REST$	Restrain state
RP	Relay plug.
RP_{max}	Highest value of RP .
RP_{min}	Lowest value of RP .
RP_s	RP interval.
rtg_{bu}	Time of the previous OCR response as a backup.
STA	Over-current relay (OCR) state operation
t	Operating time of OCR
T	Operating torque in DOCR
$t_L(i)$	Load's lower time-current border.
t_{pr}	actual time operation as primary protection.
$t_U(i)$	Load's upper time-current border.
t_x	Operating time of inverse-time (ANSI Code 51) OCR x .
$t_x(I_{x,y})$	The operating time of OCR x in accordance to $I_{x,y}$.
$td(I)$	Definite time to current function.
tdp	Predefined time delay in definite time OCR (ANSI Code 50).
TDS_{max}	Maximum value of TDS .
TDS_{min}	Minimum value of TDS .
TDS_s	TDS interval value.
tg	OCR time operating target.

tg_{bu}	tg to role as a backup protection.
tg_{min}	Minimum tg .
tg_{pr}	tg to role as a primary protection.
tg_{update}	Time increment to revise the tg .
$tl(I)$	Time-current function of equipment lower limit.
$TRIP$	Trip state
$tu(I)$	Time-current function of equipment upper limit.
U	Voltage bus
U_{th}	Voltage threshold in VCM
φ	Angle between ϕ_i and ϕ_v
ϕ_i	Polarizing values proportional to the current
ϕ_v	Polarizing values proportional to the voltage

This page is left intentionally blank.

CHAPTER 1

INTRODUCTION

1.1 Background

Among the many appealing challenges faced by the industry today, the most critical part is the ability to compete in the market by figuring and shaping the new technology revolution. The “Fourth Industrial Revolution” [1] is a movement that considers not only the quantity but also the quality and sustainability of a product or service being offered. From an electrical power system perspective, this statement expresses that the orientation of the future power delivery is shifting from generating and spreading electricity to continuously delivering electricity in a high-reliability index. A dependable electrical system requires a flexible maneuver in the distribution network and a credible protection system. In a common industrial plant, the power system consists of a generator (upstream) and load (downstream). In such a large-scale plant, the system is integrated with another plant using a transfer bus, a complex system with a complicated coordination scheme in the protection devices. As a result, engineers face no shortage of challenges to keep the plant reliability in the high index. Confronted with false or failure trips due to motor starting (MS), transformer energizing, and network maneuver, engineers need to rethink their coordination scheme to maintain the performance index.

A reliability analysis conducted by the North American Electric Reliability Corporation shows that the incorrect setting of the protection system or devices is an immense issue and does not come with a significant improvement [2]. The study shows that the two highest misoperations are caused by the protective device. Consequently, among the two, the incorrect setting/logic/design error is the highest cause (31%), followed by the relay failures/malfunctions (19%). These facts prove that the protection system needs an improvement to tackle incorrect setting or logic issues during operation.

A protection relay is a device that monitors electrical parameters and then sends a trip signal to the circuit breaker (CB) if the threshold is violated. Nowadays, relay manufacturers produce a multi-function relay that can sense multiple parameters at

once. However, each relay is working independently for every parameter. Thus, a specific threshold is needed for every parameter being monitored.

Accordingly, some standards on well-coordinated protection systems for every parameter being monitored have been published by American National Standards Institute (ANSI)/Institute of Electrical and Electronics Engineers (IEEE) [3]–[6] and International Electrotechnical Commission (IEC) [7]. These standards are very useful only if engineers can interpret the boundary of the threshold and if the circumstance is similar to the case stated in the standard. Consequently, a considerable number of research have been conducted to solve the protection coordination problem. An attempt for this particular dispute is by creating an optimization method in the power system protection domain.

Furthermore, events in electrical systems, such as ground fault, phase fault, start or cease of electrical machines, and network topology changes have their own indicators. These indicators are categorized based on electrical parameters (i.e., frequency (f), current flow (I), and voltage (V)). For instance, in the event of a short-circuit (SC) fault, the closest feeder relay to the fault location experiences a drop voltage, followed by an increase in the current flow and frequency swing rate. By contrast, in the MS event, the feeder may sense a dip voltage, surge current, and slight frequency drop. These events are clearly different even though the indicators of the voltage and current are similar. The CB is required to trip in SC conditions, whereas it is prohibited to trip during the MS event. However, due to improper settings, CB trips are often recorded during the MS event, particularly in most petrochemical or oil and gas companies [8]. The root causes to such a condition are the multi-function relay installed with a default setting and not considering the load being protected. As a containment action, engineers usually broaden the setting or disable the relay to anticipate the drop voltage or surge current during MS. This action comes with a risk, such that the relay may not trip when the SC occurs during the start process.

Another contest in the conventional protection system appears along with the new trends of the utilization of renewable energy sources (RESs) as a distributed generator (DG). RESs, such as wind, solar, tidal, and hydropower, offer less carbon footprint compared to conventional thermal power plants. However, RESs in power

generation does not come without any drawbacks. The variability in RESs results in the variable output power [9]. In a distribution network, the RES is not centralized; it is distributed in nature. As DG penetration rises, abnormalities in traditional power systems occur (e.g., reverse power flow [10], voltage rise or imbalance [11], low inertia [12], harmonics [13], and SC behavior changes [14]). The traditional distribution network protection technology heavily relied on current monitoring to isolate SCs. In this case, overcurrent relay (OCR), with ANSI code 51, gives an inverse-time response to the magnitude of the fault current [15]. The issue is that the distribution power system metamorphosis caused by DG penetration changes the principle of the distribution network's protection mechanism. Because the protection strategy is meant to anticipate various faults, recognizing the SC behavior is critical for determining the set point of the relay protection in the distribution network affected by the high DG penetration.

In this study, an attempt to improve the protection system is introduced by analyzing the behavior of the electrical system when an event occurs. In the succeeding sections, the behaviors will be categorized into several symptoms that could be understood by the relay. Then, with the improved relay ability to recognize what happens on the system, it is expected that the proposed method may lower the possibility of misoperations due to incorrect setting, although it remains sensitive to possible fault conditions. On a bigger scale, the improved relay operation may contribute to the enhancement of the reliability of power delivery.

1.2 Problem Statement

To frame the present work, the outcomes of this study are expected to answer the problems in a false trip issue in the medium voltage power system network. First, this study investigates the effect of network topology changes and maneuver in power system operation on the coordination scheme of the protection system. Once the investigation is concluded, this study aims to digest the practical consideration that must be taken care to make a defense scheme. Second, this study attempts to optimize the conventional relay, by minimizing the time operation, by merging the multi-function characteristic (inverse-time and definite-time curve). Third, this study examines the fault mitigation plan for the distribution network due

to the impact of RES utilization. Forth, this study aims to create the intelligent protection apparatus with the capability to classify the power system events such as fault (i.e., SC) and non-fault condition (i.e., MS, generator outage, and switching events).

1.3 Objectives and Benefits

One of the objectives of this work is to establish the concept and practical consideration during the optimization of the relay setting with an expectation to reduce the false trip event. Once the electrical boundary is defined, the mathematical model to optimize the conventional protection relays' setting could be addressed. Aside from maximizing the capability of the conventional protection relay, this work also aims to investigate the impact of RES penetration on the power system network. The objective is to obtain the accurate fault behavior under a high DG penetration or inverter-based resource (IBR) by concerning the suitable approach for protection relay sensitivity. The correlation between electrical parameters (i.e., frequency, voltage, and current) might be used altogether to determine a fault or no-fault condition. Thus, another objective is to define the determiner in the intelligent protective apparatus (IPA) by employing the neural network. The improved optimization method with regard to the electrical boundaries, multi-function relay for the power system network with high DG penetration, and IPA has an applicable benefit to increase the reliability and resiliency of the power system network, especially by reducing the number of false trip events.

1.4 Roadmap

The research roadmap of this work is visualized in Figure 1.1. With the aim to achieve the “Intelligent Protection Apparatus to Minimize the False Trip Issue in Medium-Voltage Industrial Power System,” the research is supported with three subtopics: 1) optimization method for the protection relay, 2) fault mitigation due to high DG penetration, and 3) multi-function tripping scheme. In the fishbone diagram, the research conducted in this work is denoted with the blue font color, whereas the black font color shows the works conducted by the other researchers in the field, with the list of titles provided in Table 1.1, Table 1.2, and Table 1.3.

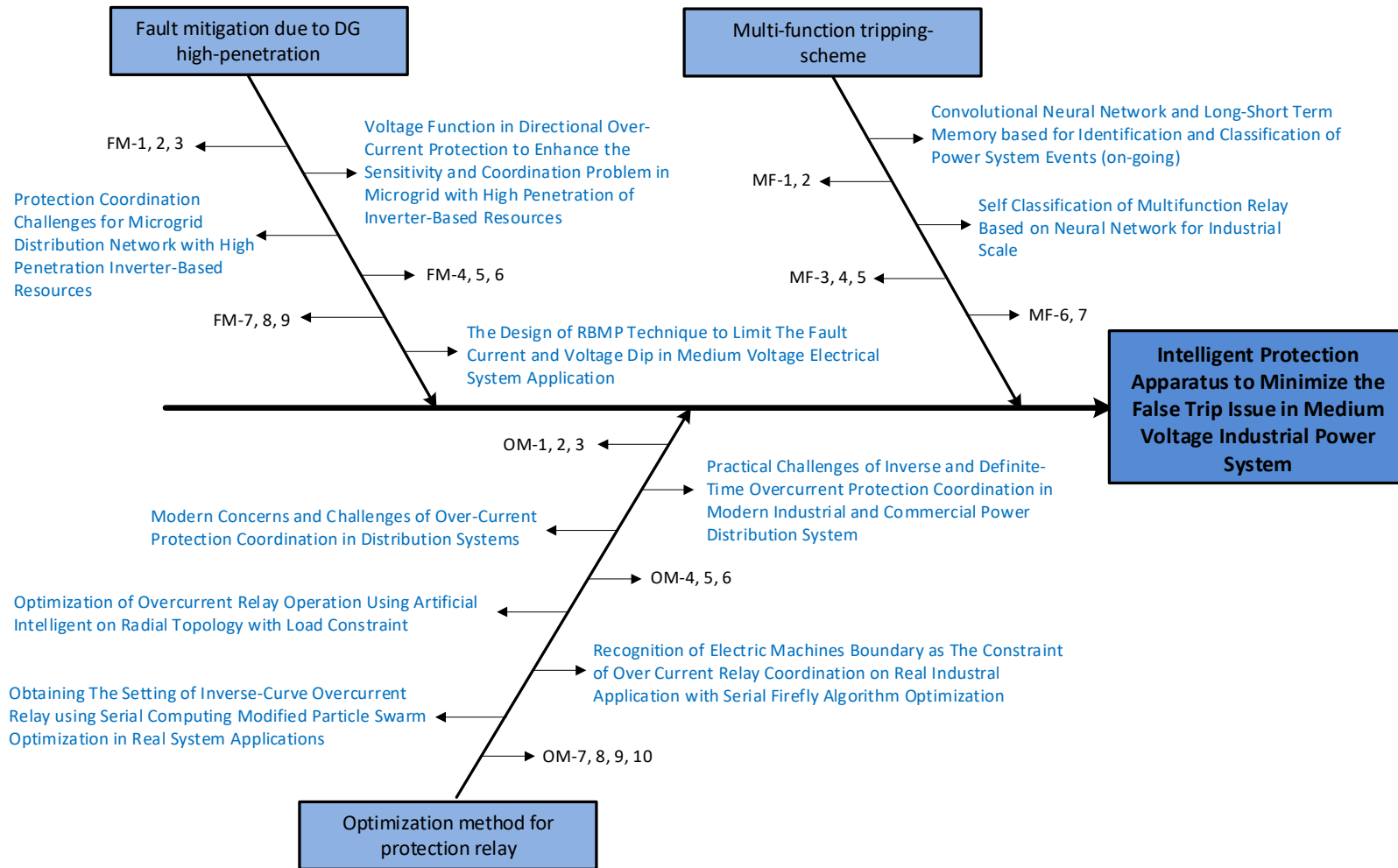


Figure 1.1. Fishbone diagram of the study.

Table 1.1. Research works in the field of optimization method for electrical protection systems

ID	Bibliography
OM-1	A. J. Urdaneta et al., “Optimal coordination of directional overcurrent relays in interconnected power systems,” IEEE Transaction on Power Delivery, Jul. 1988. [16]
OM-2	IEEE Committee Report, “Computer representation of overcurrent relay characteristics,” IEEE Transaction on Power Delivery, Jul. 1989. [17]
OM-3	C. S. Mardegan and R. Rifaat, “Considerations in applying IEEE recommended practice for protection coordination in industrial and commercial power systems—Part I,” IEEE Transactions on Industry Applications, Sep. 2016. [18]
OM-4	J. D. Pico et al., “Protection coordination analysis under a real-time architecture for industrial distribution systems based on the Std IEEE 242-2001,” IEEE Transaction in Industry Applications, Jul. 2016. [19]
OM-5	A. Tjahjono et al., “Adaptive modified firefly algorithm for optimal coordination of overcurrent relays”, IET Generation Transmission Distribution, 2017. [20]
OM-6	R. M. Chabanloo and N. Mohammadzadeh, “A fast numerical method for optimal coordination of overcurrent relays in the presence of transient fault current,” IET Generation Transmission Distribution, 2018. [21]
OM-7	P. A. Gaynor et al., “Protective relay coordination study at a petrochemical complex,” in 2019 IEEE Petroleum and Chemical Industry Committee Conference, Sep. 2019. [22]
OM-8	N. El-Naily et al., “A novel constraint and non-standard characteristics for optimal overcurrent relays coordination to enhance microgrid protection scheme,” IET Generation Transmission Distribution, 2019. [23]
OM-9	S. Saad M., “A new constraint considering maximum PSM of industrial overcurrent relays to enhance the performance of the optimization techniques for microgrid protection schemes,” Sustainable Cities and Society, Jan. 2019. [24]
OM-10	M. Ghotbi Maleki et al., “Accurate coordination method based on the dynamic model of overcurrent relay for industrial power networks taking contribution of induction motors into account,” IET Generation Transmission Distribution, 2020. [25]

Table 1.2. Research works in the field of fault mitigation due to the high DG penetration.

ID	Bibliography
FM-1	R. C. Dugan and T. E. McDermott, "Operating conflicts for distributed generation on distribution systems," 2001 Rural Electric Power Conference, Apr. 2001. [26]
FM-2	T. Ackermann et al., "Distributed generation: a definition," Electric Power System Research, 2001. [27]
FM-3	M. Dewadasa et al., "Fault isolation in distributed generation connected distribution networks," IET Generation Transmission and Distribution, Oct. 2011. [28]
FM-4	A. Ukil et al., "Current-only directional overcurrent protection for distribution automation: Challenges and solutions," IEEE Transaction on Smart Grid, Dec. 2012. [29]
FM-5	E. Muljadi et al., "Different factors affecting short circuit behavior of a wind power plant," IEEE Transactions on Industry Applications, Jan. 2013. [14]
FM-6	A. Al-Riyami et al., "An investigation into alternatives to directional overcurrent protection on grid transformers to improve the network capacity to accommodate reverse power flow," in 12th IET International Conference on Developments in Power System Protection (DPSP 2014), Mar. 2014. [30]
FM-7	F. B. Costa et al., "Overcurrent protection in distribution systems with distributed generation based on the real-time boundary wavelet transform," IEEE Transactions on Power Delivery, Feb. 2017. [31]
FM-8	M. G. Maleki et al., "Method to resolve false trip of non-directional overcurrent relays in radial networks equipped with distributed generators," IET Generation Transmission Distribution, 2019. [32]
FM-9	A. A. Balyith et al., "Non-communication based time-current-voltage dual setting directional overcurrent protection for radial distribution systems with DG," IEEE Access, 2020. [33]

Table 1.3. Research works in the field of multi-function tripping scheme

ID	Bibliography
MF-1	L. Jenkins et al., "An application of functional dependencies to the topological analysis of protection schemes," IEEE Transaction on Power Delivery, Jan. 1992. [34]
MF-2	M. Abdi-Khorsand and V. Vittal, "Modeling protection systems in time-domain simulations: A new method to detect mis-operating relays for unstable power swings," IEEE Transactions on Power Systems, Jul. 2017. [35]
MF-3	D. F. C. Rodriguez et al., "Virtual relay design for feeder protection testing with online simulation," IEEE Transaction on Industry Applications, Jan. 2018. [36]
MF-4	H. F. Albinali and A. P. S. Meliopoulos, "Resilient protection system through centralized substation protection," IEEE Transactions on Power Delivery, Jun. 2018. [37]
MF-5	C. A. Castillo et al., "Mitigation of DOCR miscoordination through distance relays and non-standard overcurrent curves," Electric Power Systems Research, Oct. 2018. [38]
MF-6	S. Mitra and P. Chattopadhyay, "Design and implementation of flexible numerical overcurrent relay on FPGA," International Journal of Electrical Power & Energy Systems, Jan. 2019. [39]
MF-7	S. A. Saleh et al., "Comparing the performance of protection coordination and digital modular protection for grid-connected battery storage systems," IEEE Transaction on Industry Applications, May 2019. [40]

1.5 Contributions

Over the decades, researchers have worked extensively to improve the protection system with the aim to improve the reliability of the power system network. The improvement of the protection system may be categorized into two subjects: 1) the enhancement of the relay architecture and 2) the coordination function among relays. In this work, both subjects are addressed to provide a solution in both sides. The contributions of this work is mainly divided into three major scopes:

First, to enhance the protection coordination using conventional protection devices, the optimization of the system model and relay tripping logic is required. In this scope, a numerical method or artificial intelligence (AI) is used to solve the coordination problem following the previous researchers (Table 1.1). This work contributes to address the practical consideration by modeling the electrical machine as the constraint during the optimization [41], [42]. Once the electrical

boundaries are recognized, the optimization process is improved by considering the possible relays in different voltage levels [43] and merging the inverse-time (ANSI 51) and definite-time (ANSI 50) relays as an objective function (OF) to be solved [44], [45]. The experiments conducted in the IEEE Std. 242 test feeder shows that the total relay time operation is reduced, and the relay mis-operation is exempted.

Second, with consideration to the recent trends of RES utilization in various locations, an effort to estimate the fault behavior in a distribution system with high DG penetration is published by some researchers, as listed in Table 1.2. The focus of this study is on the impact of IBR penetration on the distribution network [46]. The observation is made from the IEEE-13 bus test case. Compared to a rotating-machine generator, IBRs only produce low fault currents, which might cause the protection relay to fail. Thus, this work attempts to solve the problem by aiding the voltage parameter in the directional overcurrent relay (DOCR) [47]. The idea is to readjust the relay pickup current to conform to the low fault current.

Third, some approaches to increase the protection relay accuracy and sensitivity have been made by researchers, as shown in Table 1.3. In this work, an IPA is designed with the multi-parameter sensing parameters, such as voltage, frequency, and current readings [48]. The performance test shows that the IPA can distinguish the fault and fault-like event in the industrial power system scale.

To have a chronological overview regarding the study, Figure 1.2 shows the summary of cause and effects. The summary of the research flow can give a clear view regarding authors' mindset to do the research.

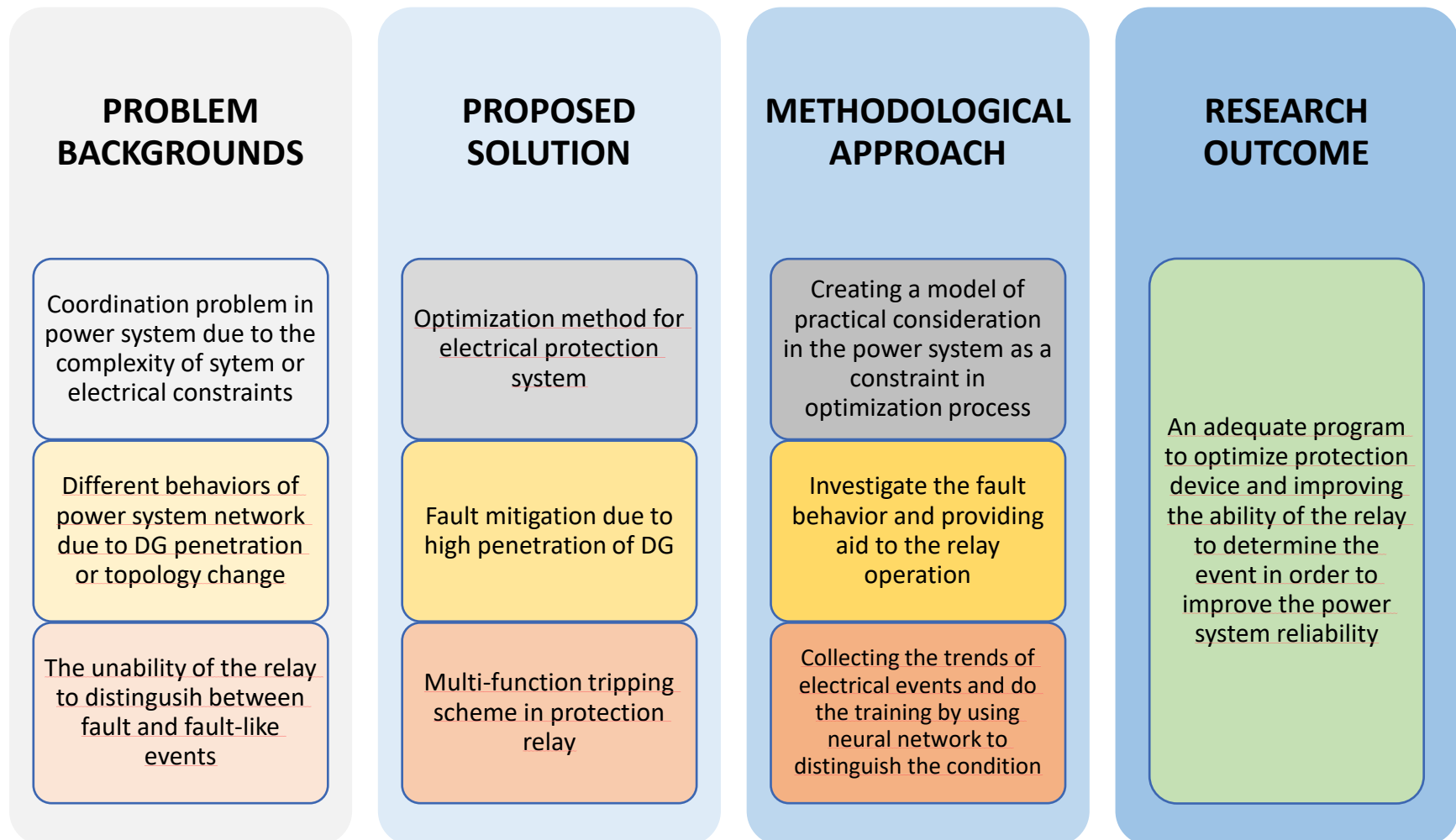


Figure 1.2. Summary of the contributions for each subtopic in this study.

1.6 List of Publications

1. V. R. Mahindara, M. G. Istiqlal, M. Pujiantara, D. A. Asfani, A. Priyadi, and M. H. Purnomo, "Obtaining The Setting of Inverse-Curve Overcurrent Relay using Serial Computing Modified Particle Swarm Optimization in Real System Applications," 2018 International Seminar on Intelligent Technology and Its Applications (ISITIA), 2018, pp. 187–192, doi: 10.1109/ISITIA.2018.8710868. [43]
2. N. A. Wibowo, V. R. Mahindara, A. Priyadi, M. Pujiantara, and M. H. Purnomo, "Optimization of Overcurrent Relay Operation Using Artificial Intelligent on Radial Topology with Load Constraint," 2018 International Seminar on Intelligent Technology and Its Applications (ISITIA), 2018, pp. 205–208, doi: 10.1109/ISITIA.2018.8711089. [49]
3. V. R. Mahindara, N. A. Wibowo, T. P. Sari, M. Pujiantara, A. Priyadi, and M. H. Purnomo, "Recognition of Electric Machines Boundary as The Constraint of Over Current Relay Coordination in Real Industrial Application with Serial Firefly Algorithm Optimization," 2019 IEEE 12th International Symposium on Diagnostics for Electrical Machines, Power Electronics and Drives (SDEMPED), 2019, pp. 153–159, doi: 10.1109/DEMPED.2019.8864828. [41]
4. M. Pujiantara, V. R. Mahindara, B. Fachrurriza, A. Priyadi, and M. H. Purnomo, "The Design of RBMP Technique to Limit The Fault Current and Voltage Dip in Medium Voltage Electrical System Application," 2019 International Seminar on Intelligent Technology and Its Applications (ISITIA), 2019, pp. 159–164, doi: 10.1109/ISITIA.2019.8937291. [50]
5. V. R. Mahindara, D. Celeita, M. Pujiantara, A. Priyadi, M. H. Purnomo, and E. Muljadi, "Modern Concerns and Challenges of Over-Current Protection Coordination in Distribution Systems," 2020 IEEE/IAS 56th Industrial and Commercial Power Systems Technical Conference (I&CPS), 2020, pp. 1–7, doi: 10.1109/ICPS48389.2020.9176749. [45]
6. V. R. Mahindara, A. Priyadi, M. Pujiantara, M. H. Purnomo, A. Y. Saber, and E. Muljadi, "Protection Coordination Challenges for Microgrid Distribution Network with High Penetration Inverter-Based Resources,"

- 2020 IEEE Energy Conversion Congress and Exposition (ECCE), 2020, pp. 1618–1622, doi: 10.1109/ECCE44975.2020.9235817. [46]
7. F. W. Rahmat, M. Pujiantara, V. Lystianingrum, V. R. Mahindara, and T. P. Sari, “Self Classification of Multifunction Relay Based on Neural Network for Industrial Scale,” 2020 International Seminar on Intelligent Technology and Its Applications (ISITIA), 2020, pp. 13–18, doi: 10.1109/ISITIA49792.2020.9163719. [48]
 8. V. R. Mahindara, D. F. C. Rodriguez, M. Pujiantara, A. Priyadi, M. H. Purnomo, and E. Muljadi, “Practical Challenges of Inverse and Definite-Time Overcurrent Protection Coordination in Modern Industrial and Commercial Power Distribution System,” in *IEEE Transactions on Industry Applications*, vol. 57, no. 1, pp. 187–197, Jan.-Feb. 2021, doi: 10.1109/TIA.2020.3030564. [44]
 9. V. R. Mahindara, D. F. C. Rodriguez, M. Pujiantara, A. Priyadi, E. Muljadi, and M. H. Purnomo, “Voltage Function in Directional Over-Current Protection to Enhance the Sensitivity and Coordination Problem in Microgrid with High Penetration of Inverter-Based Resources,” in *International Journal of Intelligent Engineering and Systems*, vol. 14, no. 3, pp. 516–527, Jun. 2021, doi: 10.22266/ijies2021.0630.43. [47]

1.7 Scope and Limitations

This works focuses on a medium-voltage distribution network that is mainly used in the industrial power system. The experiments are conducted based on the real case of an industrial plant and the test case provided by the IEEE standard (IEEE Std. 242 and IEEE Std. 3004)

1.8 Dissertation Outline

This dissertation consists of seven chapters to comprehensively discuss the research journey. In Chapter 1, an introduction about the protection system issue in the medium-voltage industrial power system and the approach taken in this study are discussed. In Chapter 2, the basics of the protection system is discussed, mainly with the consideration to the electrical boundary during the optimization process. In Chapter 3, after defining the optimization constraint, the methodology and

mathematical equations to improve the optimization of the protection relay are discussed. Because this work focuses on the trend of DG penetration in the power system network, in Chapter 4, an investigation pertaining to the fault behavior is provided. In Chapter 5, the solution to the unique condition regarding DG penetration in the distribution system is provided. Then, in Chapter 6, an attempt to design the IPA by aiding the protection relay with machine learning capability is documented. Lastly, in Chapter 7, concluding remarks and suggestions for further research are presented.

This page is left intentionally blank.

CHAPTER 2

RECOGNIZING THE ELECTRICAL BOUNDARY FOR PROTECTION RELAY SETTINGS

In this chapter, a new approach of determining the OCR setting with the recognition of the electric machine boundary is discussed [41]. The method combines the AI optimization method with a specific boundary model of the equipment being protected by the OCR. The process is started by summarizing the model of an induction motor, transformer, and generator. Then, these mathematical models are used to evaluate the possible settings of the OCR spawn by the AI. The firefly algorithm (FA) is used as the basis of AI with a modification to exempt the possibility of local minima [20]. Instead of parallel optimization, the FA will be run serially (serial firefly algorithm [SFA]) on each OCR to evaluate the whole available curve type based on the IEC standard. The best results are retrieved by comparing the possible settings from the SFA with the electric machine boundary. In addition, the validation of the proposed method is endorsed with an industrial power system.

2.1 Problem Definition

Electrical machines are a common thing used in industrial facilities. On the upstream side, a generator generates electricity, a transformer converts it to the desired voltage, and a motor drives the pump, fans, conveyor, and other factory-required loads on the downstream side. To increase capacity or reliability, the industry usually replaces existing electric machines with higher-specified machines or introduces a new line of electric machines.

The problem occurs when the new electric machines are energized using the existing system. As demonstrated in a fertilizer factory in Indonesia (PT Pupuk Kujang Cikampek), new motors and transformers frequently fail during the initial energization due to improper OCR setting. For generators, engineers were extremely concerned that the OCR would fail to operate if a fault occurred close to the generator bus due to the OCR's lower sensitivity setting. According to a

reliability analysis [51], the incorrect setting of protection devices, including OCR, is still a significant issue that has not improved significantly.

Indeed, regulations governing the protection of electric machines already exist. For motor protection, certain standards [52], [53] explicitly state that the OCR must initiate tripping and disconnecting the motor circuit from the power system when an excessive current is detected, but they permit the motor to be energized, started, and run. On other occasions, the critical conditions for transformers were enumerated in the standard [54] and [55], which most likely discuss the trough fault current limitation. In addition, [56], [57] refer to the generator standards, which classify the protection against overloads, overexcitation, and phase faults.

Although standards exist, engineers in the field continue to use the conventional method to determine the OCR settings, which is trial and error. Engineers plot the OCR on a time–current characteristic (TCC) curve using commercial software, such as Electrical Transient Analyzer Program (ETAP) [58], SKM [59], or OCR manufacturer-supplied software [60]. This traditional method is undoubtedly difficult and time-consuming. The OCR contains four variables: pickup current (I_p), time dial setting (TDS), curve type, and desired time operation (td). Thus, in the trial and error method, engineers vary one variable while maintaining the other variables constant to obtain td .

Research on OCR setting optimization has accelerated over the years. Numerous works have discussed the changes in the distribution network topology as the primary issue in coordinating OCR [21], [31]. Similarly, some works have focused on developing a new equation to provide the most precise responses to system anomalies or faults [35], [38], [61]. Moreover, in majority of cases, however, no special attention has been paid on devices being protected by the OCR. Previous research have limited the optimization boundary to the clearing time interval (CTI) between OCRs, with the OF being to minimize the total time required for all OCRs on the system under consideration. In addition, the optimization process considers only a single equation of the curve type. Indeed, OCRs in the market already include a variety of curve types that can be adjusted to address specific circumstances.

2.2 Electric Machine Model from the Protection System Perspective

This section will summarize the electric machine's model. The specification details refer to the actual machine installed in the power system plan of PT Pupuk Kujang Cikampek. The purpose of this modeling is to ascertain the boundary conditions that must be considered during OCR optimization.

2.2.1 Induction Motor

Numerous aspects should be considered in induction motor protection. These conditions are discovered through a continuous monitoring of the current and time duration. When the motor is energized (without using any starting mechanisms), a significant amount of current flows to it because of motor inertia. The amount of current consumed during an MS event can be determined using the locked rotor test and compared to the maximum load condition or full-load ampere (FLA). Equation (2.1) illustrates the relationship between FLA and locked rotor current (LRC).

$$LRC = FLA \times k_s, \quad (2.1)$$

where k_s is the LRC factor as specified on the motor's nameplate or datasheet. The LRC condition lasts several seconds in relation to the mechanical load connected or as specified in the datasheet.

During the startup, an asymmetrical lock rotor current (*AsymLRC*) may exist due to the motor's inductance. This condition may vary between 1 and 2 times the LRC in a short period of time, depending on the machine's X/R. As a result, the starting characteristic of an induction motor can be transformed into a time–current characteristic, as illustrated in Equation (2.2).

$$t_{mtr}(I) = \begin{cases} FLA; & \text{if } t > t_{startdur} \\ LRC; & \text{if } t_{asymm} > t > t_{startdur} \\ AsymLRC; & \text{if } 0 > t > \text{for } t_{asymm} \end{cases}, \quad (2.2)$$

where $t_{startdur}$ is the duration of the LRC and t_{asymm} is the duration of the asymmetrical LRC.

After the motor reaches a steady state (FLA), there is a possibility that it will be overloaded. This condition may result in an increased hot spot temperature

within the stator, which may result in an insulation failure [53]. In comparison to the LRC, the overload condition occurs over an extended period of time. The stator’s endurance under overload conditions is determined by the motor’s manufacturer. An example of a motor stator damage point summarized in Table 2.1. By connecting the points, the time–current characteristic of the stator damage curve can be plotted.

Table 2.1. Stator damage points based on a Fuji electric motor (specifications: 1320 KW, 2300 V, 50 Hz, 8 poles, 405 A, and SN: 1701J504N)

t (s)	I (p.u.)
1000	1.4
100	1.7
10	4.3

2.2.2 Power Transformer

A transformer is an intermediary device that distributes power to a different zone or voltage level, so a fast clearing fault is required. In a particular condition, the transformer draws an excessive amount of current, but this is not considered a fault. This condition occurs when the transformer is first energized following an extended period of deactivation. On the TCC, this condition is modeled using a point of current and duration as a boundary.

During a continuous operation, the transformer may dispose a large amount of current as a result of an overload or an unclear fault in the downstream zone. When a fault occurs on one of the transformer’s sides, the current flowing through the transformer may exceed the thermal winding’s limit. The transformer’s withstand capability is determined by its size as defined by the standard [55]. In this study, the experiment deals with a 5 MVA transformer, which belongs to Category II of IEEE Std. C57.109-2018. Table 2.2 shows the short-time damage point of the power transformer.

Table 2.2. Category II transformer short-time thermal load capability based on IEEE Std C57.109-2018 [55]

t (s)	I (p.u.)
1800	2
300	3
60	4.75
30	6.3
10	11.3
2	25

2.2.3 Synchronous Generator

A synchronous generator (SG), as a critical component of the power system, must be carefully protected without jeopardizing its reliability and continuity. When an SC occurs, the SG reacts by generating a large current that gradually decays. According to [62], the generator's total current generated during an SC might be calculated as follows:

$$i_{ac} = (id'' - id') \times e^{\frac{-t}{T_d''}} + (id' - id) \times e^{\frac{-t}{T_d'}} + id, \quad (2.3)$$

$$i_{dc} = \sqrt{2} \times id'' \times e^{\frac{-t}{T_a}}, \quad (2.4)$$

$$i_{total} = \sqrt{i_{ac}^2 + i_{dc}^2}, \quad (2.5)$$

where i_{ac} is the decaying SC current in the AC component, including the sub-transient, transient, and steady state component. i_{dc} is the SC current in the DC component. i_{ac} and i_{dc} are combined into i_{total} .

In this study, the generator being modeled is a gas turbine generator (GTG) with an output of 21.4 MVA at 13.8 kV and 0.8 PF, 50 Hz, 1500 RPM, and FLA of 621 A. The saturated sub-transient reactance (X_d'') is 16%, the saturated transient reactance (X_d') is 23.8%, and the synchronous reactance (X_d) is 161%. The time constant during SC on the sub-transient (T_d'') is 0.025 s and 0.87 s during transient (T_d'), whereas the armature short-circuit time constant (T_a) is 7.63 s. The field current at the rated load (I_f) is 3 pu, whereas the voltage (I_{fg}) at the no rated load is 1 pu. The terminal voltage (V_a) is 1 pu at 13.8 kV.

To calculate the sub-transient current (id''), the following equations are used:

$$E' = Va + Xd' \times \sin\theta. \quad (2.6)$$

$$id' = \frac{E'}{Xd'}. \quad (2.7)$$

During the steady state, the current generated (id) is calculated by considering the regulated field current (I_f) and field current on the no-load condition (I_{fg}) as follows:

$$id = \frac{Va}{Xd} \times \left(\frac{I_f}{I_{fg}} \right). \quad (2.8)$$

The generator's operation must also account for the possibility of overload, as mentioned in [56]. The short-term thermal capability of the armature winding is shown in Table 2.3, in accordance with the GTG datasheet.

Table 2.3. Gas turbine generator short-time thermal capability (specifications: ABB-AMS 900 LE, 14.85 MVA, 50 Hz, 0.8 PF, 13.8 kV, 621 A, and 1500 RPM)

t (s)	I (p.u.)
60	1.25
50	1.35
40	1.39
30	1.51
20	1.7
10	2.19

2.3 Basic Inverse-Time (ANSI 51) OCR Operation and Coordination

An OCR is a type of protective device that is frequently used in electrical systems. Its logic is extremely simple, relying on a specific current threshold and the delay time before a trip occurred. This straightforward logic is critical in preventing an electrical system, whether an industrial or a large network grid, from collapsing as a result of a disturbance that could result in an overload or SC. As stated in the protection system design principle [4], the objectives are to minimize the duration of service interruption and damage to the component involved in the failure. To achieve the highest performance of the electrical system, a perfect coordination among OCRs is required.

Overcurrent conditions in the power system can occur as a result of an equipment overload or a fault that leads to an SC. Given that a single relay must handle two conditions with varying current flows, an inverse curve is introduced to

provide a general response of the relay that is dependent on the current flow. The inverse-time OCR works with a mathematical model explained in IEEE C37.112 [63]:

$$t_d = \frac{k \times TDS}{\left(\left(\frac{I}{I_p}\right)^\alpha - 1\right) \times \beta}, \quad (2.9)$$

where I is the current sensed by OCR that could be an SC current and k , α , and β are the curve characteristic constant as stated in Table 2.4.

Table 2.4. Parameters of an inverse-time OCR

Curve ID	Curve Type	k	α	β
1	SI (standard inverse)	0.14	0.02	2.97
2	VI (very inverse)	13.5	1	1.5
3	LTI (long time inverse)	120	1	13.33
4	EI (extremely inverse)	80	2	0.808
5	UI (ultra inverse)	315.2	2.5	1

The curve characteristic allows users to adjust the slope of time and current response. Figure 2.1 illustrates the characteristic of each curve in the TCC.

Equation (2.9) shows that an increasing value of I (as long as k , α , β , TDS , and I_p remain constant) decreases the value of td .

The operation and coordination of the OCR are highly dependent on the network configuration and protected elements. A radial network is used in this study because it is universally used either in a distribution service or industrial power system. In general, a radial network is composed of a transformer, cable feeder, and load, which is typically an induction motor. This equipment has a maximum operating temperature and maximum thermal capability.

This study investigates how to choose an OCR curve type that is appropriate for the boundary. If only one equation curve considered to obtain td , then the problem appears, as shown in Figure 2.2. For example, an SC current is sensed by five OCRs, each of which represents a different type of curve and has the same I_p and td . The time dial setting (TDS) can be calculated for each curve type using Equation (2.9). If those five OCRs are used to protect a motor with a starting characteristic, then not all of the curves are applicable. As a result, Equation (2.9)

is simplified to form Equation (2.10) in order to emphasize the relationship between t_d and TDS.

$$t_d = a_p \times TDS, \quad (2.10)$$

where $p = 1, 2, 3, 4, 5$, which represents each curve (i.e., SI, VI, LTI, EI, and UI, respectively).

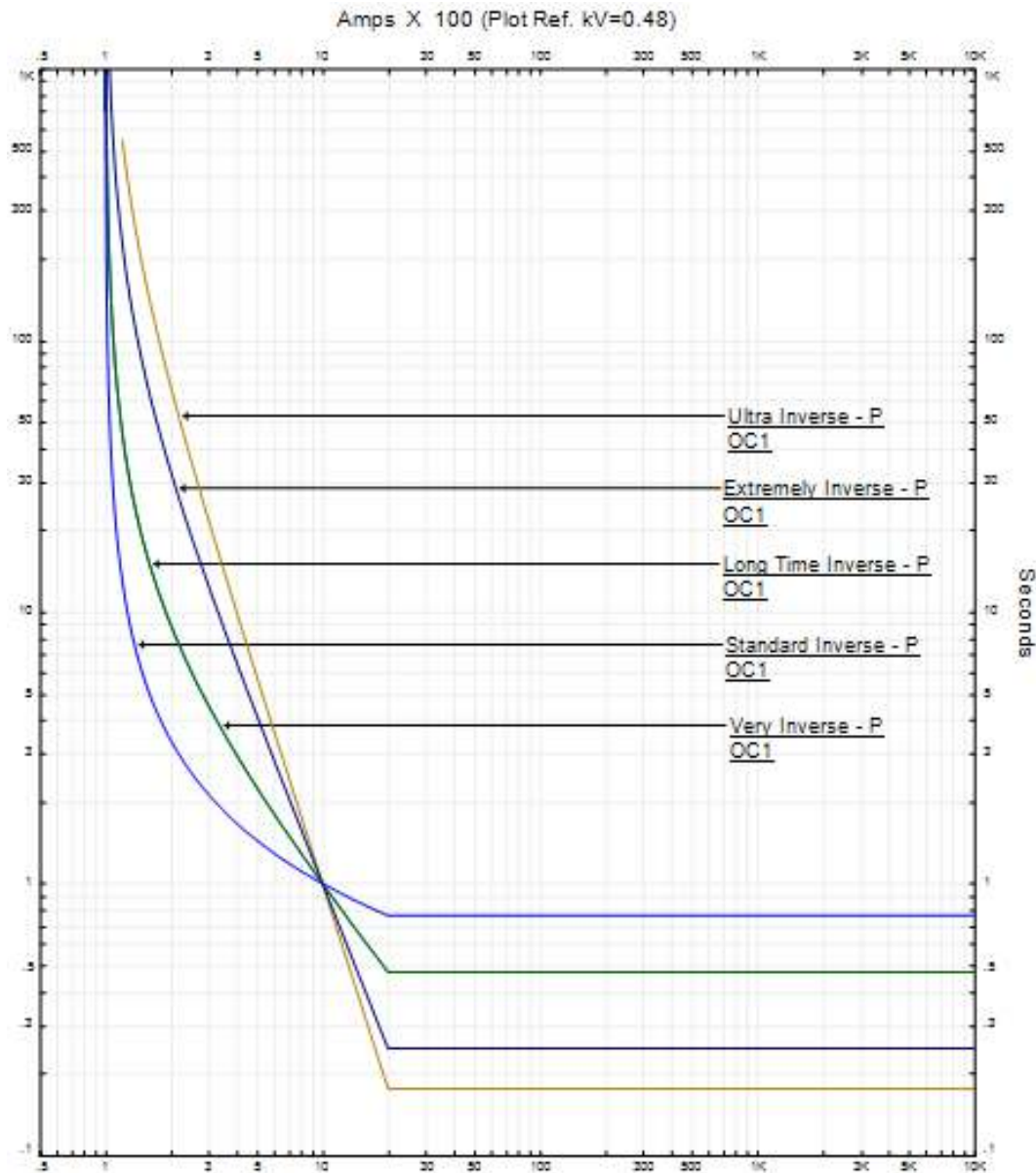


Figure 2.1. Different curve types affecting the OCR response.

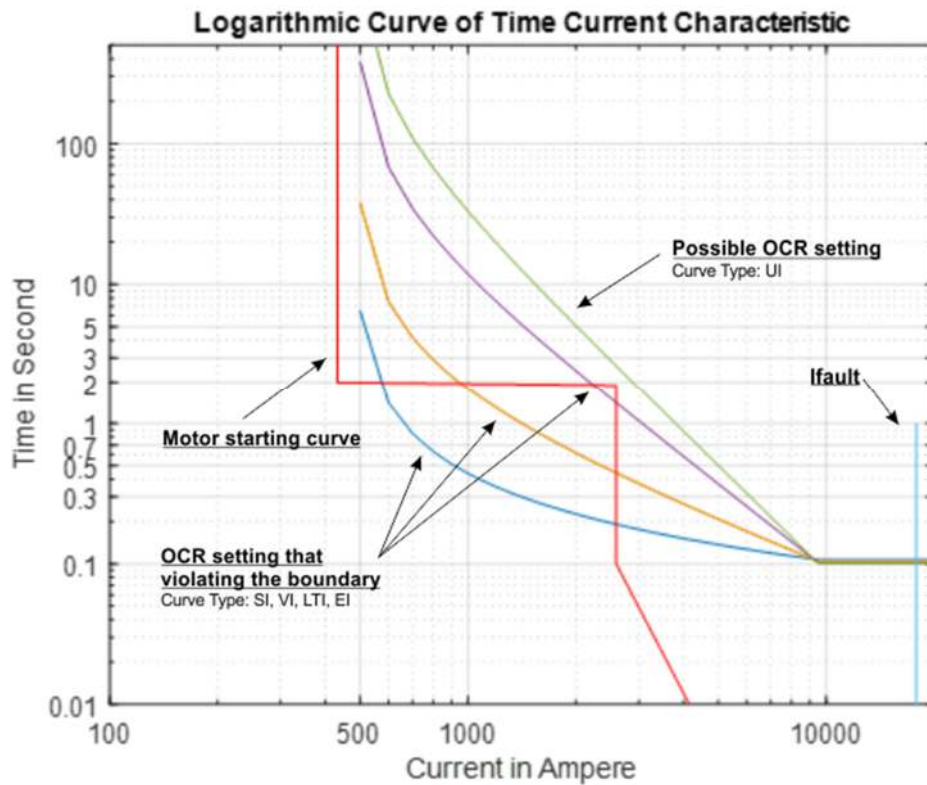


Figure 2.2. Illustration of the optimized curve type of SI, VI, LTI, EI, and UI compared to the MS behavior on the same time operation target.

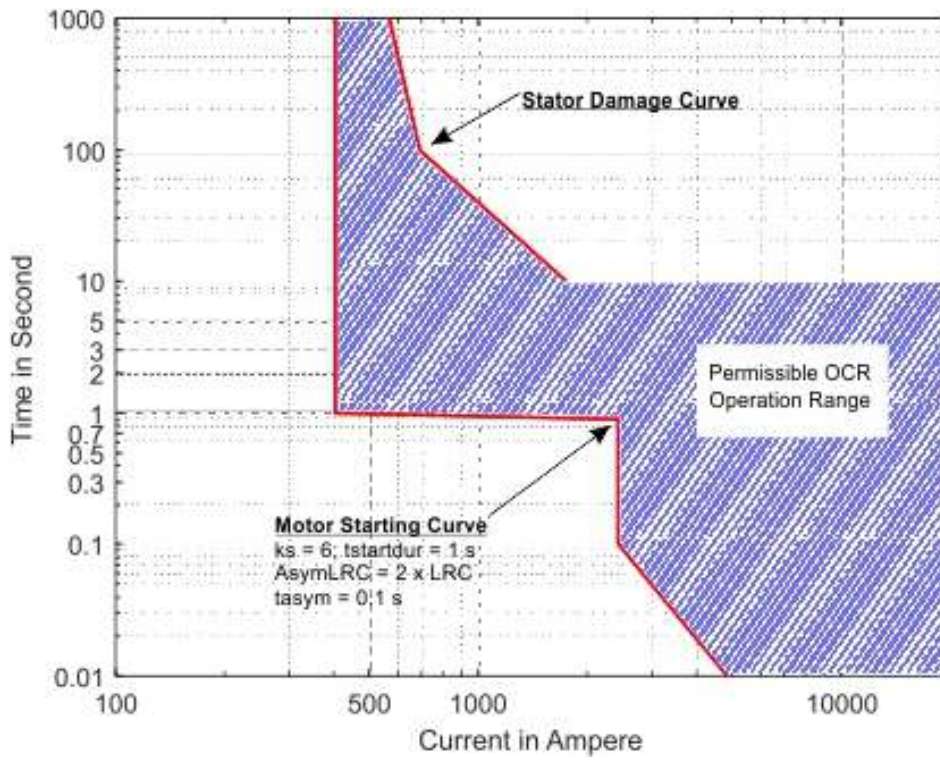
Determining the fault current contribution is critical in protection coordination studies. The fault current varies according to the type of SC: three-phase symmetrical and asymmetrical (line-to-line fault or line-to-ground fault). The three-phase symmetrical fault is discussed in this article. The magnitude of the fault current varies over time. The fault current exists in three states: sub-transient (0.5 cycles), transient (1.5–4 cycles), and steady state (more than 30 cycles). The transient condition was used in this study because it is frequently used in protection coordination studies.

2.4 OCR Optimization with the Boundary Evaluation and SFA

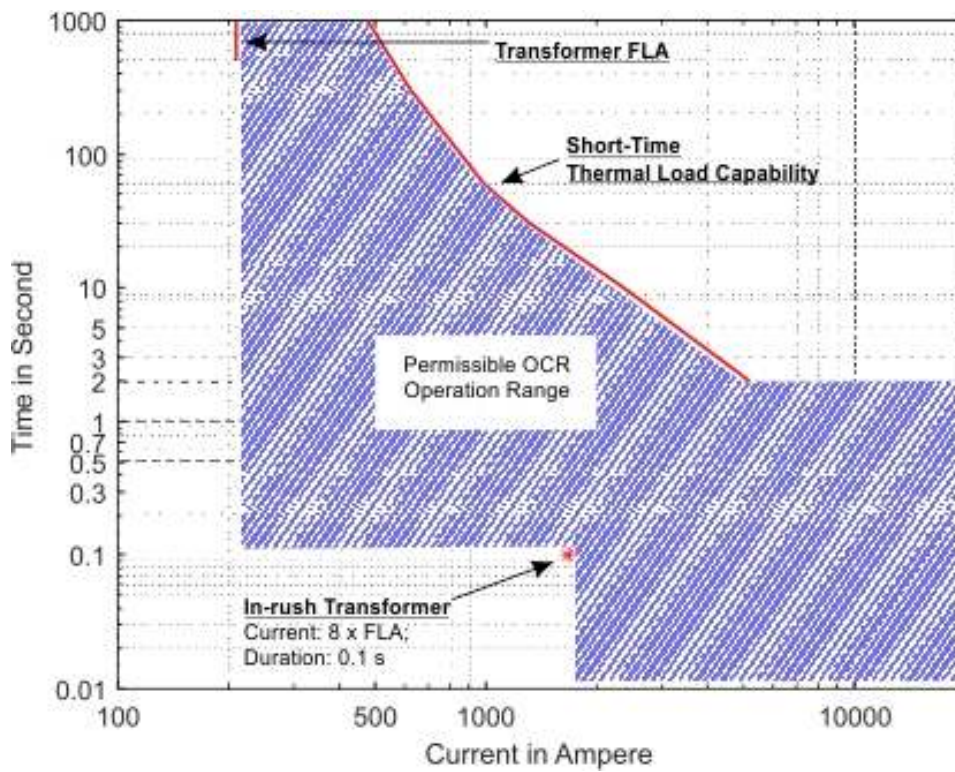
2.4.1 Objective Function

The main objective of OCR coordination in this study is to minimize the time required to clear a disturbed area without violating the device boundary using the SFA. Therefore, after figuring the boundary of the electric machine in Section 2.2, the equation or data of each machine could be formed into a $t(i)$ curve as

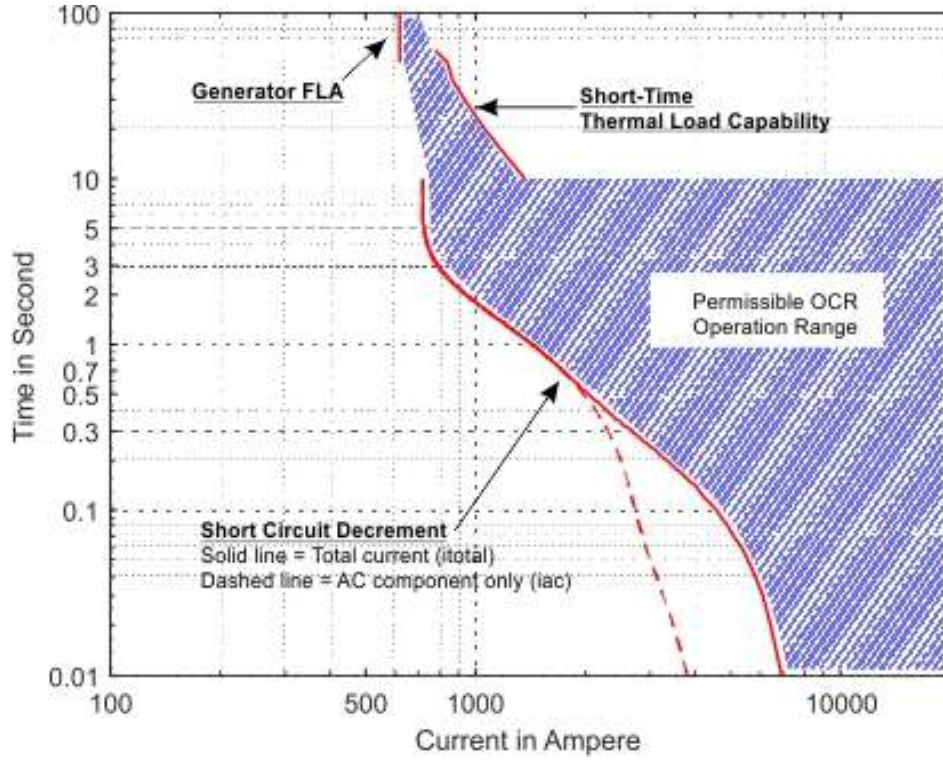
visualized by the TCC curve in Figure 2.3. The blue shade in the curve shows the allowable area of the OCR operation.



(a)



(b)



(c)

Figure 2.3. Illustration of the allowable OCR operation range with consideration of the electric machine boundary in a TCC of the (a) induction motor, (b) transformer, and (c) generator.

In the power system, more than one OCR work in series. These OCRs have a stage from the closest location to the load until the generator. This stage is notated as q , with the minimum value of 1 for the closest OCR to the load and the maximum value (q_{max}) for the closest OCR to the source. q_{max} depends on the number of OCRs being coordinated (x). Therefore, in each q , $t_d(ktd_q)$ is formulated as follows:

$$ktd_q = td_{min} + (q - 1) \times CTI, \quad (2.11)$$

where td_{min} is the minimum possible working time of the OCR and CTI is the clearing time interval.

The OF on each stage q formulated as follows (accordingly from Equation (2.10)):

$$\text{minimize } (OF_q) = \sum_{p=1}^5 a_{p-q} \times TDS_q \quad (2.12)$$

2.4.2 SFA with Boundary Evaluation

In this study, the OF is optimized using a metaheuristic optimization technique called the FA. Yang published this algorithm in 2009 [64]. The algorithm was inspired by the behaviors and flashing patterns of fireflies. Because fireflies are unisex, their attractiveness to other fireflies is determined by their brightness. Simply put, when two fireflies are present, the darker firefly will migrate to the brighter firefly. In comparison to other swarm intelligence algorithms, the FA benefits from the ability to deal with multimodality [65], which relates to the optimization of multiple curve types in OCRs.

Equation (2.12) shows that the program will perform optimization serially for each stage q . A serial computation is required because the $q + 1$ relay has to consider the curve of the q relay.

Each firefly is notated as x_a , which indicates the location, and a is the number of fireflies in a population. The movements of fireflies are based on the light intensity. In this case, each firefly will carry a TDS that varies from 0.1 to 3.2 with a step of 0.01. Then, the light intensity is indicated by the following equation:

$$L = \frac{1}{|ktd_q - td_q|}. \quad (2.13)$$

The less bright firefly will move to the brighter one and update its value as determined by

$$x_a = x_a + \beta_0 \times e^{-\gamma r_{ab}^2} \times (x_b - x_a) + \alpha_f \times \epsilon, \quad (2.14)$$

where β_0 is the attractiveness constant of the firefly, γ is an absorption coefficient, and x_b is the next firefly after x_a , which may also be notated as x_{a+1} . The Cartesian distance of x_a and x_b is notated as r_{ab} . Parameter α_f is the movement intention of the firefly that governs the convergence velocity. α_f is multiplied by ϵ , which indicates a continuous random value between -1 and 1 and divided by 2 . The constant value of α_f might result in the optimization being stuck at the local optima. Therefore, the dynamic value is proposed by updating α_f for each iteration (adaptive modified FA (AMFA)) using the following equation [20]:

$$\alpha_{n+1} = \alpha_n \times (0.5 \times n_{max})^{\frac{1}{n_{max}+1}}. \quad (2.15)$$

The pseudocode of the FA used in the optimization is shown as follows:

Step 1: Generate n fireflies for initial populations (each firefly has a value of a combination from Ip , TDS , and the curve type).

Step 2: Determine L using Equation (20) for each firefly.

Step 3: Update the movement of the fireflies.

while iteration < maximum iteration

for $a = 1:n$;

for $b = 1:n$ (this is the inner loop of a)

if ($L_a < L_b$), move firefly a using (2.14), *end if*

End for a

End for b

Step 4: Rank the fireflies and find the optimum solution.

The program is commenced after the parameters of OCRs and the boundary are inputted. For *the* q -th stage of the OCR, the SFA will generate ktd and perform the optimization for every curve type. After the optimized TDS on each curve is found, the boundary evaluation begins. From the inputted boundary, the program generates a $t(i)$ curve of each boundary that will be compared to the $t(i)$ curve of the OCR. This evaluation will determine the possible curve type of the OCR. If there are more than one curve types that can be used, the lowest total $t(i)$ on each curve is chosen as the q -th OCR setting. The program shall continue to the $q+1$ stage or shall halt if it reaches q_{max} , an optimized result, and TCC at the last part. In brief, the program has three major domains: 1) input/output, (2) SFA, and (3) boundary evaluation. Figure 2.4 shows the flowchart of the proposed method.

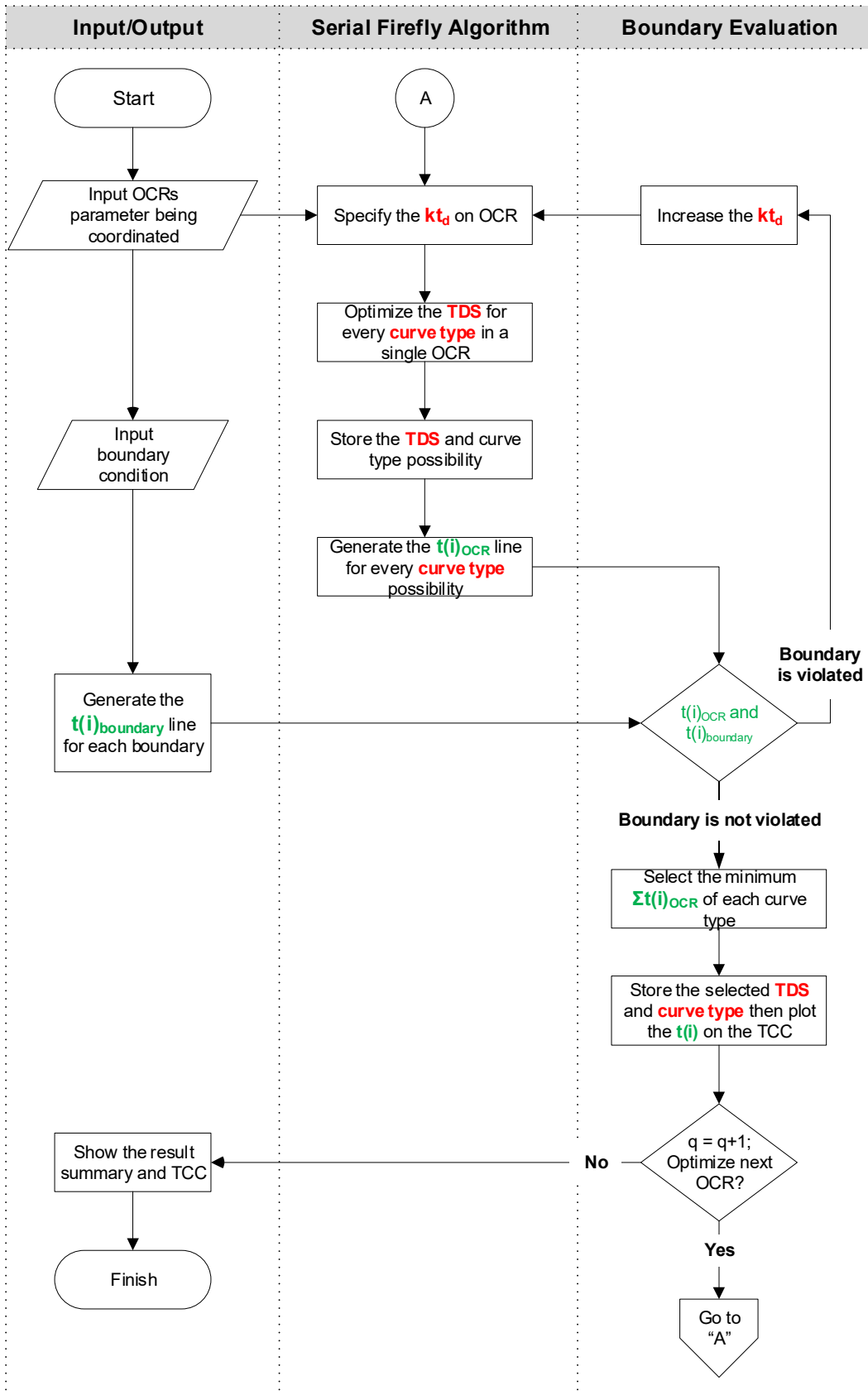


Figure 2.4. Flowcharts of the proposed method in each domain program.

2.5 Results and Analysis

2.5.1 Test Case

The proposed method is validated using the power system plan of PT Pupuk Kujang Cikampek. The system is supplied by two primary sources: 1) a GTG and 2) an electricity grid. To facilitate the experiments, the radial-active topology network is divided into three study cases.

Figure 2.5 depicts the system's single-line diagram (SLD). For the program's global input, td_{min} is set to 0.1 s, and CTI is set to 0.2 s as recommended in [4]. A saturation condition is associated with the current readings that have an effect on the calculation (2.9). If the OCR detects a current greater than 20 times its I_p , it will remain at 20 times its I_p [66]. On the SFA domain, the maximum number of iterations is limited to 15 with 75 fireflies.

2.5.2 Case Study A

Case study A consists of two OCRs that work in the downstream side in a 2.4 kV bus. On the load side, a motor (ID: 2209-JCM) operates at a maximum rating of 1320 kW. During the starting event, the motor k_s will be 3, with AsymLRC equal to 2. $t_{startdur}$ is 5 s, and t_{asymm} is 0.1 s. The FLA of the motor is 365.2 A, and the stator damage is presented in Table 2.1.

The 2209-JCM motor is protected by R-1A, with I_p set to 1.2 times higher than that of the motor FLA, which is 401.7 A. R-2A is operated as a backup of R-1A, with I_p of 1443.6 A, with respect to the 2.4 kV side of the transformer 01-TR-3. R-2A does not have any boundary except R-1A. The fault is located at the 2209-JCM terminal that is caused by a 14.08 kA SC current (If), which is sensed by R-1A and R-2A.

Table 2.5 shows the optimized results of case study A with the newly proposed method. The results are verified on the TCC, as shown in Figure 2.6. To compensate the starting behavior of 2209-JCM, the selected curve of R-1A is EI. The $t(i)$ curve of R-1A does not violate the MS curve and stator damage curve. Meanwhile, for R-2A, the curve used is SI. R-2A does not need to change the curve type because of the large difference of I_p from R-1A. The target OFs of R-1A and

R-2A are 0.5 and 1.5, respectively. Figure 2.7 shows the converging speed of SFA on the two premises of AMFA and FA for case study A.

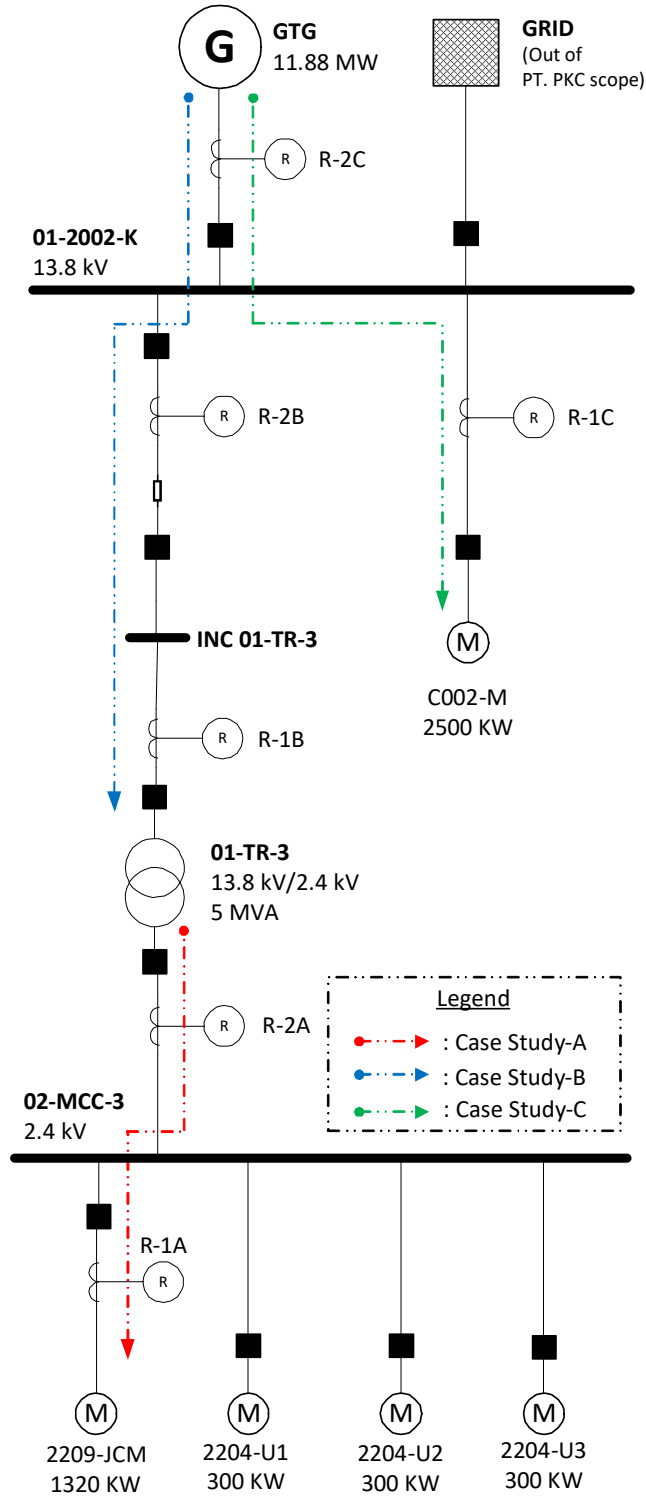


Figure 2.5. Simplified SLD of PT Pupuk Kujang Cikampek for the validation of the proposed method (SFA) and boundary evaluation.

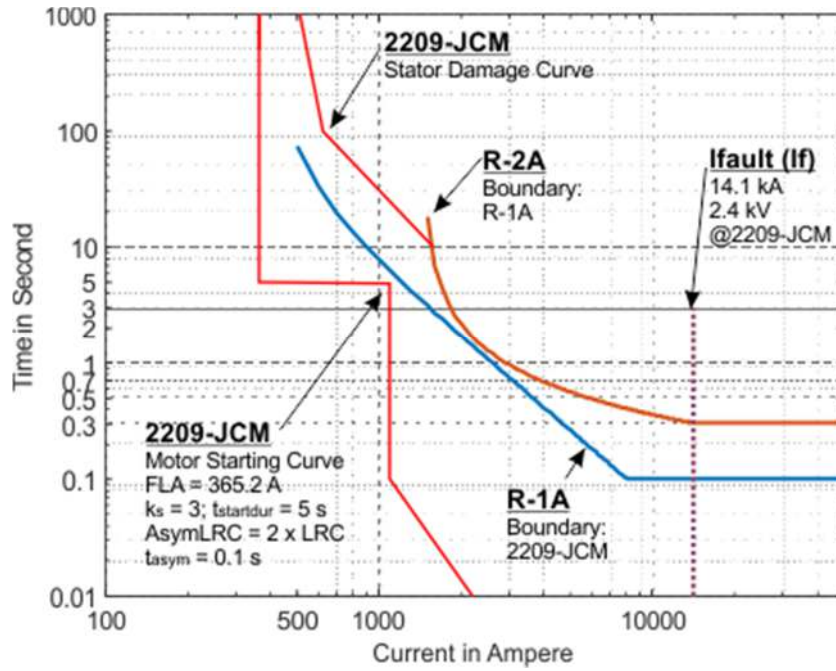


Figure 2.6. TCC of OCRs in case study A after the optimization process.

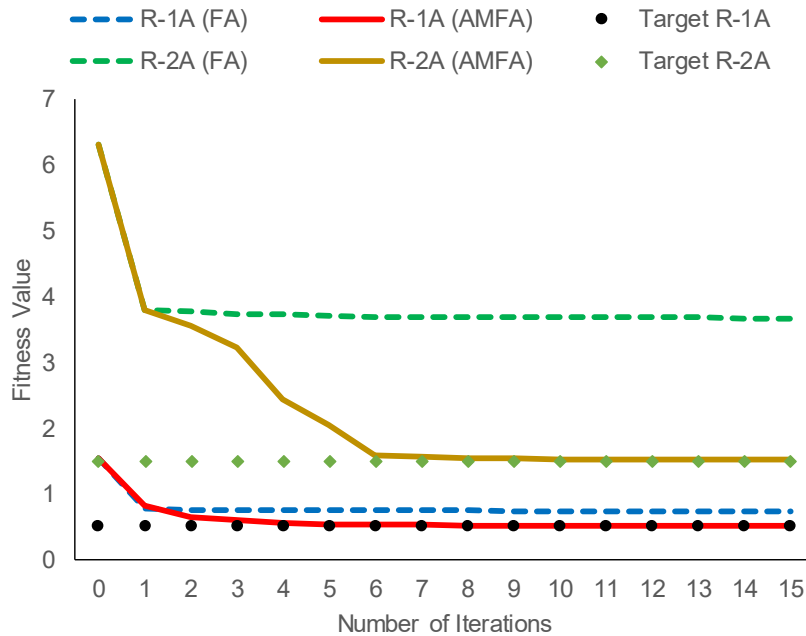


Figure 2.7. Convergence curve comparison (FA vs. AMFA) in case study A.

2.5.3 Case Study B

In case study B, the SFA and boundary evaluation are subjected to a condition with three OCRs: R-1B, R-2B, and R-GTG. R-1B is intended to protect the transformer 01-TR-3 at 13.8 kV. Therefore the I_p of R-1B is larger than the transformer FLA. The transformer itself has 6% impedance and FLA of 209.2 A,

with an in-rush point at eight times the FLA and 0.1 s. The winding thermal limit is presented in Table 2.2.

Above R-1B, R-2B is used to back up R-1B without any electric machine boundary. Lastly, R-GTG has to protect the generator and act as a backup of R-2B. In this study case, although the fault location is subjected at the terminal of 03-TR-1, different I_{fault} readings among the OCRs are obtained. For R-1B and R-2B, because it is not connected to any other feeder or generator, they receive two current supplies during the fault at 03-TR-1. The supplies are from the GTG and GRID. Hence, the R-GTG seems to sense less current during the fault compared to R-1B and R-2B.

The optimization shows that all the OCRs in this study case use the SI curve to operate, as shown in Table 2.5. By using the SI curve, R-1B can anticipate the in-rush condition of 01-TR-3 while being kept below the winding thermal limitations. By contrast, for R-GTG, the SI curve can adequate with the generator's restrictions. The OF targets of R-1B, R-2B, and R-GTG are 0.5, 1.5 and 2.5, respectively. Figure 2.8 shows the TCC, and Figure 2.9 shows the performance of the SFA.

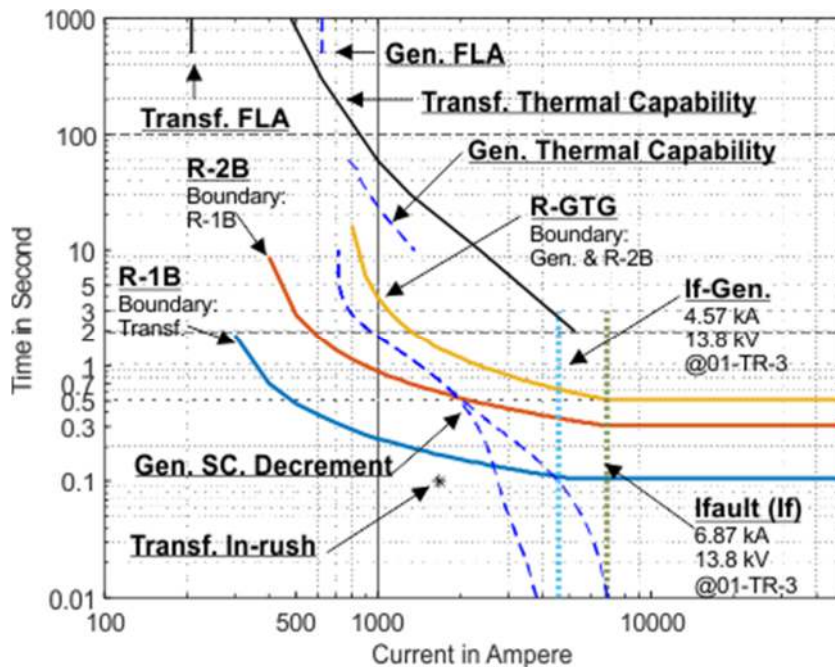


Figure 2.8. TCC of the OCRs in case study B after the optimization process.

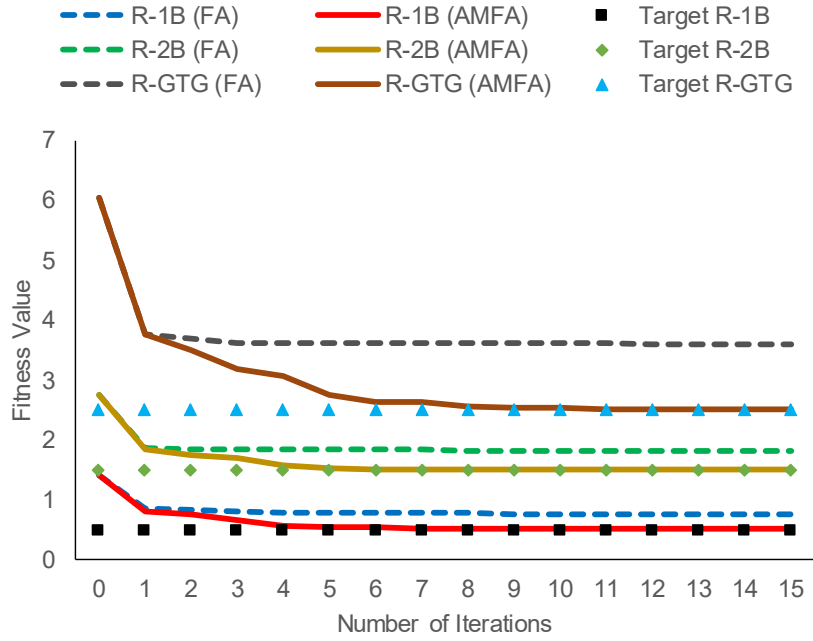


Figure 2.9. Convergence curve comparison (FA vs. AMFA) in case study B.

2.5.4 Case Study C

The proposed method is tested with a narrow gap in case study C. The system in this case study consists of a motor (ID: C002-M) that is connected in the same bus with the GTG at 13.8 kV. The FLA of the C002-M motor is 119.5 A, with k_s equal to 6 and $t_{startdur}$ of 1 s. There is no AsymLRC in C002-M. The C002-M motor is protected by R-1C and backed up by R-GTG. During an SC at the C002-M terminal, R-1C will sense the total current from two sources, whereas the R-GTG will only sense the currents from the generator. Particularly, for this study case, because the R-GTG acts as a backup for R-2B (case study B) and R-1C, the greater q is selected. That is, the R-GTG is forced with kt_d equal to 0.5 s, where q is equal to 3.

The experimental results are shown in Table 2.5 with the coordinated TCC shown in Figure 2.10. The R-GTG in case study C seems to have the same results as the optimization on case study B. Hence, the curve type and setting of the R-GTG are adequate to cover R-2B and R-1C while not violating the boundary of generators. The target OFs in case study C for R-1C and R-GTG are 0.5 and 2.5, respectively. Figure 2.11 shows the convergence curve during the optimization.

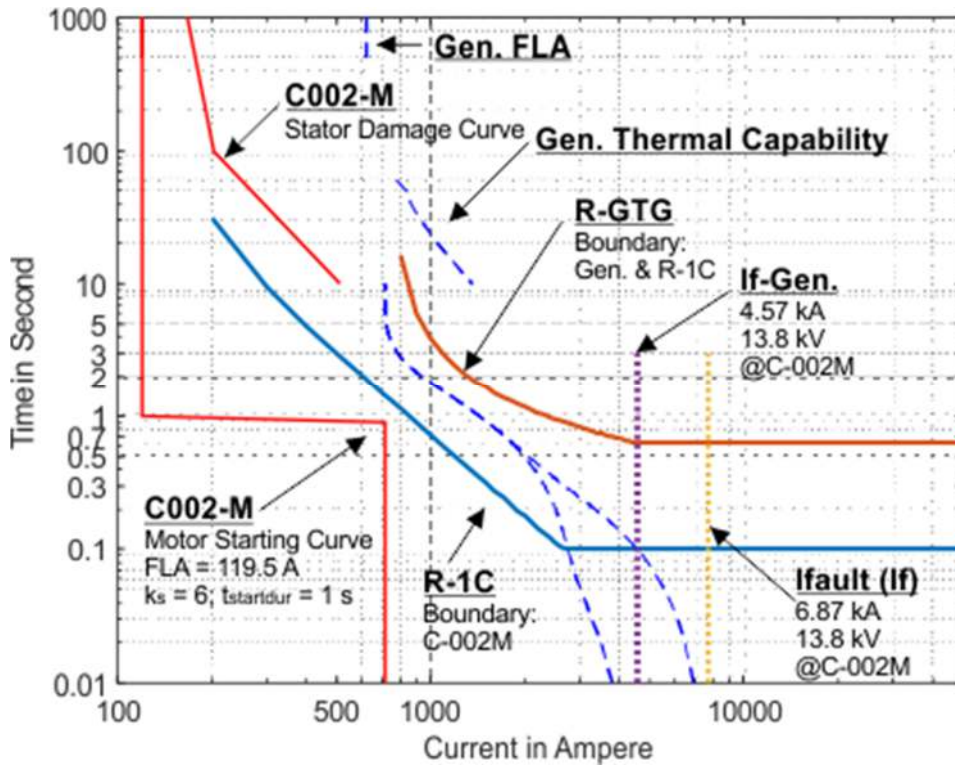


Figure 2.10. TCC of the OCRs in case study C after the optimization process.

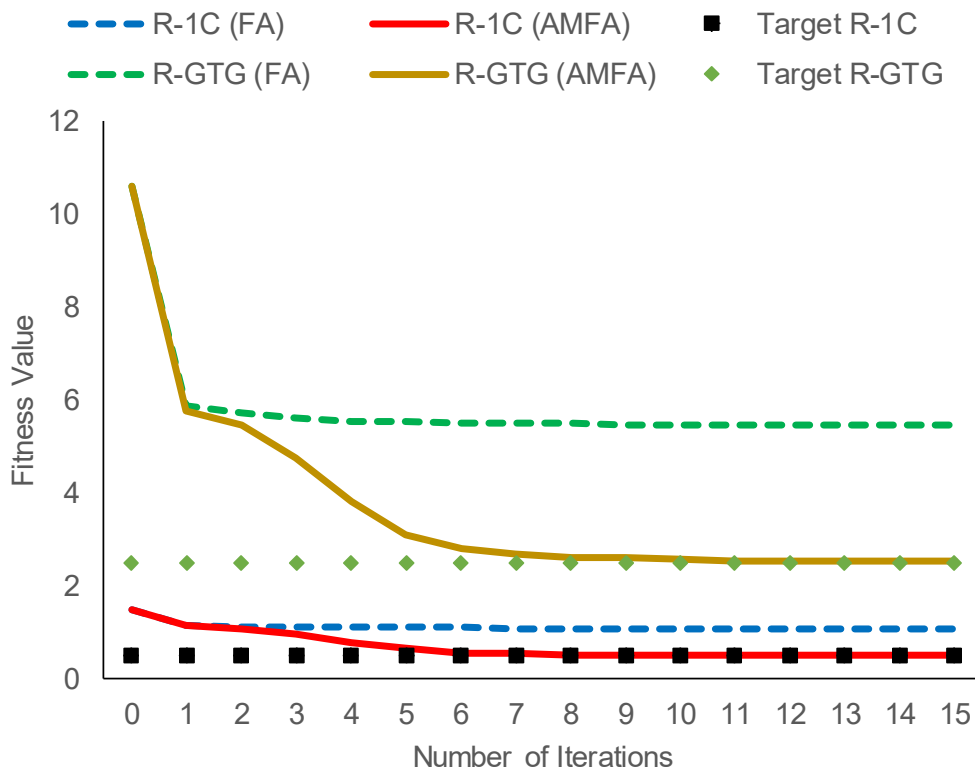


Figure 2.11. Convergence curve comparison (FA vs. AMFA) in case study C.

Table 2.5. Optimization results using the proposed method (SFA) and boundary evaluation

OCR ID	Case Study	Ip (A)	Ifault (kA)	<i>q</i>	Boundary	Curve Type	TDS (s)	<i>td</i> (s)
R-1A	A	401.7	14.08	1	Motor (2209-JCM)	EI	0.41	0.1017
R-2A	A	1443.6	14.08	2	R-1A	SI	0.3	0.3032
R-1B	B	250.8	6.87	1	Transformer	SI	0.14	0.1069
R-2B	B	360	6.87	2	R-1A	SI	0.39	0.3026
R-GTG	B	745.2	4.57	3	Generator; R-2B	SI	0.49	0.5085
R-1C	C	131.45	7690	1	Motor (C002-M)	EI	0.41	0.1017
R-GTG	C	745.2	4.57	3*	Generator; R-1C	SI	0.49	0.5085

*: OCR is forced to follow the desired *td*

2.6 Discussion

The overall hypothesis in this chapter is the recognition of the use of electric machines in solving the relay coordination problem. Optimization methods are appended with additional boundaries (e.g., induction motor, transformer, and generator) for induction motors, transformers, and generators. This proposed method is implemented serially on each OCR to analyze all possibilities for the input curve, including the type of curve. Serial optimization is the preferred method considering its capability to examine OCRs' previous stage.

During validation using three cases in an industrial power system, the results show that the proposed program is capable of 1) identifying the machine boundary, 2) identifying the previous OCR, and 3) locating the exact settings of the relay without compromising the machine operation. To obtain a perfected result, the FA is used to solve the OF. Moreover, further analysis results demonstrate its superiority compared to a single equation OCR optimization. After examining these ideas, the proposed method is found to offer a significant advancement in the field with a new boundary perspective.

CHAPTER 3

OPTIMIZING THE COORDINATION FUNCTION WITH ENHANCED MULTI-FUNCTION OVERCURRENT PROTECTION

In the previous chapter, the recognition of the electrical machine boundary has been profoundly discussed. However, the relay being optimized is limited to the inverse-time curve characteristic (ANSI 51). In this chapter, the effort to optimize not only the inverse-time curve relay but also the definite-time (ANSI 50) relay is discussed. By combining ANSI 51 and 50, it is expected that the coordination function in the power system network could be achieved and operate at a minimum time [44], [45].

3.1 Problem Definition

Figure 1 illustrates a general classification of issues and proposed solutions found in the literature and technical reports from the industry. Both are classified as traditional or modern concerns, along with their corresponding solutions, depending on the extent to which distributed energy resources (DERs) are used.

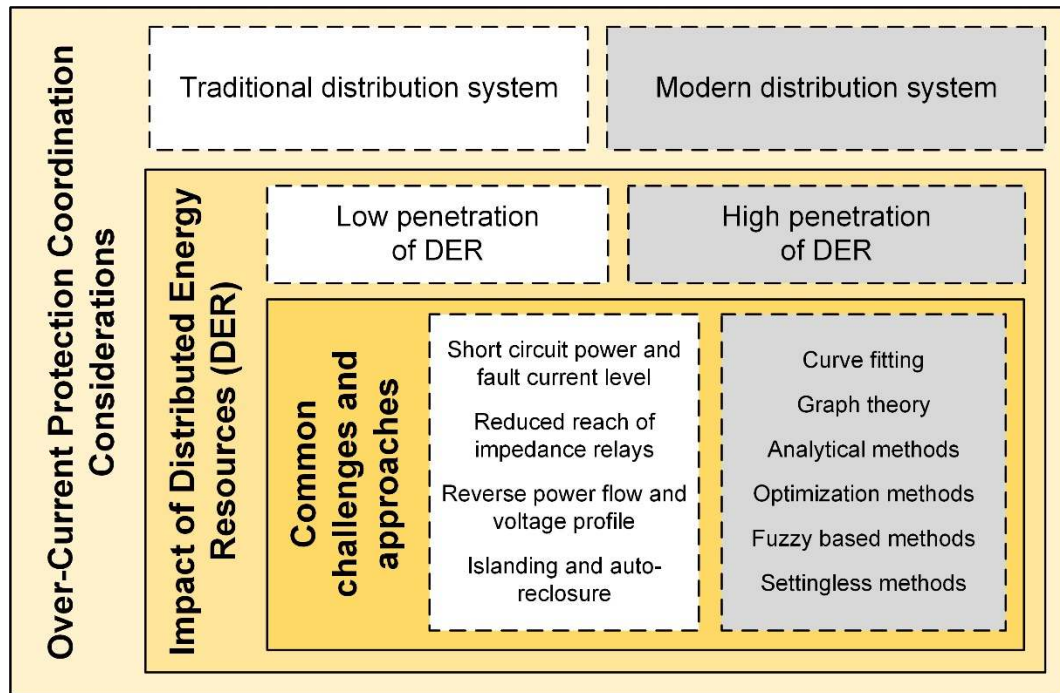


Figure 3.1. Overcurrent protection challenges and approaches in practice.

The first overcurrent protection issue was described in [26], where changes in the timing and reach of overcurrent devices degrade the reliability and power quality for other feeder customers. This issue became significantly worse as DERs became more prevalent in conventional distributed systems [67]. Prior to the publication of the standard in 1996 [63], a technical report strategically compiled the principles of one of the most traditional approaches to solve low DER penetration, i.e., curve fitting technique [68]. OCRs' time inverse relay characteristics, including TDS and operating time, are mathematically modeled.

The OCR is classified into three types based on time operations: instantaneous, definite-time, and inverse-time. The instantaneous OCR sends a trip signal immediately upon passing the current threshold, whereas the definite-time OCR sends a trip signal after a predetermined delay time [69]. The inverse-time OCR is based on a mathematical function with a parameter that defines the type of curve (discussed extensively in Section 2.3).

Optimizing the OCR is primarily concerned with the inverse-time function. In [28], a novel curve type called inverse-time admittance was proposed. The OCR includes a measured value of the protected line's admittance for a more sensitive fault detection. As a result, a shorter trip time is expected. In [70], the voltage function was incorporated into the inverse-time function. The voltage dip enables the OCR to be more sensitive to fault conditions, potentially shortening the relay operation time. In [71], the OCRs using single and dual settings were optimized. Multiple OCR settings in the distribution system contribute to the protection system's selectivity when multiple DGs penetrate. In [23], consideration of the practical limitations of commercially available OCRs is introduced. Excessive fault current occurs as a result of DGs' high penetration. Thus, during optimization, a saturation current measurement is made. This technique ensures an adequate time interval between the primary and backup relays. In [32], the sub-transient fault current contribution from induction motors is considered a dynamic model in the optimization of OCRs. According to the study, the SC current from an induction motor could cause a false trip for an OCR that is not located within the protection zone. In [41], the optimization of OCRs took into account machine constraints, such as electric MS behavior, transformer in-rush current, and thermal winding

limitation. Thus, the optimization process included the choice of curve type within the standards.

The previous research exclusively focuses on the inverse-time (ANSI 51) function as a target object. While this is true, the majority of OCRs on the market include inverse- and definite-time functions (ANSI 51 and 50) [22]. The absence of a definite-time function in OCRs is viewed as a gap that needs to be addressed in this study.

3.2 Formulation of OCR Coordination

The OCR operation has been deliberately explained in Section 2.3 and 2.4. Accordingly, a further investigation regarding the coordination function is provided in this section.

Equation (2.9) in Section 2.3 explains the inverse relay time operations. However, some OCR manufacturers and designers encounter limitations regarding the detection of I [66]. For an enormous amplitude of current, the OCR changes to a definite-time response. The maximum current detection is limited by a ratio between I and I_p , called C . If I is greater than C times of I_p , the inverse-time OCR will operate at t where I is equal to C times I_p (definite-time operation). Considering Equation (2.9), this saturated condition may be written mathematically as follows:

$$t_x(I_{x,y}) = \begin{cases} \frac{k_x \times TDS_x}{\left(\left(\frac{I_{x,y}}{I_{p_x}}\right)^{\alpha_x} - 1\right) \times \beta_x}, & \text{for } I_{x,y} < C * I_{p_x} \\ \frac{k_x \times TDS_x}{(C^{\alpha_x} - 1) \times \beta_x}, & \text{for } I_{x,y} \geq C * I_{p_x} \end{cases}, \quad (3.1)$$

where x is the notation for the number of relays and y is that for the fault location considered by the relay.

3.2.1 Time Interval in the Coordination Protection

OCRs have the capability of working in a coordinated manner. Thus, OCRs must selectively isolate the fault with the least amount of system disruption as possible. Figure 3.2 illustrates the coordination capability of two OCRs. The upper-tier OCR, which is located closer to the upstream, employs multiple time operations

to accommodate near (primary) and far (backup) fault locations. When used as a backup, the OCR must conform to the *CTI*.

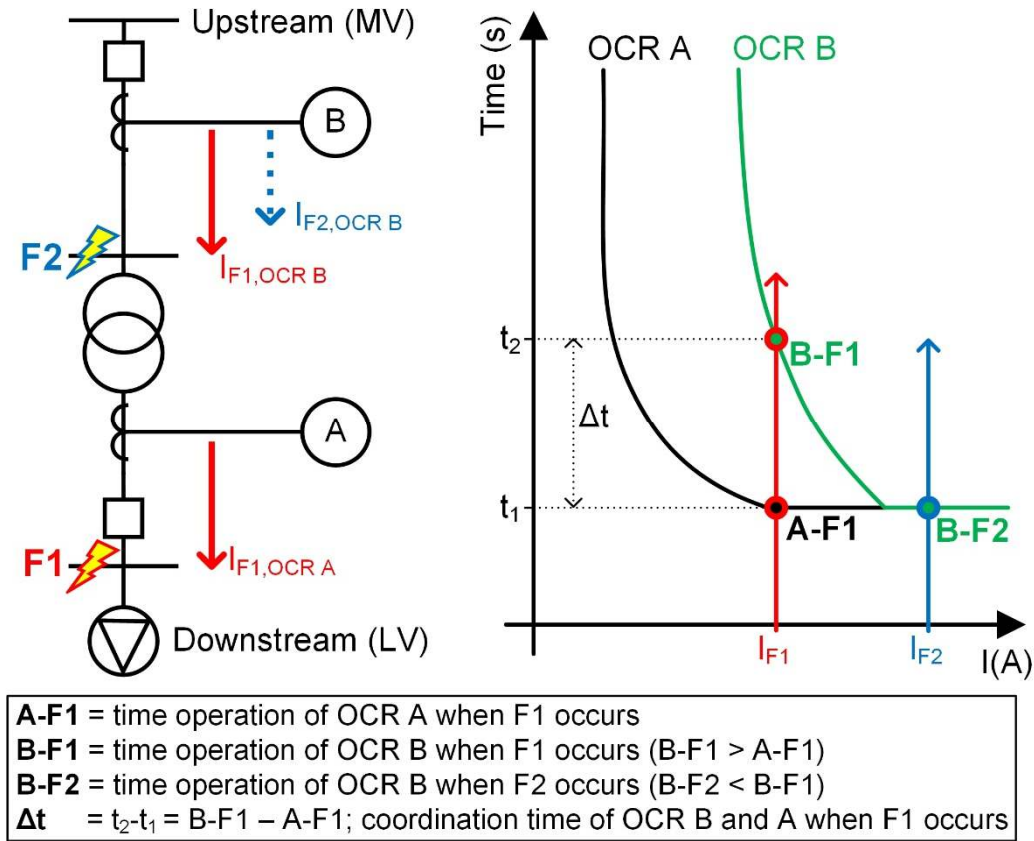


Figure 3.2. SLD and time–current curves for two OCRs (OCR A and OCR B) with a coordination function to anticipate different fault locations (F1 and F2). OCR A only anticipates F1, whereas OCR B anticipates F2 and F1.

According to IEEE 242-2001 (Table 15-3), CTI_{min} for a field-tested static relay is 0.2 s [4]. Coupled with a maximum CTI_{max} of 0.4 s, this condition can be expressed as follows:

$$t_B(I_{B,F1}) - t_A(I_{A,F1}) \geq CTI, CTI_{min} \leq CTI \leq CTI_{max}. \quad (3.2)$$

This practice is most likely used when both OCRs operate at the same voltage level. When the voltage level is different (e.g., through a transformer), the *CTI* could be reset [72].

3.2.2 Protecting but not Limiting the Load Operations

Apart from protecting the equipment from an SC, OCRs must be adaptable to the load behavior (e.g., starting current in the induction motor or in-rush current when energizing the transformer).

As discussed earlier in Section 2.4, when an induction motor is started (via the direct online (DOL) method), a spike current is generated for a specified period of time until the motor reaches its nominal rotating speed. This condition must be taken into account when determining the OCR setting. A careless selection of the curve type in an inverse-time OCR may result in an MS failure. Simultaneously, the OCR must not exceed the motor's thermal limit. As a result, the OCR setting should take into account not only the SC current but also the equipment capability limit. Simply put, the OCR has the following lower and upper boundaries:

$$t_L(i) < t(i) < t_U(i), i \in \Omega, \quad (3.3)$$

where t_L and t_U are the load's lower-time and upper-time boundaries, respectively, and Ω is the current limit (i) of the load.

Adjusting the I_p , TDS , or curve type would be a solution to maintain the OCR inverse-time function within the boundary in Equation (3.3). However, with consideration to Equation (3.2), the adjustment affects the OCR time operation and might ruin the coordination function. Hence, inverse-time (ANSI 51) and definite-time (ANSI 50) functions could be used together as a combined curve. As a result, the inverse-time curve obliges the OCR role as backup protection and the definite-time curve as the primary protection.

3.3 Optimization of the Definite-Time (ANSI 50) and Inverse-Time (ANSI 51) OCRs

This section presents a mathematical model of the proposed method, which extends previous research by incorporating the definite-time function (ANSI 50) into OCR optimization and introducing a new type of evaluation to solve the protection coordination problem in industrial or commercial power distribution systems. Simply put, the new method combines an optimization technique for locating the OCR setting value with a curve fitting technique for evaluation. The

setting obtained through this method may be directly implemented in the field, as it has been evaluated in modern and practical concerns [45].

3.3.1 Objective Function

Optimization is used to determine the best setting for each OCR. The following equation describes the OF:

$$\text{Minimize: } OF = \sum_{i=1}^{I_{x,y}} t_{x,crv}(i), \quad (3.4)$$

where:

$$\begin{aligned} x &= [1, 2, \dots, x_{max}] \\ crv &= [SI, VI, LTI, EI, UI], \end{aligned} \quad (3.5)$$

where *crv* is the list of curve type as discussed in Section 2.3 and Table 2.4 and x_{max} is the maximum number of OCRs that can be coordinated. As shown in Equation (3.4), the OF evaluates the OCR as a function ($t(i)$) rather than as a specific response time (t). This OF is founded based on Equation (3.2). The substance of concerning the OCR as a function is to deal with a downstream to upstream protection. This type of protection may operate at a different voltage level than what is typically found in a distribution network.

3.3.2 Selection of I_p

I_p ranges between two values, i.e., maximum load current and minimum SC current [32]. The OCR typically picks up on overload at 115% of the FLA [4]. In this study, 145% of the FLA is considered for the upper bound.

$$1.15 \times FLA \leq I_p \leq 1.45 \times FLA. \quad (3.6)$$

The OCR does not measure the current directly from the circuit. It requires some auxiliary equipment, such as a current transformer (CT) or Rogowski coils [73]. Therefore, the selection of I_p has to consider the CT rating. The I_p ranges of OCR are RP with RP_{min} , RP_{max} , and RP_s . Afterward, RP may be formed as an array.

$$RP = [RP_{min}, RP_{min} + RP_s, Rp_{min} + 2 \times RP_s, \dots, RP_{max}] \quad (3.7)$$

RP is defined as the ratio between current flows and the primary side of CT (CT_{prim}). Hence the selection of I_p is limited to an array ($I_{p_{array}}$).

$$I_{p_{array}} = RP \times CT_{prim} \quad (3.8)$$

Therefore, the selection of I_p for optimizing the OF (3.4) could be formulated as follows:

$$1.15 \times FLA \leq I_p \leq 1.45 \times FLA, I_p \in I_{p_{array}} \quad (3.9)$$

3.3.3 Calculating the TDS

The TDS of an OCR varies from TDS_{min} to TDS_{max} with the interval TDS_s . In an array form, TDS can be expressed as

$$TDS_{array} = [TDS_{min}, TDS_{min} + TDS_s, TDS_{min} + 2 \times TDS_s, \dots, TDS_{max}] \quad (3.10)$$

A proper TDS must be evaluated for every curve type and with a specific time operation target (tg). Thus, several fault locations have to be considered to form a supporting constraint.

The coordination of OCR could be designed in a time (chronological), current (amperometric), or time–current sequence [72]. The focus of this study is on the time–current coordination. Hence, specifying tg relates with the SC current. Accordingly, a set of SC data with the following form is required:

$$I_{sc} = \begin{bmatrix} I_{x,y} & I_{x+1,y} & \dots & I_{x_{max},y} \\ I_{x,y+1} & I_{x+1,y+1} & \dots & I_{x_{max},y+1} \\ \vdots & \vdots & \vdots & \vdots \\ I_{x,y_{max}} & I_{x+1,y_{max}} & \dots & I_{x_{max},y_{max}} \end{bmatrix} \quad (3.11)$$

I_{sc} contains the SC current of each OCR presented in columns. Consequently, this SC current is evaluated for every fault location presented in rows. The magnitude of the SC current might be used to identify the state of the OCR's role as a primary or backup protection. For the row ranging from y to y_{max} , the highest SC current ($I_{sc_{pr}}$) in column x obliges OCR X to react as the primary protection and the second-highest SC current ($I_{sc_{bu}}$) as the backup protection. To

differentiate between the primary and backup protection in the OCR, then tg might have two conditions:

$$tg = \begin{cases} tg_{pr}, I = Isc_{pr} \\ tg_{bu}, I = Isc_{bu} \end{cases} \quad (3.12)$$

By default, tg_{min} is equal to 0.1 s, which is also applied for tg_{pr} . tg_{bu} shall comply with Equation (3.2), and each OCR shall choose the backup pair. Furthermore, tg_{bu} has to consider the network topologies either in a series or multi-feeder protection. Hence, tg_{bu} has to be the maximum time of the previous OCR time with a CTI . Mathematically,

$$tg_{bu} = \max(rtg_{bu}) + CTI, rtg_{bu} \in backups \quad (3.13)$$

3.4 Consideration of Protection Limitations and Activation of the Definite-Time (ANSI 50) Function

3.4.1 Boundary Evaluation

A thorough evaluation is required to ensure that OCR operations do not exceed the load or equipment limit. This evaluation is performed in the context of a time–current function. As stated in Equation (3.3), the mathematical evaluation of OCR operation in relation to the equipment limits could be as follows:

$$t(I) - tl(I) > 0, I \in I_L. \quad (3.14)$$

$$tu(I) - t(I) > 0, I \in I_U. \quad (3.15)$$

The OCR time response for each current point in the equipment is investigated using Equations (3.14) and (3.15). The boundary may be the thermal limit of the equipment or the downstream OCR characteristic (as discussed in Chapter 2). When the OCR time response is less than the lower load limit or greater than the upper load limit criteria, a boundary violation occurs.

3.4.2 Target Remedy to Activate the Definite-Time (ANSI 50) Function

Due to the preceding constraints, it is possible that no OCR setting is available for all curves. As a result, some adjustments are required to make it work. The adjustment is accomplished by increasing tg_{min} in the following manner:

$$tg_{min} = tg_{min} + tg_{update} \quad (3.16)$$

Based on Equation (3.1), the increase in t must be followed by the variation of TDS or Ip . Thus, the increment of tg_{min} is expected to solve the situation. However, this adjustment results in a longer fault clearing time. Accordingly, a definite-time function (ANSI 50) takes place.

A definite-time function (ANSI 50) works with a specific time and current response $td(I)$. This function can be expressed as follows:

$$td(I) = \begin{cases} tdp, I \geq Ipd \\ \infty, I < Ipd \end{cases} \quad (3.17)$$

The selection of tdp is objected to tg_{pr} with the origin tg_{min} . Henceforth, Ipd shall comply with Isc_{pr} . The selection of Ipd shall conform to the following constraints:

$$Ipd_{min} \leq Ipd \leq 0.8 \times Isc_{pr}, Ipd \in Ipd_{array} \quad (3.18)$$

The form of Ipd_{array} is similar to Equations (3.7) and (3.9). It also has its minimum and maximum RP called RPd_{min} and RPd_{max} , respectively. Ipd_{min} shall consider the lower limit and the previous OCR Isc_{pr} to avoid miscoordination. Consequently, Equation (3.18) is merged with Equation (3.1) to form a new time–current function that is evaluated on the next optimization iterations.

3.5 Program Demonstration and Testing

3.5.1 Test Case and Adjustment

To demonstrate the proposed method, a simulation using a case study from IEEE 242.2001 Chapter 15 Section 7 is conducted. Figure 3.3 illustrates the SLD. The test system utilizes a single high-voltage feeder (138 kV), which is then distributed via a medium-voltage (13.8 kV) switchgear to serve two branches

operating at low voltage (0.48 kV) and medium-voltage (4.16 kV). Numerous electrical components exist, each with its own operating characteristics and thermal damage characteristics. Appendix 1 details the detailed parameters for each piece of equipment (grid parameter, transformer specification, cable impedance, and motor information) based on [19]. The dataset is available in [74].

The test system is slightly adjusted. In comparison to the standard, the test system employs static relays and CBs to protect all protective devices. All CBs, including the low voltage CB, are driven by the OCR. The OCR labels are also renamed as A1, A2, A3, A4, B1, B2, B3, B4, B5, 51-5, and 51-6 to correspond to the CBs. Certain buses (4.16 F-01, 13.8 F0-1, 0.48 F0-1, 13.8 F0-2, and 138 F0-1) are also added to the test system to simplify the process of tracing the fault location. As illustrated in Figure 3.3, this additional bus is named according to its voltage level and unique tag.

An SC analysis is conducted in advance to determine the current reading for each OCR with varying fault locations. There is some discrepancy between the results of the SC study and the standard, although the SC analysis results remain plausible [19], as illustrated in Table 2 with the arrangement according to Equation (3.11). The three-phase symmetrical fault in the transient domain (1.5–4 cycles) is considered in this study.

In the simulation, RP_{min} , RP_{max} , and RP_s are defined as 0.1, 2.4, and 0.1, respectively, to comply with Equation (3.7). TDS_{min} , TDS_{max} , and TDS_s are valued as 0.1, 12.5, and 0.01, respectively, to conform to Equation (3.10). The OCR operation is limited to one backup. Based on the SLD, A4 and B5 select 51-5 as the backup. Hence, 51-5 has to select the maximum values of $tg_{bu,A4}$ and $tg_{bu,B5}$ to conform to Equation (3.13). The evaluation of the upper limit commences from 0.1 s with regard to tg_{min} . Hence, the thermal limit function below 0.1 s is neglected. tg_{update} is equal to 0.1 s. When the target remedy is performed, RPd_{min} , RPd_{max} , and RPd_s are denoted as 1, 24, and 0.1, respectively, to shape Equation (3.18). The FA is used with 75 populations and 15 times iterations. Figure 3.4 illustrates the proposed method's flowchart, which combines the optimization and time–current evaluation altogether.

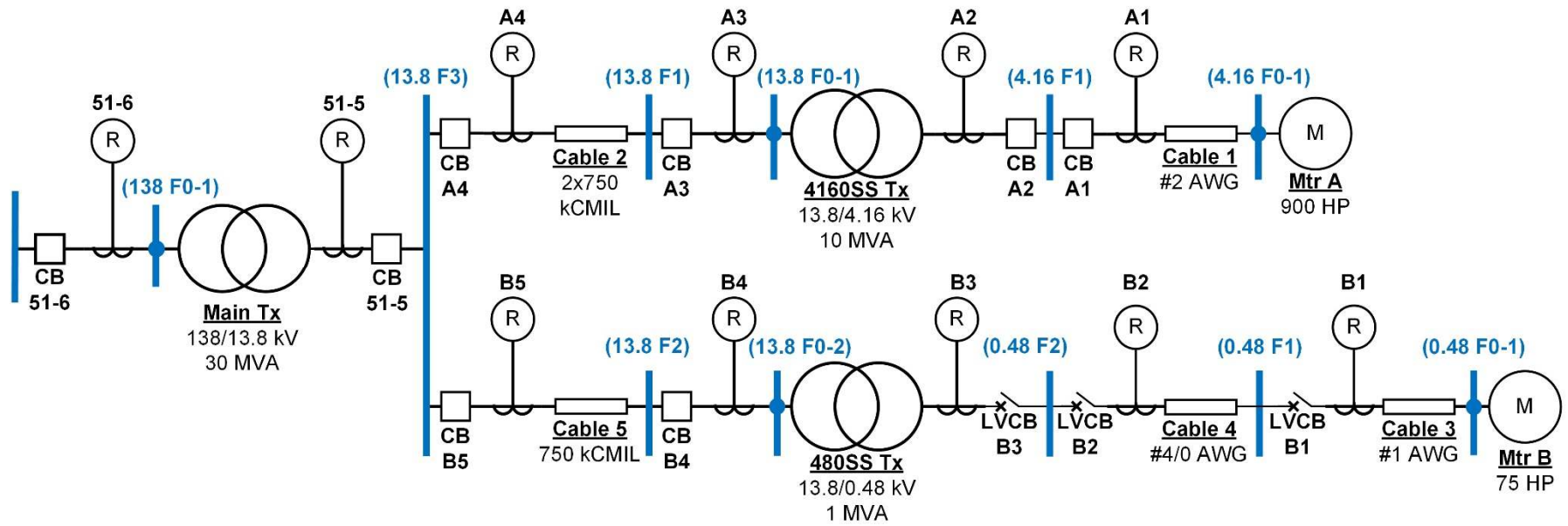


Figure 3.3. SLD used as the test bench according to the IEEE Std. 242.

Table 3.1. Fault current in various locations on the IEEE Std. 242 test case measured by each OCR

Fault Location	Current Sensed by Relay (A)										
	A1	A2	A3	A4	B1	B2	B3	B4	B5	51-5	51-6
4.16 F0-1	17066	17066	5144	5144	0	0	0	0	0	5144	514
4.16 F1	0	17984	5421	5421	0	0	0	0	0	5421	542
13.8 F0-1	0	0	15396	15396	0	0	0	0	0	15396	1542
13.8 F1	0	0	0	15396	0	0	0	0	0	15396	1542
0.48 F0-1	0	0	0	0	8599	8599	8599	299	299	299	30
0.48 F1	0	0	0	0	0	14540	14540	506	506	506	51
0.48 F2	0	0	0	0	0	0	19981	695	695	695	69
13.8 F0-2	0	0	0	0	0	0	0	15396	15396	15396	1540
13.8 F2	0	0	0	0	0	0	0	0	15396	15396	1540
13.8 F3	0	0	0	0	0	0	0	0	0	15396	1542
138 F1	0	0	0	0	0	0	0	0	0	0	20918

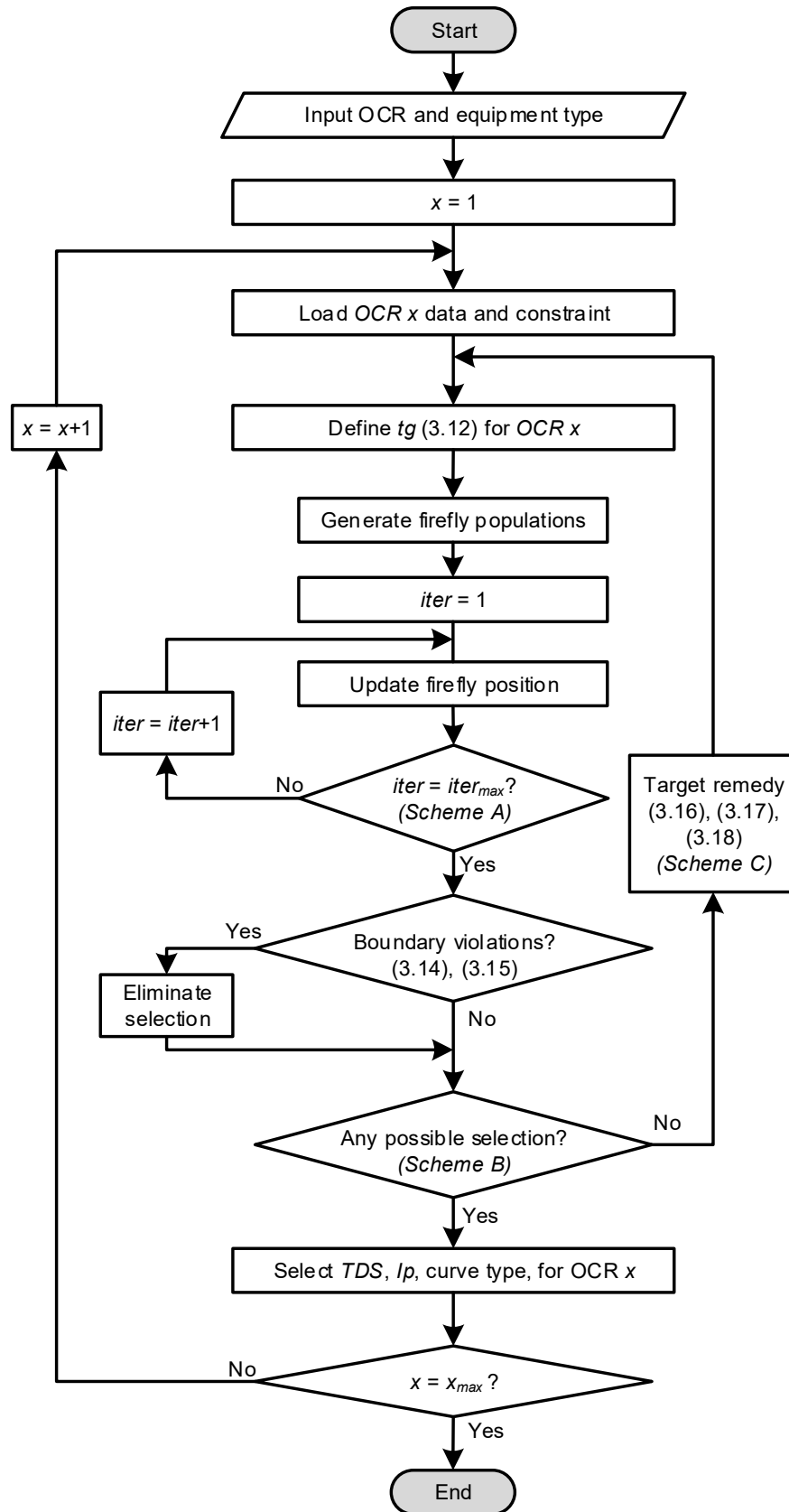


Figure 3.4. Flowchart of the method to perform OCR optimization and time-current evaluation.

3.5.2 Testing Results

Three distinct simulation approaches are used to evaluate the proposed method's effectiveness. The difference between the approach schemes is illustrated in Table 3.2.

The OCR setting is optimized in Scheme A in accordance with the coordination rules. By incorporating the boundary evaluation into the optimization process, Scheme B improves Scheme A. Finally, Scheme C is implemented with an additional target treatment and the addition of a definite-time function (ANSI 50) to improve Scheme B.

Table 3.3 summarizes the results of Schemes A, B, and C for determining the optimal OCR setting. Each scheme's output is evaluated by calculating the error (εt_{pr} and εt_{bu}), which is presented in Table 3.4. The extensive analysis of Table 3.3 and Table 3.4 is provided in the next subsection.

Table 3.2. Optimization scenario

Scheme	OCR optimization using the FA	Boundary evaluation	Target remedy and definite-time function (ANSI 50)
A	Yes	-	-
B	Yes	Yes	-
C	Yes	Yes	Yes

Table 3.3. Optimized results of the OCR settings

Relay ID	Scheme A				Scheme B				Scheme C					
	Curve	<i>TDS</i>	<i>Ip</i>	OF	Curve	<i>TDS</i>	<i>Ip</i>	OF	Curve	<i>TDS</i>	<i>Ip</i>	OF	<i>Ip_d</i>	<i>tdp</i>
A1	SI	0.14	150	2.103	UI	0.8	150	92.396	UI	1.14	135	130.371	1200	0.1
A2	SI	0.28	2000	4.293	SI	0.32	2000	4.906	SI	0.28	2000	3.718	17200	0.1
A3	SI	0.3	560	4.581	SI	0.34	560	5.192	SI	0.27	720	4.107	8000	0.1
A4	SI	0.34	1120	5.347	SI	0.37	1120	5.819	SI	0.35	1120	4.295	8000	0.3
B1	SI	0.14	105	2.103	UI	0.8	135	92.396	UI	1.14	135	130.371	1200	0.1
B2	SI	0.4	240	6.008	SI	0.45	240	6.759	UI	1	540	115.597	9000	0.1
B3	SI	0.3	1500	4.581	SI	0.34	1500	5.192	UI	0.28	1500	32.289	15000	0.1
B4	SI	0.32	60	4.862	SI	0.37	60	5.622	UI	0.44	60	50.863	1000	0.1
B5	SI	0.1	540	2.357	SI	0.1	540	2.357	SI	0.1	540	0.631	1200	0.3
51-5	SI	0.3	2000	4.979	SI	0.32	2000	5.311	SI	0.31	2000	2.224	8000	0.5
51-6	SI	0.73	240	11.314	SI	0.73	240	11.314	VI	0.68	200	17.313	2000	0.1

Table 3.4. Time operations and errors of the OCR using the optimized settings

Relay ID	tg_{pr}	tg_{bu}	Scheme A				Scheme B				Scheme C			
			t_{pr}	εt_{pr}	t_{bu}	εt_{bu}	t_{pr}	εt_{pr}	t_{bu}	εt_{bu}	t_{pr}	εt_{pr}	t_{bu}	εt_{bu}
A1	0.1		0.107	0.007			0.141	0.041			0.1	0.000		
A2	0.1	0.3	0.294	0.194	0.301	0.001	0.336	0.236	0.344	0.044	0.1	0.000	0.301	0.001
A3	0.1	0.3	0.229	0.129	0.305	0.005	0.260	0.160	0.345	0.045	0.1	0.000	0.309	0.009
A4	0.3	0.5	0.298	-0.002	0.500	0.000	0.324	0.024	0.544	0.044	0.3	0.000	0.514	0.014
B1	0.1		0.107	0.007			0.141	0.041			0.1	0.000		
B2	0.1	0.3	0.305	0.205	0.305	0.005	0.344	0.244	0.344	0.044	0.1	0.000	0.312	0.012
B3	0.1	0.3	0.266	0.166	0.304	0.004	0.302	0.202	0.345	0.045	0.1	0.000	0.303	0.003
B4	0.1	0.3	0.244	0.144	0.300	0.000	0.283	0.183	0.347	0.047	0.1	0.000	0.304	0.004
B5	0.3	0.5	0.008	-0.292	0.932	0.432	0.076	-0.224	0.932	0.424	0.3	0.000	0.932	0.432
51-5	0.5	0.7	0.339	-0.161	0.702	0.002	0.362	-0.138	0.749	0.049	0.5	0.000	0.725	0.025
51-6	0.1	0.9	0.557	0.457	0.908	0.008	0.557	0.457	0.908	0.008	0.1	0.000	0.910	0.010

3.6 Result Analysis

In this section, a detailed analysis for each scenario explained in Table 3.2 is provided. Also, the manual calculation to obtain the relay setting is exposed in section 3.6.1.

3.6.1 Manual Calculation (Conventional Method)

This subsection shows a manual calculation to obtain the relay setting (A1). In a conventional way, the setting for relay can be obtained by firstly determine the I_p using Equation (3.6). OCR A1 protect induction motor Mtr A, therefore the FLA depend on the maximum capacity of Mtr A (the nameplate information provided in Appendix). Once the FLA obtained, the I_p can be estimated as follows:

$$1.15 \times 110 \leq I_p \leq 1.45 \times 110 \quad (3.19)$$

$$126.5 \leq I_p \leq 159.5$$

$I_p = 140$ is selected.

After concluded the I_p for A1, the next step is to determine the TDS . To determine the TDS , it is important to anticipate the short circuit condition. In this case, the fault current at Mtr A (Fault location: 4.16 F0-1) which sensed by A1 is 17066 A, as indicates in Table 3.1. $C = 20$ is considered in the calculation to comply with the maximum relay detection capability (explained in section 3.2). When short circuit occurs, A1 must operate at 0.1 s (primary protection). By using Equation (3.1), the TDS for each curve type can be calculated with result shown in Table 3.5. The VI, LTI, EI, and UI curve does not comply with the TDS_{min} of 0.1. Thus, the SI curve is selected in this iteration. To evaluate the calculation, a TCC is provided in Figure 3.5.

Table 3.5. TDS value for each curve type by using manual calculation for OCR A1

Curve Type	TDS
SI (standard inverse)	0.131
VI (very inverse)	6.86E-04
LTI (long time inverse)	6.86E-04
EI (extremely inverse)	6.24E-05
UI (ultra inverse)	1.96 E-05

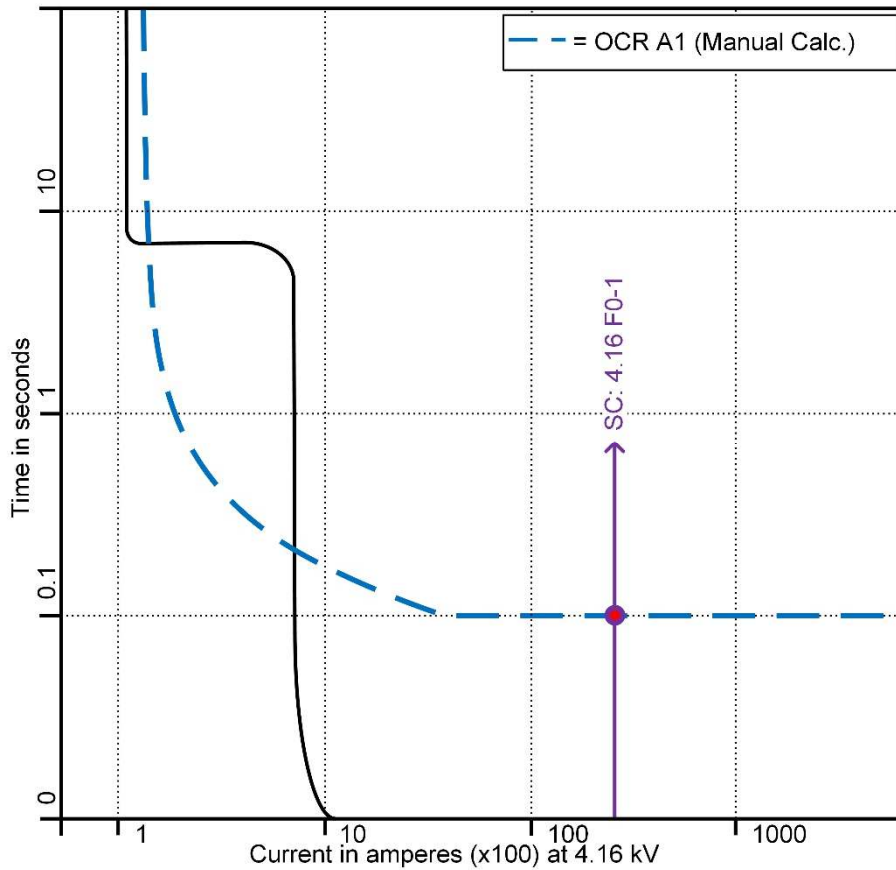


Figure 3.5. Time–current curve of A1 using manual calculation (conventional method)

As it can be seen from Figure 3.5, the relay operation of A1 will cause a false trip during Mtr A energization. Thus, a correction shall be made to prevent the false trip. To accommodate the Mtr A energization, the *TDS* is increased to be 4.88 with the same curve type. The increment of *TDS* cause A1 become insensitive to the fault current. Thus, the definite-time function is applied. The definite time function work to anticipate the fault current at 0.1 s. With regard to the Equation (3.18), the *I_{pd}* might be determined as follows:

$$140 \leq I_{pd} \leq 17066 \quad (3.20)$$

I_{pd} = 1400 is selected.

Once the correction is concluded, the curve evaluation is performed using TCC as shown in Figure 3.6. It can be seen that the A1 characteristic does not intersect with the Mtr A1 energization curve.

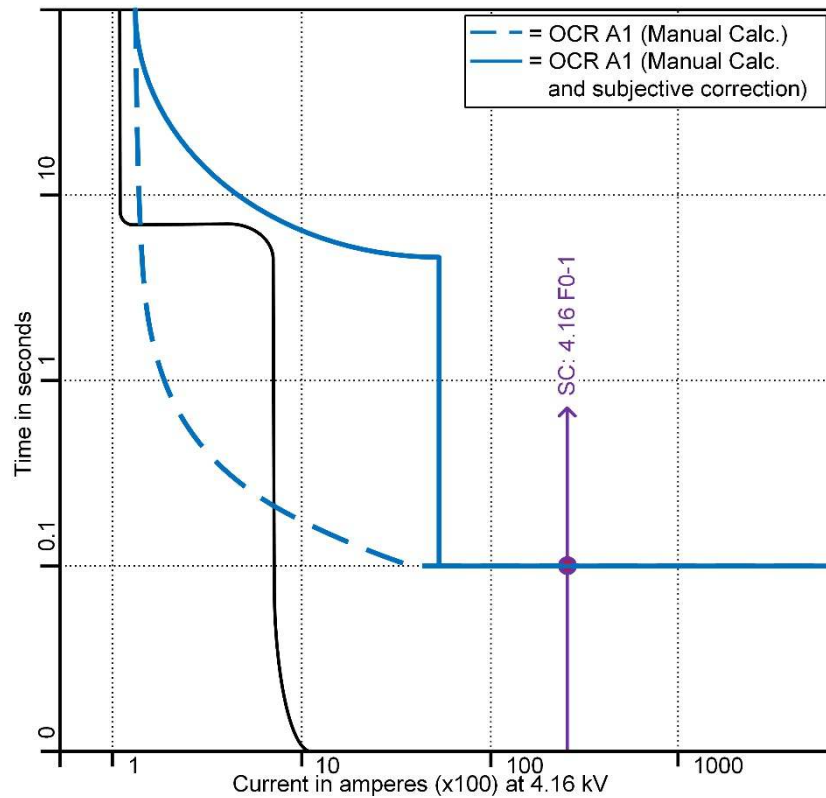


Figure 3.6. Time–current curve of A1 using manual calculation (conventional method) with subjective correction in curve-evaluation technique.

3.6.2 Scheme A

By following the coordination rules (3.2) in the optimization method, the values of TDS , I_p , and the curve type for each OCR can be obtained, as indicated in Table 4 (column *Scheme A*). Because the OF in Equation (3.4) aims to minimize the time–current function of the OCR, then the SI curve is selected for all OCRs. The calm–contour slope of the SI curve results in a smaller total value of Equation (3.4) compared with the other curves.

Table 3.4 (column *Scheme A*) shows the accuracy of the operating time to the target after testing the OCR setting to the fault current. In some cases, the OCR operations could not achieve t_{pr} , which result in εt_{pr} not equal to zero. The condition of εt_{pr} being less than zero occurred when the difference between $I_{sc_{pr}}$ and $I_{sc_{bu}}$ was insignificant. A4, B5, and 51-5 might trip swiftly, faster than the target, during $I_{sc_{pr}}$. This outcome occurred because the OCR only had one curve

to achieve the two current points (as the primary and backup protection). Thus, if the OCR had to anticipate $t_{g_{pr}}$, then it sacrificed t_{bu} .

Figure 3.7 shows the time–current response in a coordinated manner after the optimization using Scheme A. When faults occur in Bus 4.16 F0-1, the interval between A1 and A2 is 0.194 s (both relays are located in the 4.16 kV system). Although the A1 setting achieves the minimum tripping, it might cause a false trip during the MS event. This is because the response of A1 overlapped with the starting behavior of Mtr A. A fault in Bus 4.16 F1 trips A2 and A3 at approximately the same time. A3, which is located in the 13.8 kV system, could not reach $t_{g_{pr}}$ when a fault occurs in 13.8 F0-1.

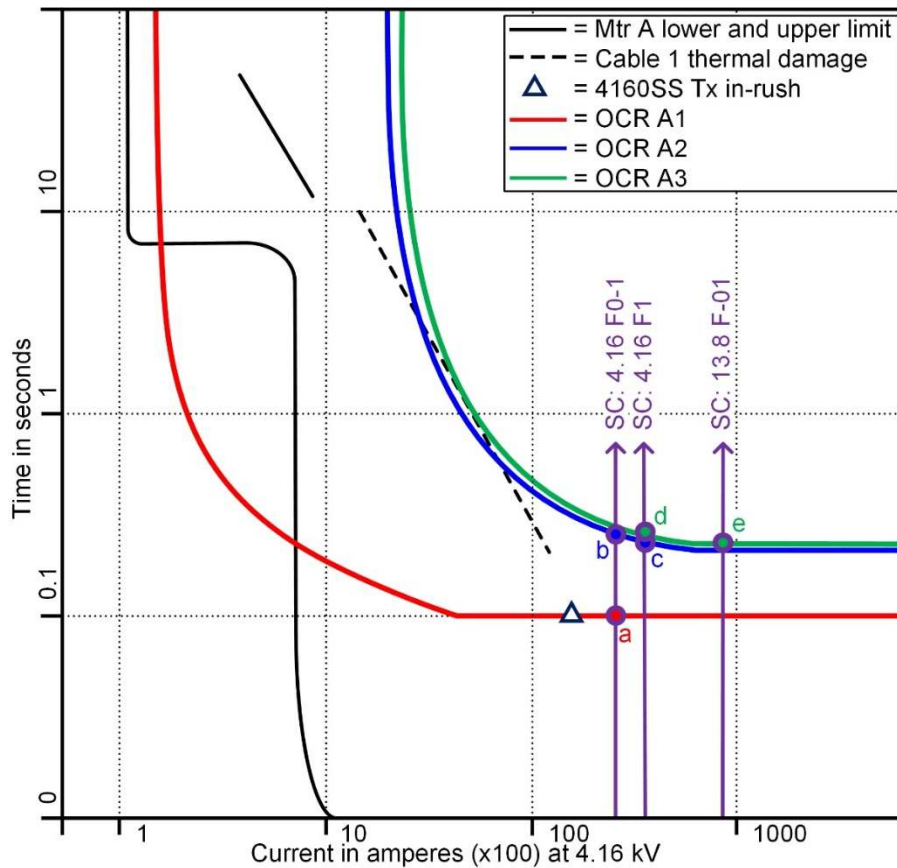


Figure 3.7. Time–current curve of A1, A2, and A3 using Scheme A optimization. **a** and **b** are the time responses of A1 and A2 during a fault in 4.16 F0-1, respectively. **a** = 0.107 s. **b** = 0.301 s. **c** and **d** are the time responses of A2 and A3 during a fault in 4.16 F1, respectively. **c** = 0.294 s. **d** = 0.305 s. **e** is the time response of A3 during a fault in 13.8 F-01. **e** = 0.229 s.

3.6.3 Scheme B

The boundary evaluation is introduced in Scheme B. The main purpose of the boundary evaluation is to prevent the false trip due to the load behavior. Compared to the OF in Scheme A (see Table 3.3), the OF (3.4) in Scheme B is greater. The increment of OF mainly occurs to A1 and B1, where the UI curve is selected. Because the relays work in a coordinated manner, the cascading effect happens. The upper-tier relays have an increment of the OF as the result of the downstream relay. Although Scheme B mitigates the possible false trip issue, a discrepancy between the operating and target times still occurs, as shown by εt_{pr} in Table 3.4 (column *Scheme B*).

Figure 3.8 shows the time–current response of the optimized OCR setting using Scheme B. The boundary evaluation improves Scheme A with the ability to avoid load operations by selecting the appropriate curve type within the I_p and TDS limits, which is very useful for A1. However, Scheme B causes the t_{pr} of A1 to increase, as compared to Scheme A.

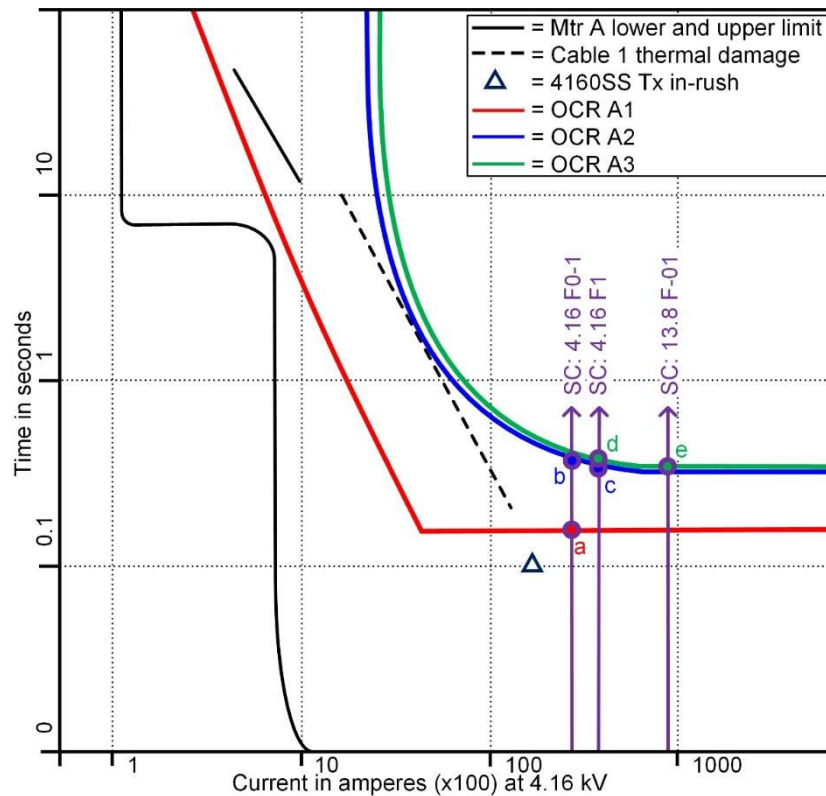


Figure 3.8. Time–current curve of A1, A2, and A3 using the Scheme B optimization. **a** and **b** are the time responses of A1 and A2 during a fault in 4.16 F0-1, respectively. **a** = 0.141 s. **b** = 0.344 s. **c** and **d** are the time responses of A2 and A3 during a fault in 4.16 F1,

respectively. $\mathbf{c} = 0.336$ s. $\mathbf{d} = 0.345$ s. \mathbf{e} is the time response of A3 during a fault in 13.8 F-01. $\mathbf{e} = 0.26$ s.

3.6.4 Scheme C

In Scheme C, a target remedy evaluation is proposed to improve the optimization (Scheme A) and boundary evaluation (Scheme B). The target remedy considers the definite-time function (ANSI 50) in the optimization process. In Table 3.3 (column *Scheme C*), new parameters (Ipd and tdp) for the definite-time function are provided. The inclusion of the definite-time function affects the OF of each OCR because the total $t(i)$ is now a combination of two curves (inverse- and definite-time functions). The presence of the definite-time function results in a significant impact to εt_{pr} and εt_{bu} . Table 3.4 (column Scheme C shows that εt_{pr} is zero for all relays. Furthermore, εt_{bu} is close to zero for all relays except for B5.

Figure 3.9 shows the time–current response of the optimized OCR using Scheme C. The deployment of the definite-time function to anticipate Isc_{pr} helps OCR to achieve tg_{pr} , i.e., trips in the exact target time. Conversely, tg_{bu} is anticipated by the inverse function. The time–current curve of A1 in Scheme C provides a better protection to Mtr A, as compared to Schemes A and B. Scheme C allows the OCR to avoid the load operations and solve the εt_{pr} problem without sacrificing t_{bu} .

3.7 Discussion

This chapter discusses modern issues and concerns and proposes a novel method for resolving the overcurrent protection coordination problem in the distribution power system. The state of the art in this study is a combination of an optimization method for inverse-time functions, a curve fitting technique for the relay operation evaluation, and the inclusion of a definite-time function in the optimization process to achieve an exact target time. IEEE Std. 242 is used to validate the proposed method.

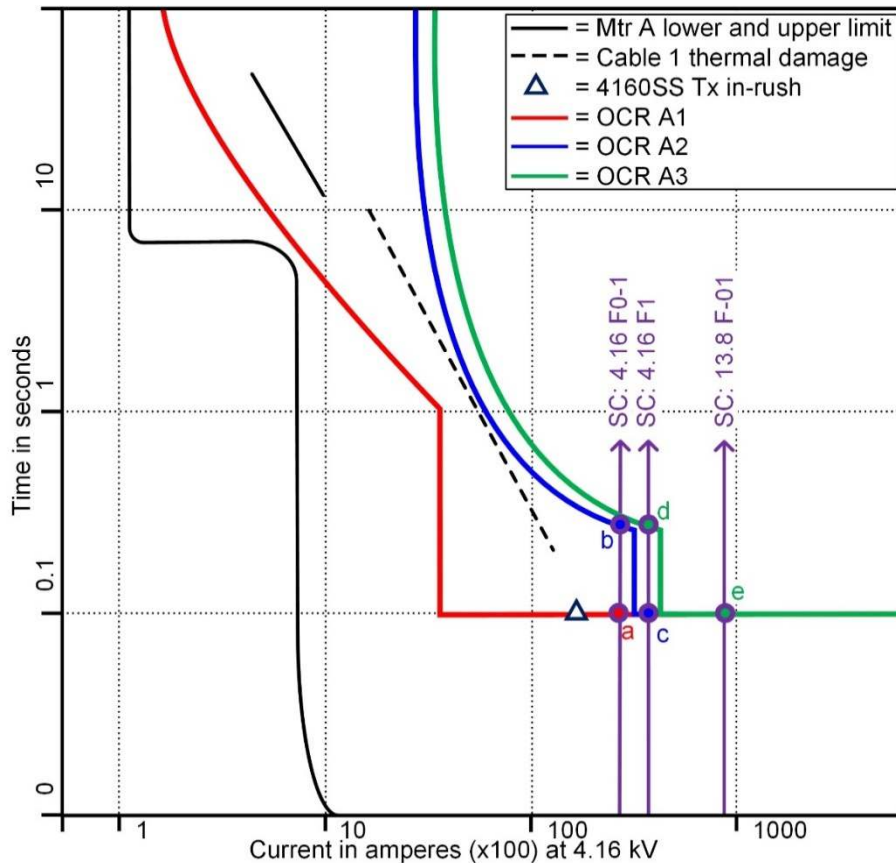


Figure 3.9. Time–current curve of A1, A2, and A3 using the Scheme C optimization. **a** and **b** are the time responses of A1 and A2 during a fault in 4.16 F0-1, respectively. **a** = 0.1 s. **b** = 0.301 s. **c** and **d** are the time responses of A2 and A3 during a fault in 4.16 F1, respectively. **c** = 0.1 s. **d** = 0.309 s. **e** is the time response of A3 during a fault in 13.8 F-01. **e** = 0.1 s.

During the optimization process in Scheme A, the OCR operation may achieve its objective but violate load operations, resulting in a protection system malfunction trip. Thus, the OCR constraint is expanded to include the load operation behavior and thermal limit, referred to as the boundary evaluation method in Scheme B. However, the boundary evaluation method is incapable of performing precisely to the time target when the fault current during the primary operation is insignificant to the backup operation, resulting in the primary time operation being sacrificed. As a result, a separate curve is required to denote the primary and backup roles. In Scheme C, a target remedy is introduced that utilizes a solution of the definite-time function (ANSI 50) as the primary protection and the inverse-time function (ANSI 51) as the backup protection. Therefore, the OCR is capable of precisely serving as a primary or backup.

Figure 3.10 shows the comparison between the conventional (manual calculation) and the proposed method. From the TCC, it can be concluded that the conventional method might result a false trip if not followed by a subjective correction. This work proposes a complementary tool to help protection engineers set existing OCRs in the power distribution system infrastructure.

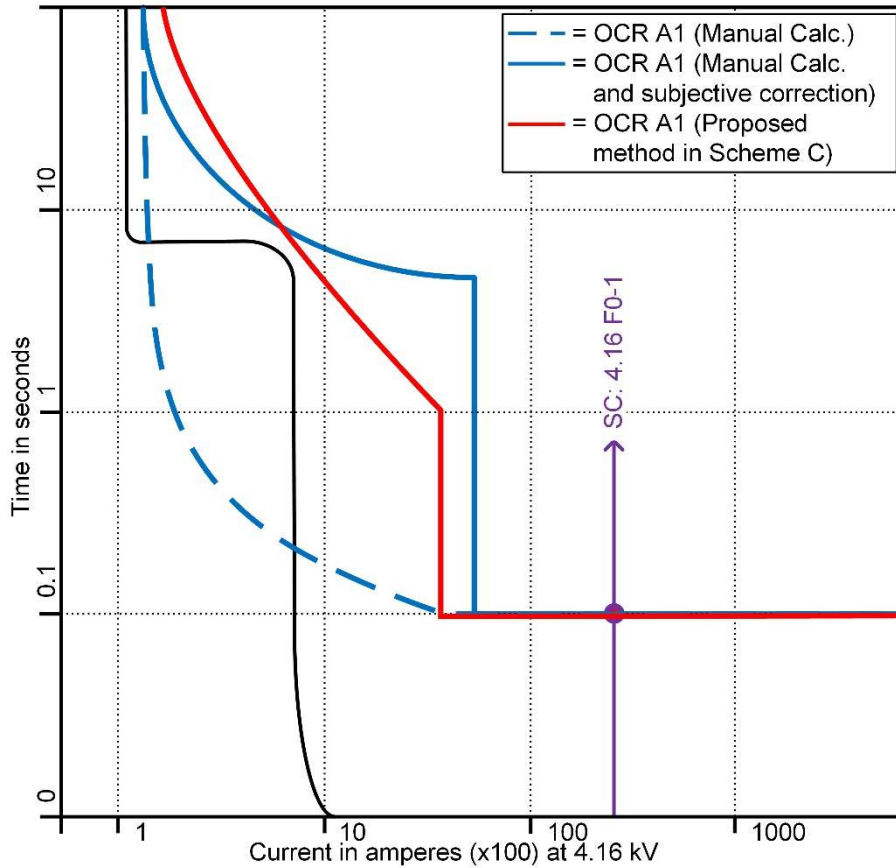


Figure 3.10. The result comparison of conventional method, conventional method with correction, and the proposed method for obtaining setting of relay A1.

CHAPTER 4

CHALLENGE OF THE PROTECTION SYSTEM IN A DISTRIBUTION NETWORK WITH A HIGH PENETRATION OF IBRs

The trend toward the use of RESs as DGs within a distribution network poses new challenges on the power system protection. The output power variability, location of the point of common coupling (PCC), and characteristics of the DG all have an effect on the power system's dynamic stability. The traditional distribution network and its protection system were not designed with the high penetration RES in mind. The majority of RESs are IBRs. Hence, a thorough understanding of the impact of IBRs with a high penetration rate on the distribution network is required.

This chapter examines the effect of high-density RESs on the IEEE 13 bus system. The proposed protection system is designed using scenarios and case studies, which include a comparison of DG types and various fault points. Moreover, this chapter investigates the relation of current, voltage, and tripping time in developing a credible protection coordination scheme.

4.1 Problem Definition

When an SC occurs in a power system network, all generators, including DG, contribute a fault current to the SC location. In this context, the PCC and the type of DG, whether SGs or IBRs, affect the direction and magnitude of the fault current, which in turn influences the protection coordination design philosophy.

The magnitude of the fault current when the IBR type of DG contributes to the fault current is less than that when the SG type of DG contributes to the fault current [75]. The implication is that the conventional OCR will take longer to clear when the distribution network is heavily penetrated by the IBR as opposed to the SG. If the distribution network fault is not isolated immediately, then it could result in an unstable operation, which could eventually result in a blackout [76].

As such, the purpose of this work is to specifically identify the protection system issues and challenges associated with the microgrid distribution network. The investigation begins with an assessment of the impact of DG penetration on the

distribution network. The evaluation focuses on the SC behavior and the effect of the DG penetration point. After the assessment is complete, the protection coordination problem can be described in detail. After establishing the context for the problem, a proposed protection scheme is presented, referencing IEEE Std. 1547 [77] and IEEE Std. 2030 [78], for utilizing the OCR with a unique voltage restraint operation. The proposed protection scheme is based on the current and voltage measurements as inputs that must be processed to address the time response requirements of each relay in the distribution network. The experiment is conducted using the modified IEEE 13 bus system with DG penetration. The proposed scheme is evaluated using a three-dimensional (3D) curve consisting of the voltage, current, and time.

4.2 SC Behavior of DGs

The DGs could be SGs or IBRs. The fundamental distinction between the SG and IBR is the source's characteristic and the controlled system's dynamic behavior. While SG is typically controlled as a voltage source, IBR can either be a voltage or current source. Under certain conditions, such as an islanding mode, the IBR is controlled as a voltage source to operate in a grid forming mode.

The SC current produced by the SG (i_{SG}) is determined by the generator's impedance and capacity. i_{SG} consists of the AC and DC components, as expressed below [41]:

$$i_{SG} = \sqrt{i_{ac}^2 + i_{dc}^2}. \quad (4.1)$$

The AC component (i_{ac}) consists of the sub-transient (id''), transient (id'), and steady state (id) with the respective time constants (Td'' , Td'). The following equation shows that the current contribution from SG decays on the sub-transient and transient domain [62]:

$$i_{ac} = (id'' - id') \times e^{\frac{-t}{Td''}} + (id' - id) \times e^{\frac{-t}{Td'}} + id \quad (4.2)$$

The DC component (i_{dc}) appears as the trapped flux in the stator winding. i_{dc} only appears at the sub-transient domain with a specific armature time constant (T_a) with the following equation:

$$i_{dc} = \sqrt{2} \times id'' \times e^{\frac{-t}{T_a}}. \quad (4.3)$$

For the RES, previous works [14] examined the SC behavior of a wind turbine generator in detail (WTG). The SC maximum (sub-transient) or minimum (steady state) current values for WTG Types 1 and 2 are dependent on the timing of the fault and the characteristics of the machine. For WTG Type 3, the SC current response is affected by the crowbar control and dynamic braking, whereas the WTG Type 4 depends on the power converter capability. The SC behavior of photovoltaic (PV) generators is relatively similar to that of WTG Type 4, which is dependent on the inverter capability [79]. The maximum and minimum SC behaviors of the SG and each type of WTG are summarized in Table 4.1 and Table 4.2.

4.3 Observation of the SC Behavior in a Microgrid

4.3.1 Test Case and Adjustment

The trial is simulated using ETAP 19 software [58] with the modified IEEE 13 bus system, as shown in Figure 4.1. Compared to the original test case, several DGs are added to Buses 650, 632, and 675. The model of the DG is shown in Figure 4.2. Each bus is equipped with a CB and protection relay along with its current and potential transformer. The nomenclature of the CB is based on $i - j$, where i is the CB location and j is the feeder connection, as shown in Figure 4.3. The grid in the modified IEEE 13 bus system is modeled using an SG (11 MW, 25 kV). For the sake of diversity, the DG could be an SG or WTG Type 4.

Table 4.1. Maximum (sub-transient) SCs of the various DG types

SG	WTG Type 1	WTG Type 2	WTG Type 3	WTG Type 4
$\sqrt{i_{ac}^2 + i_{dc}^2}$	$\frac{2\sqrt{2}V_s}{X'_s}$	$\frac{2\sqrt{2}V_s}{X'_s}$	$\frac{2\sqrt{2}V_s}{X'_s}$	$1.1 \times I_{FLA}$

Table 4.2. Minimum (steady state) SCs of the various DG types

SG	WTG Type 1	WTG Type 2	WTG Type 3	WTG Type 4
i_{ac}	$\frac{\sqrt{2}V_s}{X'_s}$	$\frac{\sqrt{2}V_s}{\sqrt{(X'_s)^2 + (9R'_r)^2}}$	$1.1 \times I_{FLA}$	0

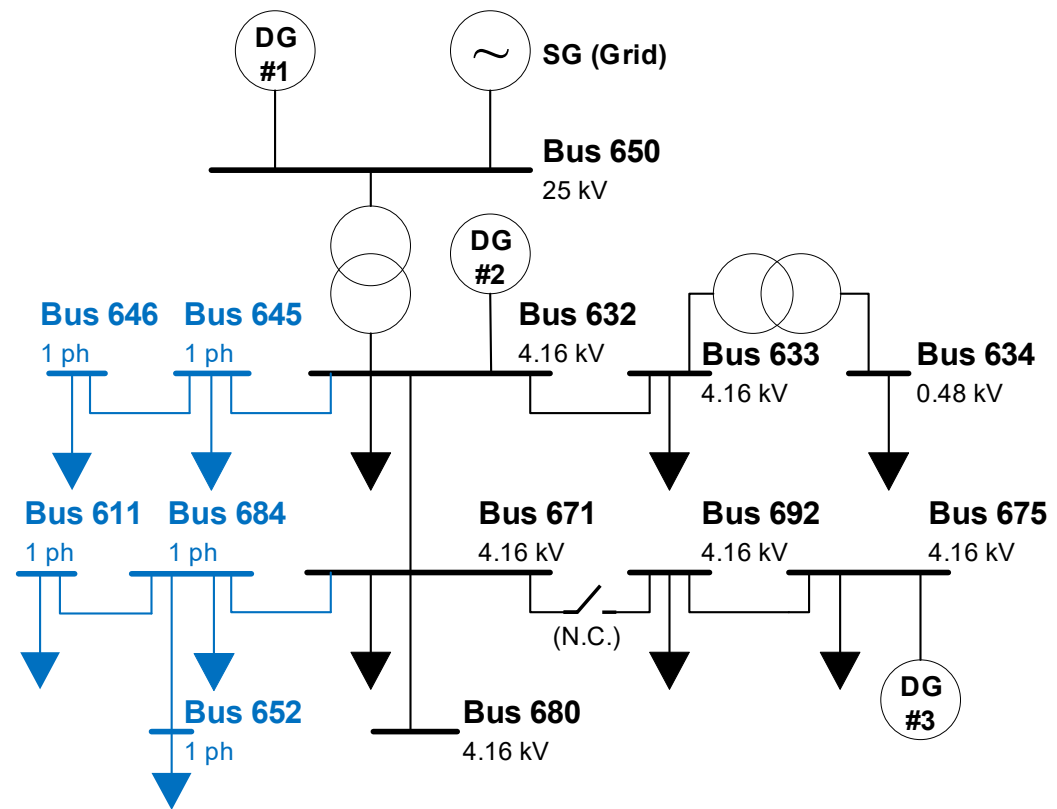


Figure 4.1. SLD of the IEEE 13 bus with DG penetration.

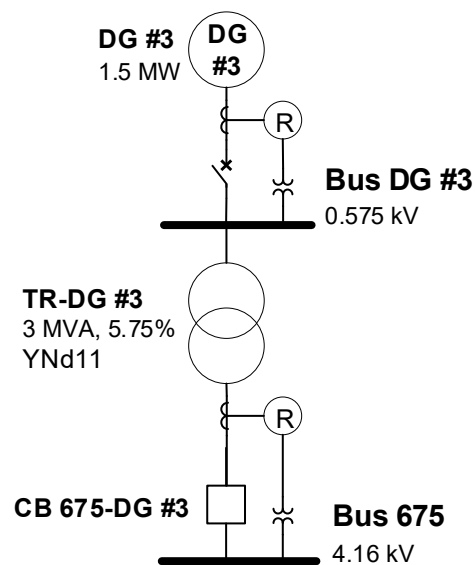


Figure 4.2. Model of the DG used in the simulation.

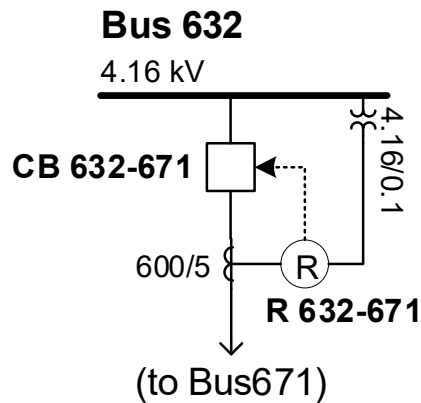


Figure 4.3. Example of the protection model used on feeder Bus 632 to Bus 671.

4.3.2 Observation Scenario

The effect of DG penetration on a microgrid distribution network has been observed in a variety of scenarios. Table 4.3 summarizes the variations used in this work. Case A represents the initial condition, in which power flows unidirectionally from the grid to the load without any DG penetration. Cases B and C illustrate the presence of DGs as an SG and IBR, respectively. In Cases B and C, the grid was assumed to be turned off to form a microgrid. Each case is classified according to the DG type. In Case B, an SG is used to model a diesel engine generator, whereas in Case C, a WTG Type 4 is used. Due to the WTG's inability to operate a swing bus, DG #1 is assumed to be the SG, with some adjustments to replicate the Type 4 SC and dynamic response of the WTG.

Bus 632 is chosen as the observation point to assess the impact of DG penetration and the type of DG. There are six scenarios are considered: 1) a normal condition (pre-fault), for which a load flow analysis is conducted. Several SCs at various fault points are simulated. To obtain the reverse SC current, fault points on 2) Bus 632 and 3) Bus 634 are selected. Then, to observe a spike current traveling in the same direction as the normal condition, fault points in 4) Bus 671, 5) Bus 675, and 6) Bus 680 are chosen. The SC occurred in the sub-transient domain, resulting in the maximum SC current.

Table 4.3. Case study used in the experiment

Case Study	SG (Grid)	DG #1	DG #2	DG #3
Case A	ON	OFF	OFF	OFF
Case B	OFF	ON (DG as: SG)	ON (DG as: SG)	ON (DG as: SG)
Case C	OFF	ON (DG as: WTG Type 4)	ON (DG as: WTG Type 4)	ON (DG as: WTG Type 4)

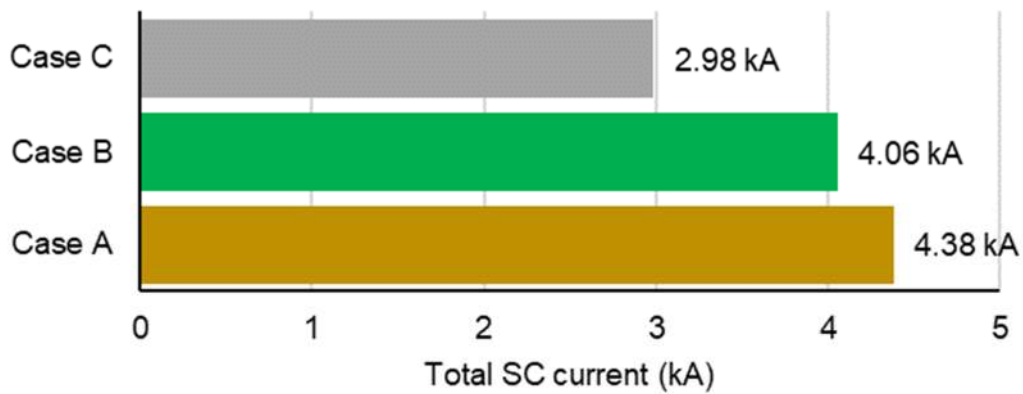


Figure 4.4. Total SC current under various case studies.

4.4 Effects of DG Penetration on the SC Behavior

By conducting a single scenario with a variable case, the impact of DG penetration and its type can be determined. The total current flows to the fault point during the SC on Bus 680 vary between the simulated cases, as illustrated in Figure 4.4. Case A has the highest current draw on Bus 680, followed by Cases B and C.

The total SC current is generated by the generator and consumed by the load, as illustrated in Figure 4.5.a, Figure 4.5.b, and Figure 4.5.c. During an SC, the load is modeled as an induction machine that acts as a voltage source. As presented previously in Equation (4.1), in Case A, the large-capacity grid represented by the SG results in a high SC current. As illustrated in Figure 4.5.a, the grid dominates the total SC current contribution (Case A). Due to the smaller capacity of the SG used in Case B, the total SC current is less than that in Case A. However, because the system contains three DGs modeled as SGs, the SC current in Case B is comparable to that in Case A.

The combined contribution of the three DGs is comparable to the load, as illustrated in Figure 4.5.b. Although Case C has the same number of DGs as Case B, the total SC current is less. In Case C, the DG is an IBR (WTG Type 4), which generates a much lower SC current than the DG as SG, as shown in Table 4.1. As illustrated in Figure 4.5.c, the majority of the SC current in Case C is generated by the load. This fact explains why the DG as IBR (WTG Type 4) produces less current during the SC.

4.5 Modernized Protection Coordination Philosophy and Strategy

A credible protection coordination must take into account all possible scenarios in the power system in all circumstances. This is because the protection device has a fixed set point and is installed in the same location. For the sake of simplicity, this section will focus on the observation point at Bus 632 and CB 632-671 (feeder between Bus 632 and Bus 671). The voltage bus and current flow are monitored and depicted in Figure 4.7 and Figure 4.8, respectively, for a variety of scenarios and case studies.

According to the voltage observation in Figure 4.7, prior to the fault condition (pre-fault), the voltage measurement in Bus 632 indicates a typical value in all cases. When the fault scenario occurs, the voltage on Bus 632 drops. Case C, in comparison to the other cases, has the most vulnerable voltage condition during the SC. The voltage drop when the DG is modeled as WTG Type 4 (Case C) is greater than that when the DG is modeled as SG (Case B) or in grid mode (Case A).

In the other observation, more precisely on the current flows between Bus 632 and Bus 671, as illustrated in Figure 4.7, the pre-fault condition has a different current measurement among Cases A, B, and C. Cases B and C exhibit decreased current flow as a result of the addition of DGs to the load side. As a result, less power was transferred from Bus 632 to Bus 671. When the SC scenario is introduced, the current flow can move backward, as indicated by the current measurements' negative polarity. If the focus is on the impact of the DG penetration, as represented by Cases B and C, it would appear that Case C contributes less to the current state of the economy than Case B. This is due to the

fact that the SC behaviors of the DG when modeled as the SG and WTG Type 4 are quite different.

As a result, the protection coordination design shall take Case C as the starting point. The CB 632-671 shall trip at a specified time (top), measured in seconds (s), depending on the location of the fault. When an SC occurs on either Bus 632 or 671, the CB 632-671 serves as the primary protection, with the top triggered faster than when the SC occurs on Bus 680 or 675. In addition, the top of the SC in Bus 680 or 675 shall be lower than that on the top of the SC in Bus 634. This condition can be expressed mathematically for the top of CB 632-671:

$$top_1 < top_2 < top_3, \quad (4.4)$$

$$\begin{aligned} & top_1: SC \text{ in Bus 632 or 671} \\ \text{where: } & top_2: SC \text{ in Bus 680 or 675} \\ & top_3: SC \text{ in Bus 634} \end{aligned}$$

Hence, top_2 on CB 632-671 is the backup protection that has to wait for the other CBs to operate. The waiting time shall comply with a certain time interval (CTI), as mandated in [80]. Mathematically, this condition is expressed as

$$top_n = \begin{cases} top_{min}, n = 1 \\ top_{n-1} + CTI, n > 1 \end{cases} \quad (4.5)$$

where top_{min} is the predefined minimum top , which is 0.1 s in this work.

After defining the top , the CB shall define the trigger. The conventional protection system uses a single-function OCR as the trigger. This condition may present a problem if the SC currents at different fault locations are not significantly different. For example, during the SC on Bus 675, the feeder experienced an electric current of 0.89 kA, whereas during the SC on Bus 671, the feeder experienced an electric current of 0.94 kA. Conversely, the relay serves as the primary when the SC is connected to Bus 671 and as a backup when the SC is connected to Bus 675. This slight difference is insufficient to coordinate the relay operation using a conventional inverse-time OCR curve. However, with the help of the bus voltage, the relay may determine the location of the fault.

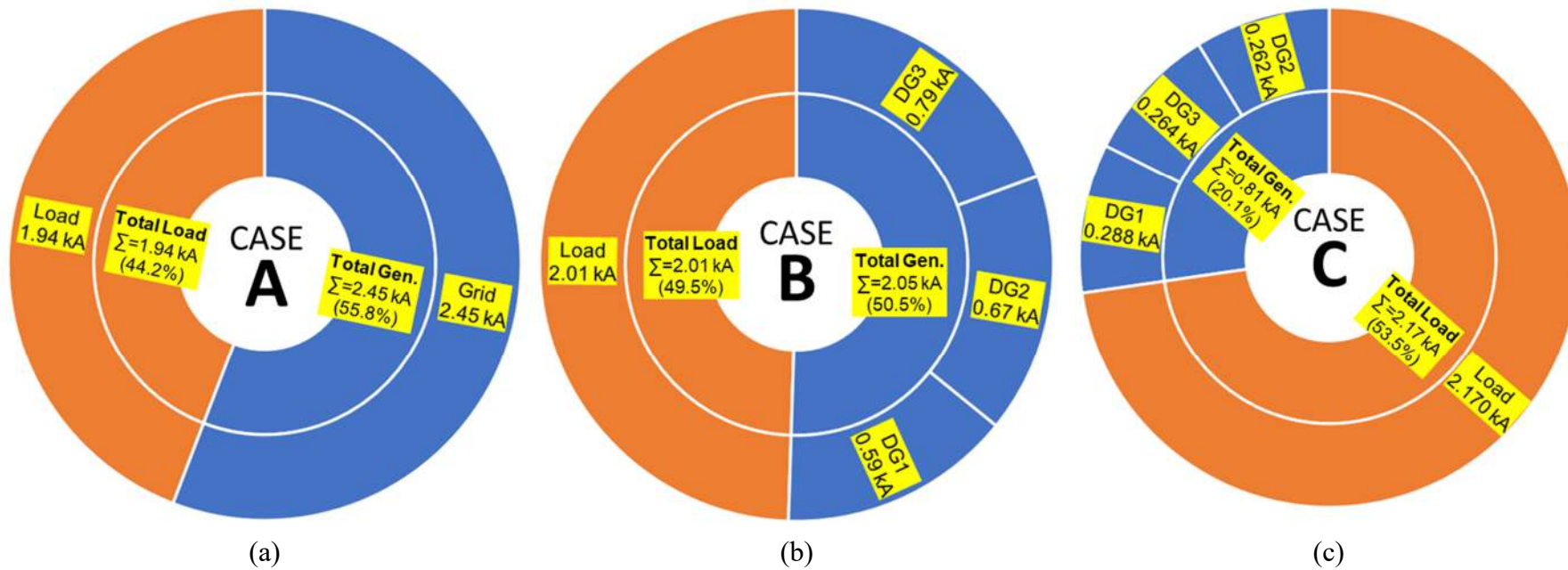


Figure 4.5. Sunburst diagram of the SC contributions for (a) Case A (grid only), (b) Case B (DG-SG penetration), and (c) Case C (DG-IBR penetration).

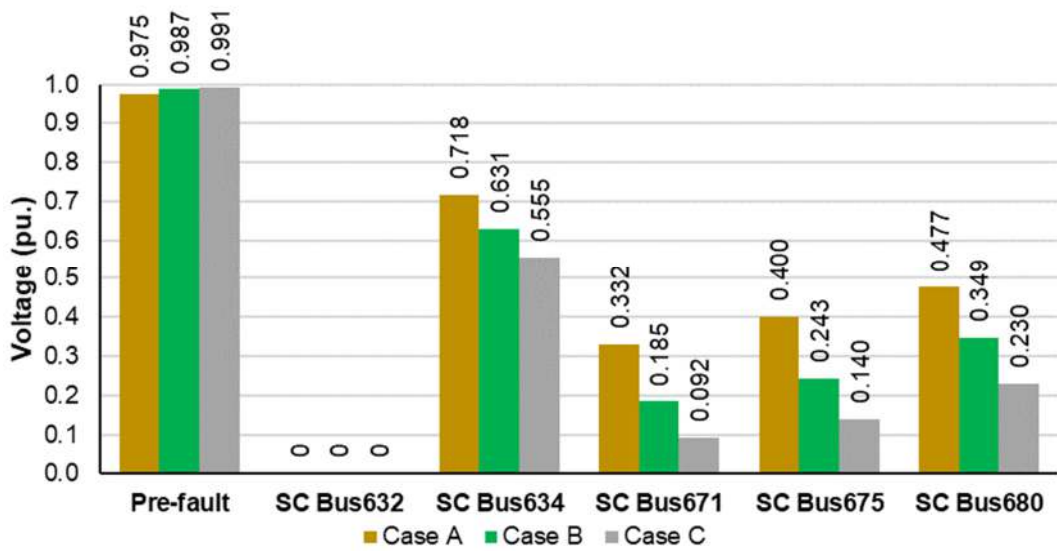


Figure 4.6. Voltage observation on Bus 632 in various SC locations.

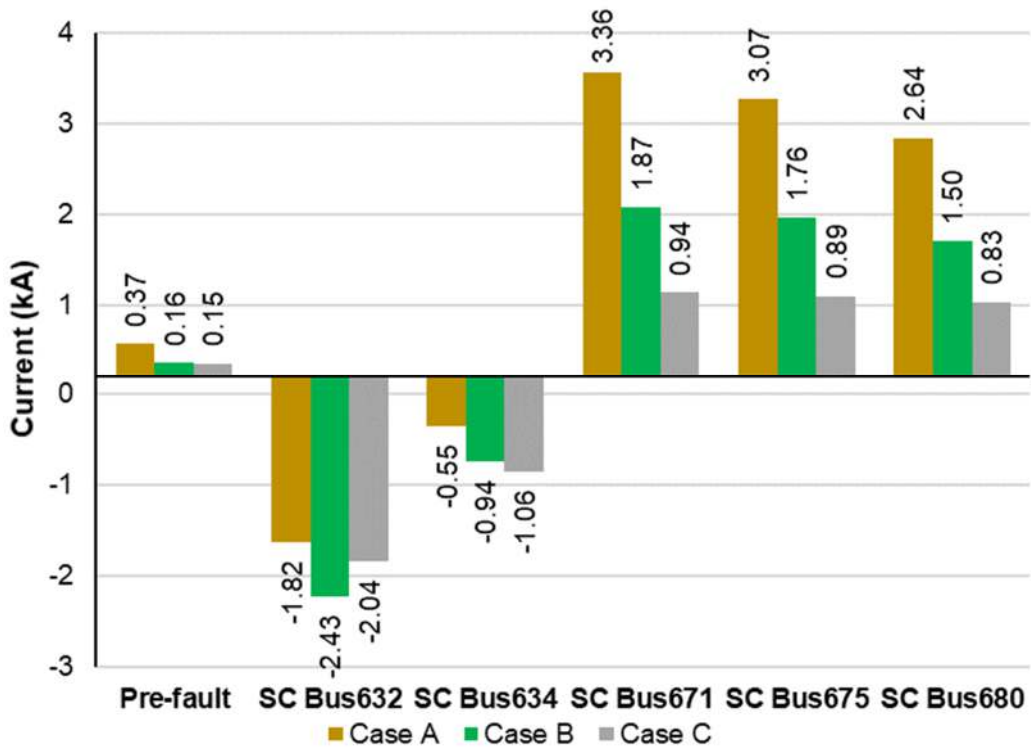


Figure 4.7. Current observation between Bus 632 and Bus 671 in various SC locations. The positive polarity means that the current flow is from Bus 632 to Bus 671. By contrast, the negative polarity means that the current flow is backward.

The CB operation is defined based on its status. The CB 632-671 signal was originally restrained (*REST*), means the CB is standby and wait the command to operate. The trigger starts when the measured current (I) is greater than the

predefined current set point (I_p), allowing the current trigger command (IST) to activate the voltage trigger command (VST):

$$IST(632 \text{ to } 671) = \begin{cases} VST, I \geq I_p \\ REST, I < I_p \end{cases} \quad (4.6)$$

The VST compares the voltage bus (V) to the predefined set point (V_p). In VST , when $V > V_p$, the CB remains $REST$, which indicates a load increment that can be handled by the system. However, if $V \leq V_p$, then the system might experience a fault. $V \leq V_p$ also activates the time selection (TVI):

$$VST(\text{Bus } 632) = \begin{cases} TVI, V \leq V_p \\ REST, V > V_p \end{cases} \quad (4.7)$$

The TVI is based on a logic function. It has several top candidates that comply with the voltage range (V_s). V_s helps the relay to recognize the fault location. The lower V_s represents the closer fault location to the CB. Hence, several V_s (V_{sn}) are employed to set the hierarchy. V_{sn} is compiled with a certain top_n , which can be written as follows:

$$TVI(\text{CB } 632 - 671) = \begin{cases} top_1, V < V_{s1} \\ top_2, V_{s1} \leq V < V_{s2} \\ top_3, V_{s2} \leq V < V_{s3} \\ top_4, V_{s3} \leq V < V_{s4} \\ \infty, otherwise \end{cases} \quad (4.8)$$

After obtaining top_n from TVI , the status of the CB (ST) can be determined, i.e., whether it has to trip ($TRIP$) or $REST$. This condition can be written as follows:

$$\begin{aligned} ST(\text{CB } 632 - 671) & \\ = \begin{cases} TRIP, IST = VST, \text{ and } VST = TVI, \text{ and } t \geq TVI \\ REST, otherwise \end{cases} \end{aligned} \quad (4.9)$$

An advanced digital curve is needed to establish the proposed operational characteristics of the protection system because the voltage, current, and time are related (voltage, current, and time are shown as a line graph). In the standard time–current chart, the previously separate curves for time–current, time–voltage, and current–voltage–time (CVT) are connected to form a 3D curve.

The chart in Figure 4.8 shows the CVT curve with several points that represent various scenarios. By using Equation (4.9), the CB 632-671 trip time,

when the SC occurs in Bus 632 or 671, is 0.1 s. When the SC occurs in Bus 675 or 680, the trip time of CB 632-671 is 0.3 s, and when the SC occurs in Bus 634, the trip time is 0.5 s, as per the criterion stated above. Thus, this condition fulfills the criterion stated above (4.4).

4.6 Discussion

Incorporating a DG into the traditional distribution network may help reduce losses, but it will negatively impact the power system's traditional protection design principles. Particularly, this work recognizes the issue and complexities inherent in designing a protection scheme for a high penetration IBR's distribution network.

When an IBR-based DG, such as a WTG Type 4 (or PV) system is connected to the distribution network, the system's SC behavior changes. All buses will experience a lower voltage drop during the SC as compared to that when the system is supplied by a grid- or SG-based DG. In addition, the IBR-based DG generates a negligible amount of fault current when compared to an SG-based DG. The low fault current may not be sufficient to initiate a standard OCR function, particularly if the fault current is less than the pickup value.

This work provides a major contribution by gauging the CB operation using voltage and current profiles. Once the current exceeds the predetermined value, the bus voltage is evaluated. By specifying the voltage range, the relay can approximate the location of the fault. The voltage range is inversely proportional to the time function. Thus, the CB can serve as a primary or backup protection mechanism. Accordingly, a 3D current-voltage-time curve can be used to evaluate this technique.

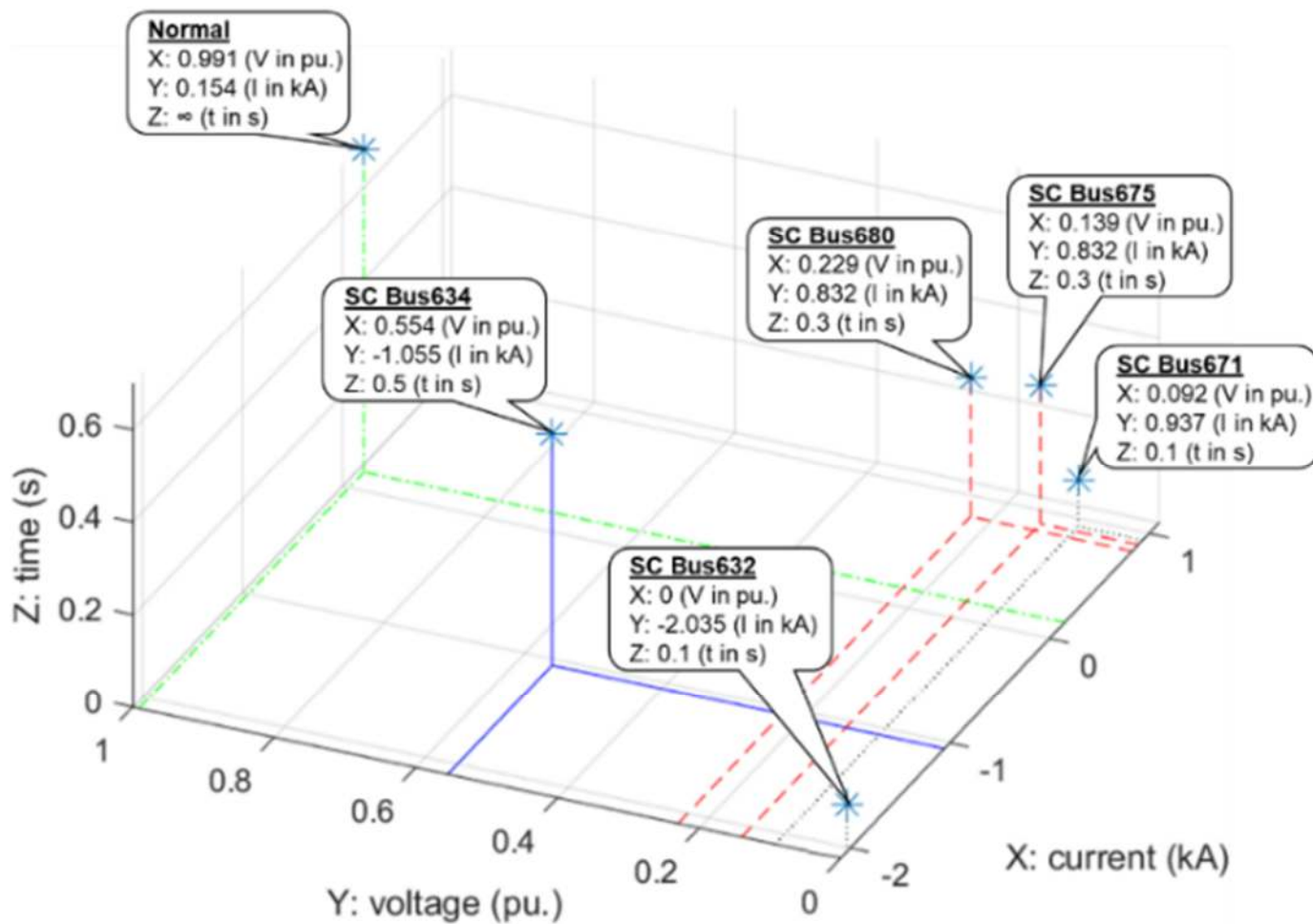


Figure 4.8. 3D diagram of the current (x-axis), voltage (y-axis), and time response (z-axis) for the protection coordination on CB 632-671 under various events.

CHAPTER 5

ADAPTIVE PROTECTION IN MICROGRIDS WITH THE VOLTAGE–CURRENT PARAMETER

In the previous chapter, we identified the challenge of the protection system in a microgrid with the high penetration of IBRs. Accordingly, we propose a breakthrough solution to ensure the reliability and resiliency of the power system network.

This chapter discusses a novel voltage–current model for DOCRs that enable the relays to operate efficiently [47]. The proposed relay architecture is a state of the art in that it anticipates the small fault current caused by the IBR using an adaptive pickup current threshold that varies with the magnitude of the voltage. A novel approach to the standard equation incorporates the magnitude of the voltage as a factor to spontaneously adjust the current threshold of the OCR in the feeder protection. The self-adjustment of the pickup value based on the OCR current threshold enables the relay to be highly sensitive to the low fault current and selective in a coordinated manner. By supplementing the voltage variable dependability to the traditional time–current response, the proposed method inherits the device requirements for selectivity, sensitivity, and adequate protection coordination.

5.1 Problem Definition

One of the primary challenges confronting modern power distribution systems is the inevitability of integrating RESs and microgrids [81]. Such subsystems are designed and implemented in accordance with the availability and location of modules based on power electronics. Thus, understanding how conventional overcurrent protection coordination may evolve in the modern context of microgrids, which are constantly interacting with existing distribution system infrastructure, is critical [82]. Without a doubt, the fault behavior will be altered by the addition of new components and physical constraints imposed by RESs, prompting a rethinking of practical protection schemes designed to prevent the spread of a fault.

Certain challenges are expected in the context of microgrids with a high penetration of IBRs in distribution networks:

1. Multi-time-inverse relay optimization
2. Variation in the level of fault current
3. Current flow in both directions during a fault
4. Topologies that are dynamic
5. Coordination with distribution networks
6. Operability of microgrids in a variety of modes
7. Adaptability of protection schemes

The existing OCR operates according to a conventional inverse-time standard, such as ANSI/IEEE or IEC. The OCR compares pre-set current thresholds to actual current flows. Once the current exceeds the threshold, the OCR begins operating at a designated time. The OCR's time operation is determined by the inverse-time function. When the sensed current exceeds the threshold, the relay rapidly operates. Conversely, when the sensed current is slightly greater than the threshold, the relay produces a long delay.

When used in conjunction with a distribution system that has a high penetration of power electronics resources, the converter's fault current is not as large as that when used in accordance with an SG. As a result, the conventional OCR requires a lengthy delay before isolating the fault practically.

5.2 Abnormal Events in Microgrids

In a power system, the microgrid concept refers to a network that consists of a source and sinks with local control and the ability to operate independently or in conjunction with the grid [83]. A source is a DER in a microgrid. The term "distributed" expresses that penetration points may be located throughout various buses or nodes. Thus, at some point, DER penetration may be extremely beneficial in minimizing system losses. However, penetration may pose another perilous threat to the conventional distribution network.

Initially, the distribution system's regular infrastructure is designed for a radial topology with a single source of power [79]. As a result, when the DER

penetrates, it may have an effect on the operation and protection system of the conventional distribution network [69].

The illustration in Figure 5.1 depicts one of the consequences of DER penetration on the distribution network. When the system is supplied from a single source, the direction of the current flow from the grid is unidirectional. This condition necessitates the operation of R1 only in the event of a fault (illustrated as F in B-1). In comparison, when a DG is included in the system, the presence of the DG may result in a reduction in the amount of power transferred from the grid. However, another protection device is required to operate during fault conditions because the faulted bus is supplied by two sources in the forward and reversed directions of R1 and R2. Hence, R1 and R2 shall trip simultaneously to mitigate the fault caused by $I_{F(Grid)}$ and $I_{F(DG)}$, respectively.

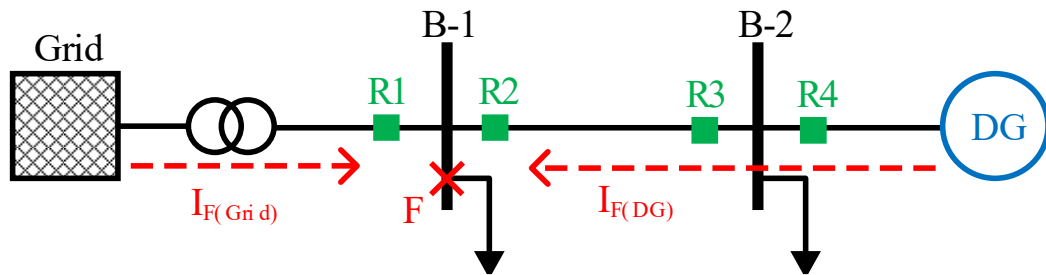


Figure 5.1. SLD for a distribution network with the DG penetration. During the fault, the fault current from DG ($I_{F(DG)}$) has an opposite direction from that of the grid fault current.

The DER encompasses all possible types of generators (e.g., fossil or biomass-fired energy, PV modules, wind turbines, and hydropower) and storage devices (e.g., batteries, flywheel, and supercapacitor). The DER in microgrids can be classified as an electrical machine, either induction or synchronous, or as an IBR, depending on the type of connection, as discussed in Chapter 4. Hence, this type of DER responds dynamically and differently to an SC event.

The SC response of a machine-based source, such as a SG, is dependent on the reactance value, which varies over the sub-transient, transient, and steady state time domains. As a result, the SG is modeled as a voltage source during the SC analysis. Conversely, the IBR responds entirely differently to the SG. The majority of the IBR is modeled as a voltage-controlled current source [84], with the rotating

reference frame control unit serving as the control unit. The IBR's SC response is limited to 1.2 p.u. during the operation to avoid damaging the internal electronic component. IBR's fault current magnitude is significantly less than that of SG. As a result, the small fault current generated by the IBR may not be detected by the conventional protection device or may require a longer response time.

To demonstrate the comparison of the fault current from the SG and IBR, Figure 5.2 depicts the time–current curve for the same fault location, as shown in Figure 5.1, under various DG models. When the DG is modeled as the SG (DG = SG), the primary relay in the reverse direction, i.e., R2, immediately trips and may be backed up by R4 at a specified time interval (t_{R4-R2} (DG = SG)). When the DG is modeled as the IBR (DG = IBR), the response time of R2 and R4 is significantly longer than that when the DG is modeled as the SG. Similarly, the interval time (t_{R4-R2} (DG = IBR)) may be affected.

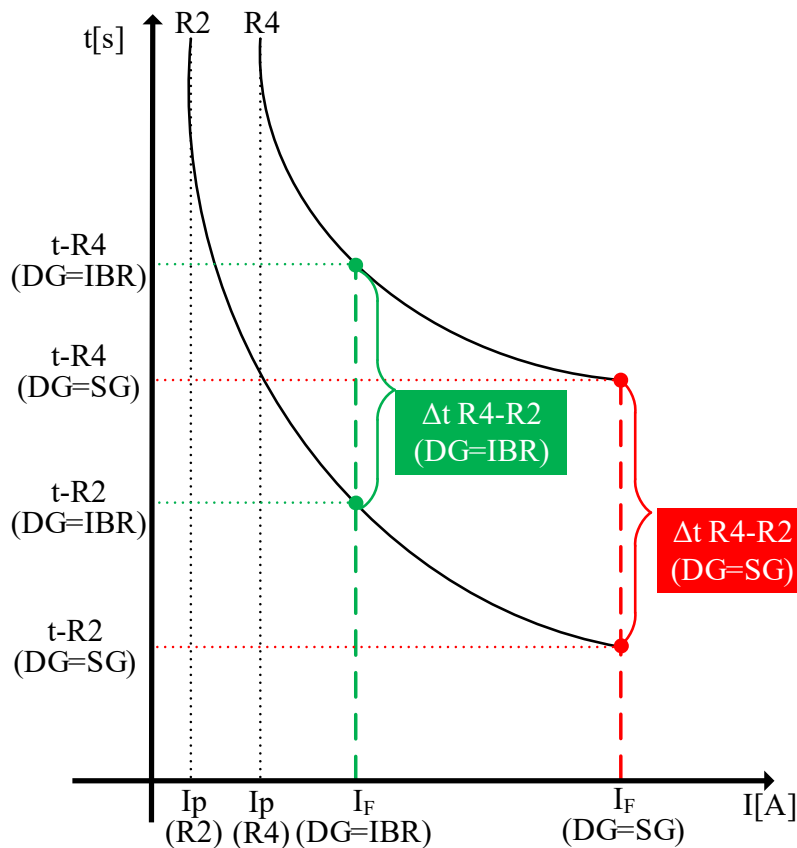


Figure 5.2. Time–current curve showing the impact of varying fault current magnitudes to the relay time response.

The protection system for a distribution network bears a significant responsibility for isolating any abnormal event, in any condition, whether with DG penetration or single-power-source operation, with the least amount of damage and impact zone. Thus, the protection system must find the right balance between the reliability and stability of the power system [40]. It must be sensitive and selective to mitigate the out-of-the-ordinary condition. The protection system is composed of several devices that work seamlessly. Each device performs a unique function but shares the common goal of securing the power system.

5.3 Voltage-Aided OCR

5.3.1 Review of the Basic Concept

The operation of OCR is determined by its state (*STA*), either a pickup (*PICK*), trip (*TRIP*), or restrained (*REST*) condition. The OCR operates in a restrained state under normal conditions. When the sensed current (G) exceeds the pre-set current threshold value (G_S), the relay goes to the pickup state. Once the timer (t) passed the time delay ($t(G)$), the relay shall send a trip signal to the CB. Thus, the relay goes to the trip state. *TRIP* is also known as the timeout state. This operation might be described by the following equation:

$$STA(OCR) = \begin{cases} PICK, G > G_S \\ TRIP, G > G_S \text{ and } t \geq t(G) \\ REST, G \leq G_S \end{cases} \quad (5.1)$$

$t(G)$ in inverse-time characteristics varies with the sensed current. Given this context, the time delay shall form a function, where the increasing magnitude of G shall be followed by the decreasing value of the time delay. To provide a certain limit to $t(G)$, the magnitude of G shall be compared to that of G_S , forming a ratio called M . This ratio might be formulated as follows:

$$M = \frac{G}{G_S}. \quad (5.2)$$

The ratio of M could be used to update the status of OCR in Equation (5.1). Then, the relation between M and OCR operation could be written as

$$STA(OCR) = \begin{cases} PICK, M > 1 \\ TRIP, M > 1 \text{ and } t \geq t(G). \\ REST, M \leq 1 \end{cases} \quad (5.3)$$

Because the relation between the current reading and relay status has been defined, the inverse-time–current function might be represented in accordance with the standard (or as discussed in Chapter 2 and presented in Equation (2.9)) as

$$t(G) = TMS \times \left(\frac{k}{M^\alpha - 1} + c \right). \quad (5.4)$$

Due to the multiple injection points of the DER, a directional element is a necessary component of the OCR operation. One method for determining the direction of current is to use a voltage reference, which is frequently used in commercial relays. Hence, the direction of power is determined by the angle formed by the current and voltage [85]. When the current and voltage are considered magnetic fluxes, the induced current produces a rotating torque, which can be defined as [86]

$$T = K \times \phi_i \times \phi_v \times \sin \varphi, \quad (5.5)$$

where K is a constant. The torque direction is determined by the value of φ , which is positive when $0^\circ < \varphi < 180^\circ$ and negative when $180^\circ < \varphi < 360^\circ$. Positive and negative torques can be used to determine the direction of the current flow. Normally, the relay operates in the forward direction, that is, when it is connected to a downstream power system.

5.3.2 Concept of the Proposed Method

An inverse OCR's time response is primarily dependent on the current flow. According to Equation (5.3), the OCR begins to respond when G exceeds G_s or when $M > 1$. As mentioned in Section 5.2, the insignificant fault current from IBR, presumed to be G , may not trigger ($M \leq 1$), resulting in a significant time delay for the OCR, as G is only slightly greater than G_s .

To address this issue, in this study, we propose that the voltage measurement can be included as a factor in $t(G)$. The basic concept is to increase M by decreasing G_s during a fault condition. The voltage suppression events that occur during a fault

serve as the trigger for reducing G_s . The following subsection discusses the relationship between G_s and the bus voltage.

5.3.3 Formulation of the Voltage-Aided Approach

The basic idea is to take advantage of the voltage drop due to a fault to lower G_s , current threshold, or relay pickup value, which increases the ratio of M . To conjoin the voltage parameter (U) into the OCR time response, Equation (5.2) might be updated as

$$M = \frac{G}{G_s(U)}. \quad (5.6)$$

By substituting Equation (5.6) to Equation (5.2), the OCR response is no longer dependent on a constant G_s , but on $G_s(U)$ as a function. $G_s(U)$ is expressed mathematically as

$$G_s(U) = G_s \times VCM. \quad (5.7)$$

The voltage–current multiplier, VCM , is a factor that varies along with the measured voltage bus. The VCM ranges from 0.1 to 1 and become unity when the bus operates at a normal voltage condition. In other words, Equation (5.6) is equal to Equation (5.2). Thus, the relays' sensitivity remains unchanged in a normal condition. However, when the voltage drops due to an SC in the system, the VCM value decreases. To have a specific trigger on when the VCM has to start decreasing, a voltage threshold (U_{th}) is introduced. The decreasing value of VCM leads to a decrement of $G_s(U)$, as shown in Equation (5.7), and increment of M , as shown in Equation (5.6). The rising value of M urges a short OCR time operation in Equation (5.4). Conversely, when the bus experiences an overvoltage phenomenon, the value of VCM shall remain at the unity point. Considering this boundary, the following expression limits the value of VCM :

$$VCM = \begin{cases} VCM, & 0.1 < U \leq U_{th} \\ 1, & otherwise \end{cases}. \quad (5.8)$$

To construct the VCM , a specific equation is used as follows:

$$VCM = \left(\frac{U}{n_a}\right)^{n_b} + n_c, \quad (5.9)$$

where n_a , n_b , and n_c are constants that form the contour of *VCM*. n_a , n_b , and n_c are self-tuned. The default value of n_a is 1. n_a affects the linear sensitivity of the *VCM*. When n_a is less than 1, the *VCM* becomes more sensitive. By contrast, to make *VCM* less sensitive, n_a must be greater than 1. The value of n_b has an exponential influence on *VCM*. Such a feature is essential when dealing with significant voltage suppression. By default, n_b must be greater than 0. n_c could be denoted as a positive offset for the *VCM*. Hence, n_c should be limited between 0.1 and 1 to comply with Equation (5.8).

To control the sensitivity of the *VCM*, an appropriate tuning between n_a and n_b is compulsory. If the OCR responds linearly with the voltage drop, then the value of n_a and n_b becomes 1. Conversely, if the OCR response is not too sensitive to the voltage drop, then the value of n_a becomes greater than n_b . To put it differently, when the OCR is susceptible to the voltage drop, then the value of n_a should be less than n_b . The combination of n_a , n_b , and n_c forms a *VCM* solution that obeys the rule in Equation (5.8). Figure 5.3 gives an illustration of several forms of Equation (5.9). To summarize, Equation (5.4) can be amended to yield the following final form of the time–current response in terms of the voltage function:

$$t(G) = TMS \times \left(\frac{k}{\left(\frac{G}{G_s(U)} \right)^\alpha - 1} + c \right). \quad (5.10)$$

5.3.4 Protection Relay Architecture and Connection

The relay connection and measuring apparatus are depicted in Figure 5.4. The relay monitors the current flowing through the bus and transmits the trip signal to the CB.

The relay's architecture is depicted in Figure 5.5. As previously stated, the relay utilizes the voltage and current inputs. In comparison to a conventional relay, the presence of *VCM* reduces G_s to $G_s(U)$, which improves the time of operation, $t(G)$, and enables a faster tripping.

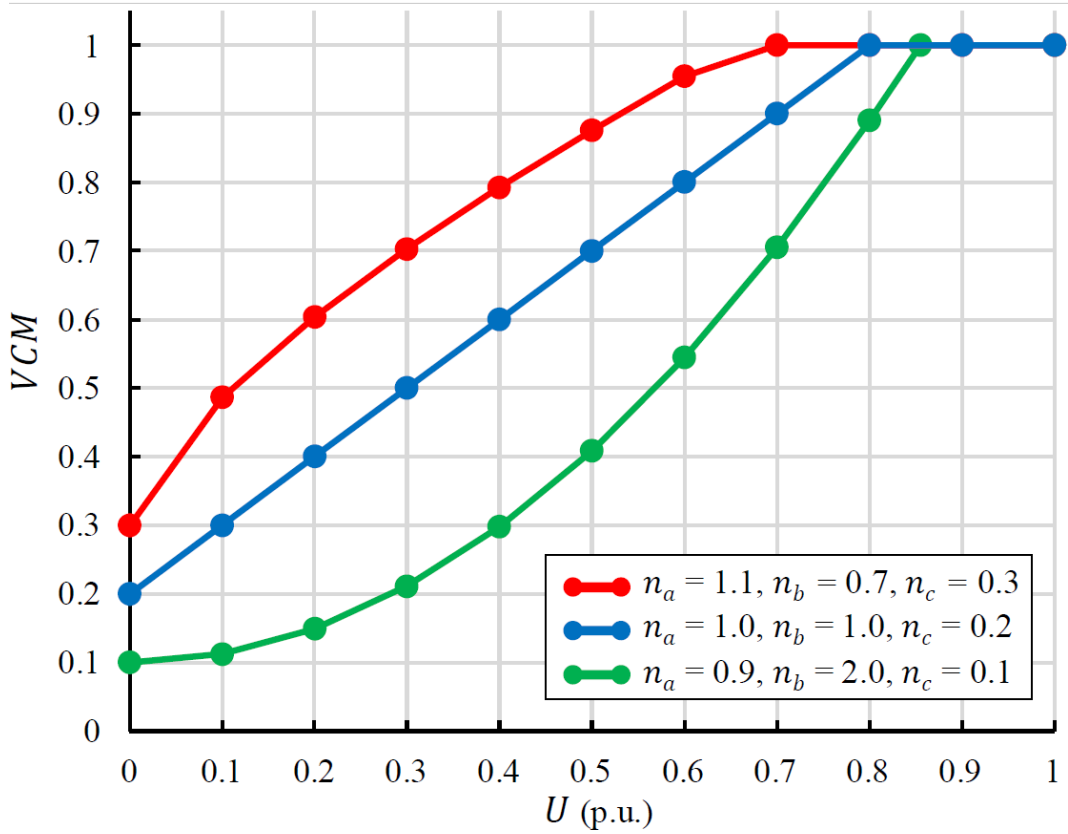


Figure 5.3. *VCM* response to the drop under some combinations of coefficients n_a , n_b , and n_c in Equation (5.9).

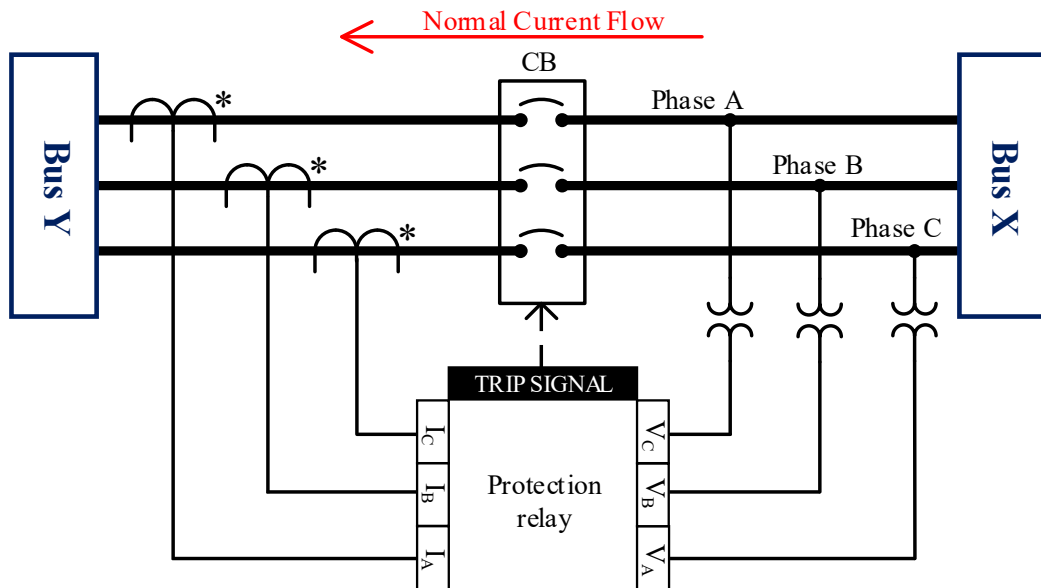


Figure 5.4. General assembly of the proposed relay connection.

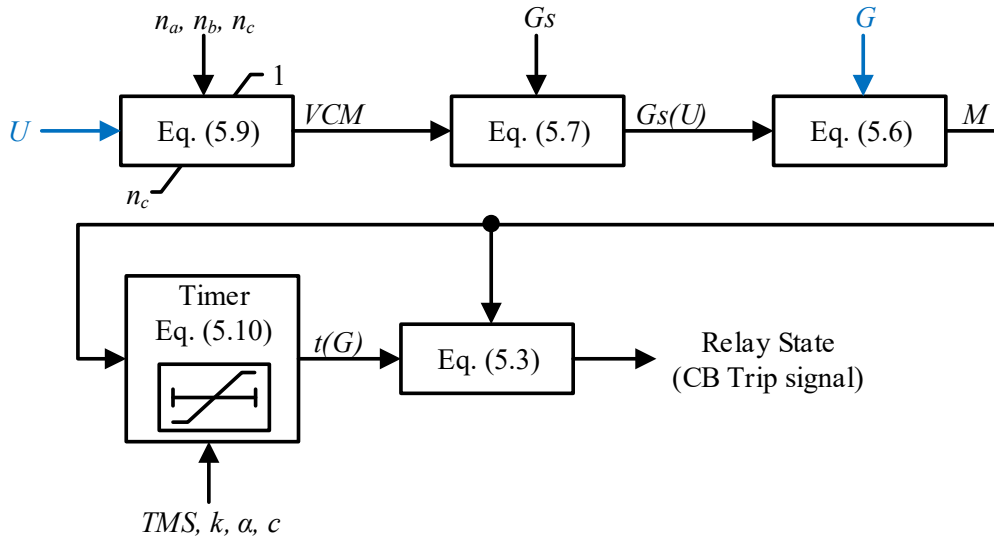


Figure 5.5. Block diagram of the proposed relay architecture. The blue line shows the analog input from the voltage and current measurements.

5.4 Simulation Setup

The relay coordination objective is to minimize the total relay operating time in the system without violating the conditions. Hence, OF could be written as

$$\text{Minimize: } OF = \sum_{x=1}^Q \sum_{y=1}^R (tp_{f,xy} + tp_{r,xy}). \quad (5.11)$$

The PSCAD software is used to conduct an experimental simulation. As illustrated in Figure 5.6, the IEEE 13 bus radial distribution system is chosen as the test bench. The IEEE 13 bus system's normal power supply is solely from the grid. Afterward, the original IEEE 13 bus test system is modified by replacing the DG with a 3 MVA IBR. The DG is regarded as an IBR that operates at full capacity and with a constant power factor. The test system considers five possible fault points (F1 to F5) and seven relays (R1 to R7). The test system's relays can measure the current flow and bus voltage. R1, R2, and R3 are used to determine the voltage on Bus 632. R4 and R5. R6 is used to determine the voltage on Bus 671. Finally, R7 is used to determine the voltage on Bus 675.

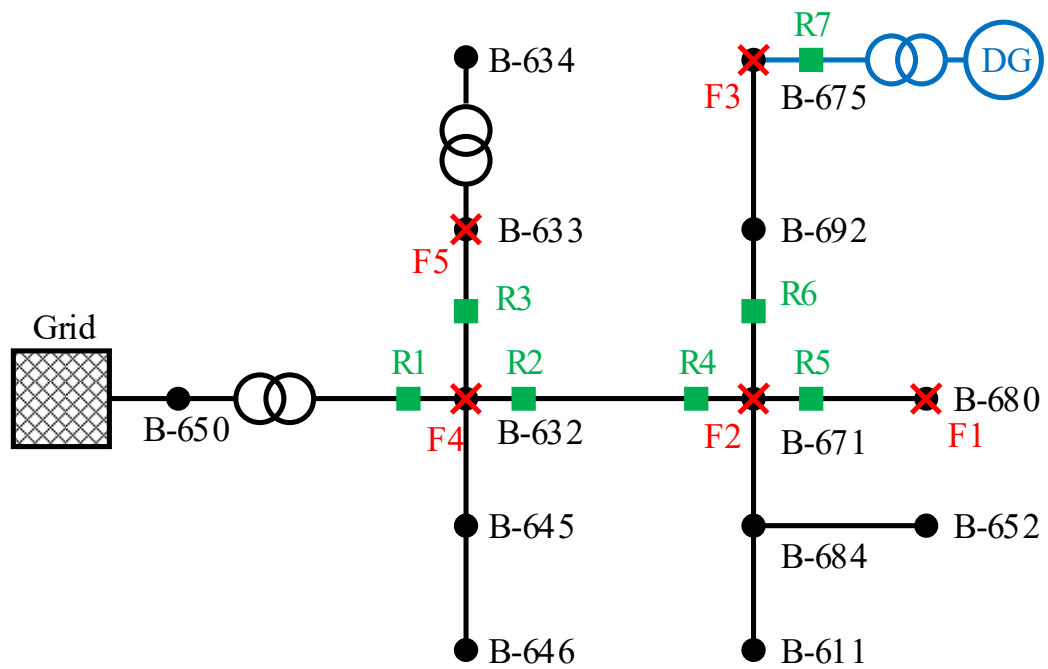


Figure 5.6. IEEE 13 bus distribution network with the DG penetration at the end point feeder.

An SC analysis is performed prior to the testing. Each fault point simulates and observes a three-phase symmetrical SC. The magnitude of the bus voltage measured during the fault is shown in Table 5.1, which is used as U in the optimization process.

Table 5.2 shows the fault current measured by the relay in the feeder. In the optimization process, the value in Table 5.2 is referred to as G .

Table 5.1. Voltage in each relay during the fault

Fault Point	U (pu)						
	R1	R2	R3	R4	R5	R6	R7
F1	0.43	0.43	0.43	0.15	0.15	0.15	0.16
F2	0.33	0.33	0.33	0.00	0.00	0.00	0.01
F3	0.38	0.38	0.38	0.08	0.08	0.08	0.00
F4	0.00	0.00	0.00	0.05	0.05	0.05	0.06
F5	0.16	0.16	0.16	0.17	0.17	0.17	0.18

Table 5.2. Current flows in each relay during the fault

Fault Point	G (A)						
	R1	R2	R3	R4	R5	R6	R7
F1	2850	2850	0	2850	3010	-442	442
F2	3350	3350	0	3350	0	-519	519
F3	3120	3120	0	3120	0	3120	524
F4	4990	-509	0	-509	0	-509	509
F5	4210	-430	4360	-430	0	-430	430

The negative value in Table 5.2 denotes the direction of the current flow in the opposite direction. Accordingly, the relay must include a directional feature. The normal direction of the current flow (supplied solely by the grid) is considered to be forward. R2 and R4 provide protection for the same feeder. Thus, R2 is only considered in the reverse direction (R2r), where the current flows from Bus 671 to Bus 632), whereas R4 is only considered in the forward direction (R4f, where the current flows from Bus 632 to Bus 671). R6 is the bidirectional relay, which is modeled as R6f when the current flows from Bus 671 to Bus 692 and as R6r when the current flows from Bus 692 to Bus 671. As a result, the total number of optimized relays increases to eight.

Because multi-direction fault currents are possible, coordination is classified into three types. First, a unidirectional relay pair performing primary and backup functions is required: 1) R4f and R1f and 2) R6r and R7f for the fault at F2, 3) R6f and R4f for the fault at F3, and 4) R2r and R6r for the fault at F4. Second, a bidirectional relay pair with two backup relays from a different feeder is required. For instance, in the event of a fault at F1, the primary relay is R5f, and the backup pairs are R4f (to anticipate grid current) and R6r (anticipate the current from the DG). A similar situation occurs during the F5 fault, where R3f serves as the primary relay and is backed up by two backups, R1f on the grid side and R2r on the IBR side. Third, a relay without a backup pair is required, such as R7f for the fault at F3 and R1f for the fault at F4.

To evaluate the proposed method's effectiveness, the overcurrent protection problem is solved using three different approaches: the conventional technique [7] (based on Equation (5.4)), the technique described in [33], and the proposed method (based on Equation (5.10)). Accordingly, certain parameters are required for the simulation, as detailed in Table 5.3. Certain parameters are consistent across all

methods, including the selection curve type based on [7], the tp_{min} value suggested in [44], the CTI_{min} value suggested in [80], TMS_{min} and TMS_{max} , and the G_s factor. In this work, the values of TMS_{min} , TMS_{max} , and G_s are pre-assumed. In addition, a unique parameter, denoted by β , is required for the technique described in [33], which is obtained throughout self-tuning. When voltage suppression occurs, the parameters n_a , n_b , n_c , and U_{th} are self-tuned to form a sensitive relay.

Table 5.3. Parameters used in the simulation.

Parameter	Conventional [7]	Balyith [33]	Proposed
Curve type	Inverse type [7] ($k = 0.14, \alpha = 0.02,$ $c = 0$)	Inverse type [7] ($k = 0.14, \alpha = 0.02,$ $c = 0$)	Inverse type [7] ($k = 0.14, \alpha = 0.02,$ $c = 0$)
tp_{min} [37]	0.1s	0.1s	0.1s
TMS_{min}	0.05	0.05	0.05
TMS_{max}	10	10	10
CTI_{min} [38]	0.2s	0.2s	0.2s
G_s factor to the nominal current	1.1	1.1	1.1
Internal parameter for the voltage factor	-	$\beta = 0.7$	$n_a = 0.9, n_b = 2,$ $n_c = 1, U_{th} = 0.8$

5.5 Results and Analysis

Each method's effectiveness is determined by the total operating time of the relays in the test system. In addition, the techniques are analyzed in terms of two concepts: 1) optimal setting and timing of relay coordination and 2) relay response during a fault and its changing state response.

5.5.1 Optimum Setting for the Coordination Purpose

The optimization variable in Equation (5.11) is the setting for the whole relay in the test case system, considering several fault points. The optimization model is solved using MATLAB's linear programming toolbox.

Table 5.4 provides the results of the optimized relay settings using various methods. As can be seen from the results, the TMS value is different for each method. In the conventional method based on the standard equation (Equation (5.4)) [7], the TMS is obtain without any consideration to the voltage bus. The difference

of the optimized TMS value in the proposed method appears because of the varying value of $G_s(U)$ compared to the fixed G_s in the conventional method.

Once the optimized TMS is obtained, its value is used to calculate each relay time operation. Table 5.5 presents the relay operating times under various fault locations and coordination scenarios. All methods satisfy the coordination constraints, i.e., tp_{min} and CTI_{min} .

The effectiveness of each method is examined from the total relay time operation in the test system. As formulated in Equation (5.11), the total relay time operation, known as OF , considers all fault points in the test system. Table 5.6 presents the OF of each method. The total relay time operation in the conventional method is 4.516 s, which is considered a benchmark. The technique in [33] results in an OF with a value of 2.702 s, which is equivalent to a 40.16% reduction from the benchmark value. The proposed method's OF result with a value of 2.363 s is equivalent to a 47.67% reduction from the benchmark value and 12.54% reduction from that of the technique proposed in [33]. Therefore, the proposed method offers a more effective result when dealing with a microgrid with IBR penetration as compared to the other methods.

Table 5.4. Optimized relay settings among the methods

Relay	G_s (A)	TMS		
		Conventional [7]	Balyith [33]	Proposed
R1f	625.1	0.124	0.185	0.237
R2r	139.7	0.050	0.087	0.139
R3f	77.8	0.060	0.108	0.092
R4f	457.9	0.089	0.160	0.201
R5f	80	0.054	0.098	0.086
R6f	186.1	0.050	0.079	0.096
R6r	393.1	0.050	0.050	0.171
R7f	438.2	0.050	0.050	0.236

Table 5.5. Relay operating times among methods in various fault points

Fault Point	Relay	Role	Conventional [7]		Balyith [33]		Proposed	
			$t(G)$	CTI	$t(G)$	CTI	$t(G)$	CTI
F1	R5f	Primary	0.100		0.100		0.100	
	R4f	Backup	0.336	0.236	0.331	0.231	0.348	0.248
	R6r	Backup	2.984	2.884	1.644	1.544	0.536	0.436
F2	R4f	Primary	0.308		0.273		0.314	
	R1f	Backup	0.508	0.200	0.473	0.200	0.514	0.200
	R6r	Primary	1.256		0.624		0.451	
	R7f	Backup	2.065	0.809	1.035	0.411	0.651	0.200
F3	R6f	Primary	0.121		0.100		0.126	
	R4f	Backup	0.321	0.200	0.300	0.200	0.326	0.200
	R7f	Primary	1.955		0.971		0.648	
F4	R2r	Primary	0.267		0.232		0.261	
	R6r	Backup	1.352	1.084	0.695	0.463	0.461	0.200
	R1f	Primary	0.409		0.302		0.363	
F5	R3f	Primary	0.100		0.100		0.100	
	R1f	Backup	0.446	0.346	0.370	0.270	0.407	0.307
	R2r	Backup	0.308	0.208	0.300	0.200	0.300	0.200

Table 5.6. Total operation time based on the objective function and effectiveness among methods.

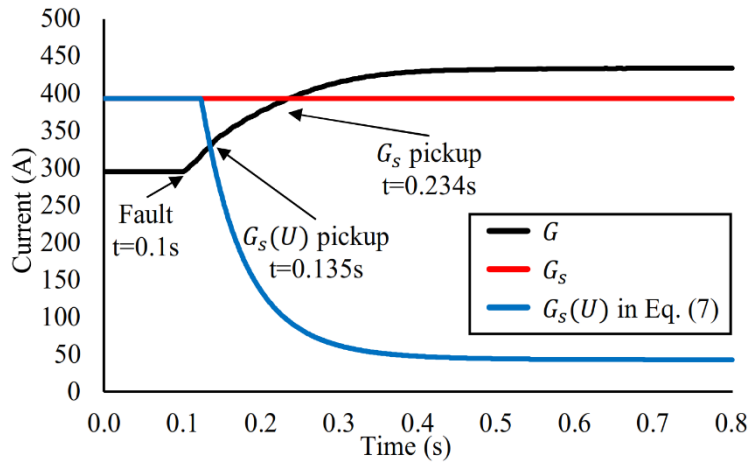
Method	OF	Time reduction benchmark (%)
Conventional [7]	4.516	-
Balyith [33]	2.702	40.16%
Proposed	2.363	47.67%

5.5.2 Relay Response

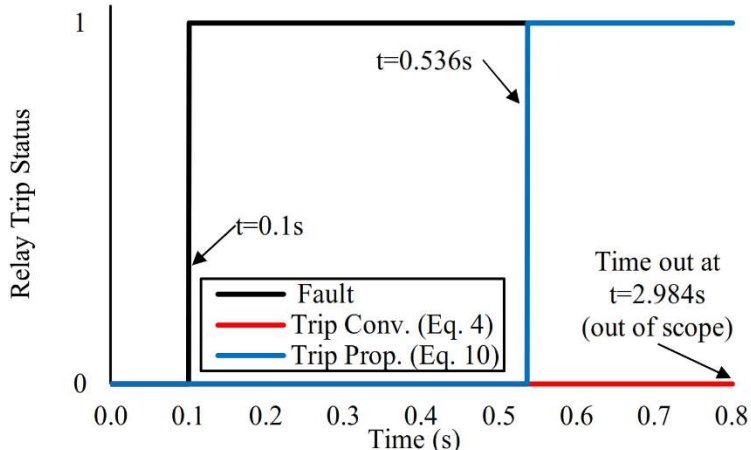
This subsection analyzes the proposed method's performance on a time response oscillograph. We presume that the fault occurs in F1 and R5f fails to trip the CB (which is supposed to act as primary protection). R4f and R6r provide backup protection against a fault at F1. The analysis is focused on R6r, which detected the IBR's fault current.

Figure 5.7.a shows the current response during the simulation. In a normal condition, G_s and $G_s(U)$ of R6r have the same value of 393.1 A, whereas the current flow is below the relay pickup value. When the fault occurs at $t = 0.1$ s, the current raising and $G_s(U)$ decrease from their original values. The decrement of $G_s(U)$ in the proposed method results in a 0.099 s faster pickup time as compared to that in the constant G_s in the conventional method. Because the increase in current and the decrease in $G_s(U)$ occur simultaneously, the M ratio in the proposed method expands faster than that in the conventional method. The faster relay pickup time gives an advantage to the relay to start the counter before tripping.

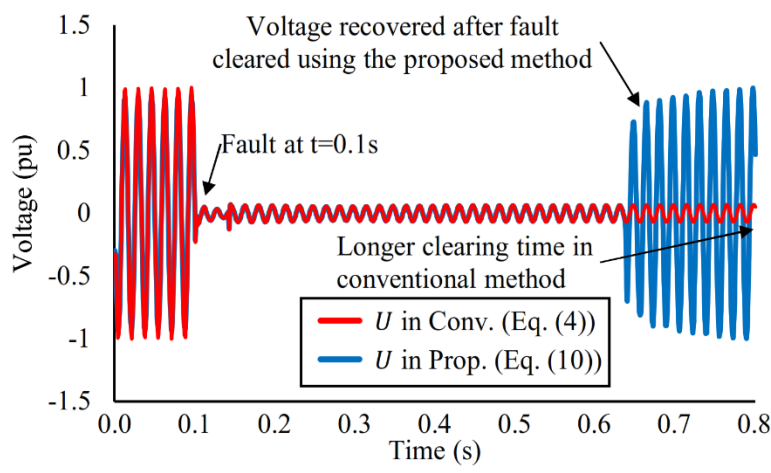
Figure 5.7.b shows the relay tripping status. The proposed method has a faster tripping time (0.401 s after the relay pickup) than the conventional method (2.75s after the relay pickup). The superiority of the faster pickup and tripping time in the proposed method relies on the voltage measurement, as shown in Figure 5.7.c. During the fault at F1 (Bus 680), the voltage in Bus 671 drops and affects the $G_s(U)$ of R6r. Once the fault is cleared, the voltage returns normal. By contrast, if the relay is insensitive to the fault (as simulated in the conventional method), the voltage drop still occurs at the bus.



(a)



(b)



(c)

Figure 5.7. Comparison between the conventional method and proposed method: (a) RMS current oscillography at R6r during the fault at F1 compared to the relay pickup current. (b) Tripping chart of R6r. (c) Comparison of the voltage oscillography at Bus 671.

5.6 Discussion

This chapter acknowledges the high penetration of IBR in the microgrid and proposes the inclusion of a voltage function in the operation of DOCRs. The state of the art in this study is the voltage–current model that enables the relay to readjust the pickup value in response to the IBR’s small fault current. In a coordination scheme, adjusting the pickup value in the protection relay results in a faster tripping time.

The proposed method is validated by inserting the DG into a standard IEEE 13 bus distribution system and comparing its performance to the conventional overcurrent relay model. The relay setting is determined by solving an optimization problem to minimize the primary time operation of the relay under the constraints imposed by the coordination scheme. Numerous fault points are applied to the test system to evaluate the model’s performance. The results demonstrate unequivocally that the proposed method requires less total relay operating time than the standard equation and that it works without violating coordination constraints. The proposed method reduces the total relay operating time to 2.363 s, which is 47.67% more efficient than the conventional method. The time-domain analysis demonstrates that the proposed technique enables the relay to adjust the pickup value (current threshold) in response to the location of the fault. As a result, the relay’s sensitivity and selectivity are increased when compared to the conventional method of fault anticipation.

This page is left intentionally blank.

CHAPTER 6

INTELLIGENT PROTECTION RELAY WITH IDENTIFICATION AND CLASSIFICATION CAPABILITY

This chapter aims to fill the gap of providing a timeless power system monitoring to witness the symptoms by planting an AI-based model in IPA [48]. The IPA has to determine the activities in the system and decide the precise action to overcome the situation. This chapter intends to show the prospects of implementing a deep learning computation to solve a protection scheme problem in power system operations.

6.1 Problem Definition

Undoubtedly, everyone demands a reliable power system. When a blackout occurs, every second of the power outages leads to an economic loss in every business sector. To tackle this issue, the power system must be fortified with a defense scheme that considers the possible fault. With the recent trends of DERs, several intermittent generators have penetrated the systems, which might cause system instability [12]. The combination of numerous operation schemes and the possibility of DG penetrations presents considerable challenges on engineers.

A reliable and sustainable power system network has tons of operation maneuvers and a dependable protection system. The operation and protection of the power system must work independently but in a correlated purpose. The false or unsafe operation during a power system maneuver, which might be caused by a DER penetration [87], sudden load injection or rejection, network topology variation, and a fault condition, shall be anticipated by a proper protection system [45]. However, the protection system shall not limit the flexibility of power system operations. For this particular reason, a trade-off point is compulsory to achieve a robust power system [15]. An illustration regarding the correlation between a power system operation and protection is presented in Figure 6.1.

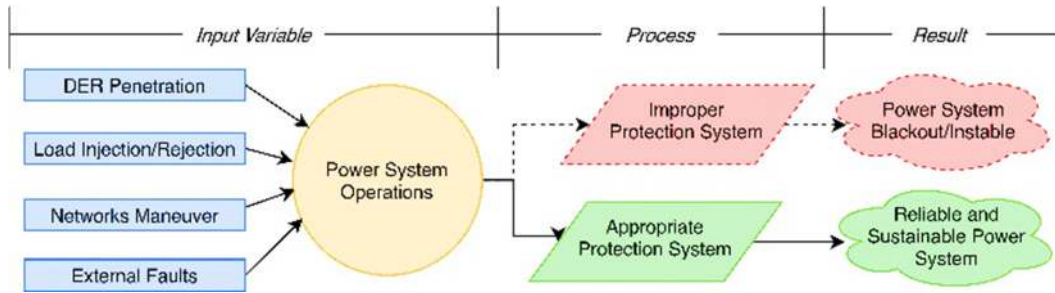


Figure 6.1. Reliable and sustainable power system as a result of an appropriate protection system and proper power system operations.

The fault in the power system can be categorized into two types, i.e., series faults, such as an open line condition, and shunt faults, such as the SC condition [88], [89]. The type of fault in a direct observation can be easily distinguished by witnessing the broken equipment or conductor. On the contrary, if the fault is located in a remote area, then the observation can only be proceeded by examining electrical parameters, i.e., voltage, current flow, and frequency. Thus, generally, it is impossible to witness every single equipment on the system, so a protection device should be used.

Deep learning has an undoubtable performance in image processing [90]. In this case, the pattern of data series based on the simulated power system events will be used as a feature to be extracted. Deep learning is based on convolutional neural networks (CNNs) and has a powerful ability to recognize patterns [91]. The objective of deep learning is to use CNN to perform an event classification based on large datasets gathered in the operation of medium-voltage power system distribution networks. Then, the CNN is combined with the long-short-term memory (LSTM) technique to increase the accuracy of recognizing and classifying the power system distribution network symptoms.

6.2 Event-Based Classification Based on CNNs

Recently, AI has witnessed a massive development that can bridge the divide between human and machine capacities. The aim of this field is to allow computers to see the environment as people do, to interpret it in the same way, and even to use understanding for many functions, such as the identification of images

and videos, image analyses and classification, recommendation systems, and linguist processing.

In power system generation with increasing intelligent electricity meters and the widespread use of power generation technologies, such as solar panels, considerable information with regard to the use of electricity may be recorded. This information is a multivariate time sequence of power that could be used in turn for modeling and even predicting future energy usage. The progress made in AI by deep learning, mainly through one specific algorithm, i.e., CNN, has been built and improved over time.

CNNs can learn characteristics from sequence information, assist multiple-variate information automatically, and immediately generate a multi-step forecasting vector [90]. They are a deep learning algorithm capable of capturing input data, assigning significance (learnable weights and biases) to multiple aspects/objects, and being able to distinguish them [92]. Figure 6.2 depicts a typical CNN block scheme, which is used on power system operations.

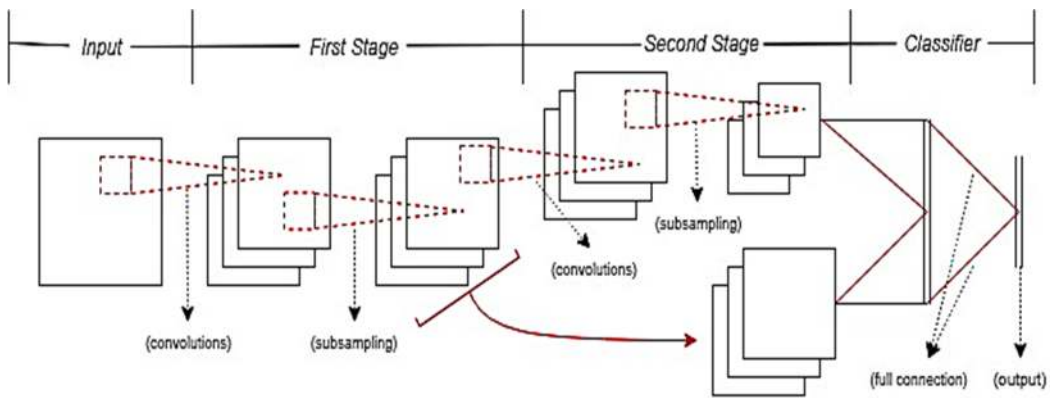


Figure 6.2. Typical CNN block scheme.

The fundamental objective in implementing deep learning is to eliminate the complicated and eventually restricting choice of features. The role of a convolutional layer can be merely articulated as follows: it uses a 3D quantity of data to generate a fresh 3D quantity of data.

Figure 6.3 illustrates the 3D convolution process used in CNNs, where input features are used for the convolution operation. The first convolutional layer uses low-level characteristics, such as edges, rows, and angles. The input is $N \times N \times D$

and is converted with H kernels, each of which is separately presented as $k \times k \times D$. The convolution with one kernel generates an output function and separately generates features map with kernels. Each kernel passes one element at a time from the top-left corner. One element will be moved downward from the kernel, and one item will be passed over again from left to right. This method is performed until the kernel hits the bottom-right corner. If the input height and width are equal to 32 and the kernel value is 5, then there will be 32 distinctive places from left to correct and 32 distinctive places from the top to upper that the kernel can hold. Based on these locations, each function in the output will comprise $32 \times 32 ((N - k + 1) \times (N - k + 1))$ components. To achieve a single component in a single output, multiplier activities between two components, i.e., $input = (k \times k \times D)$ and $kernel = (k \times k \times D)$, are needed for each place in the sliding window method.

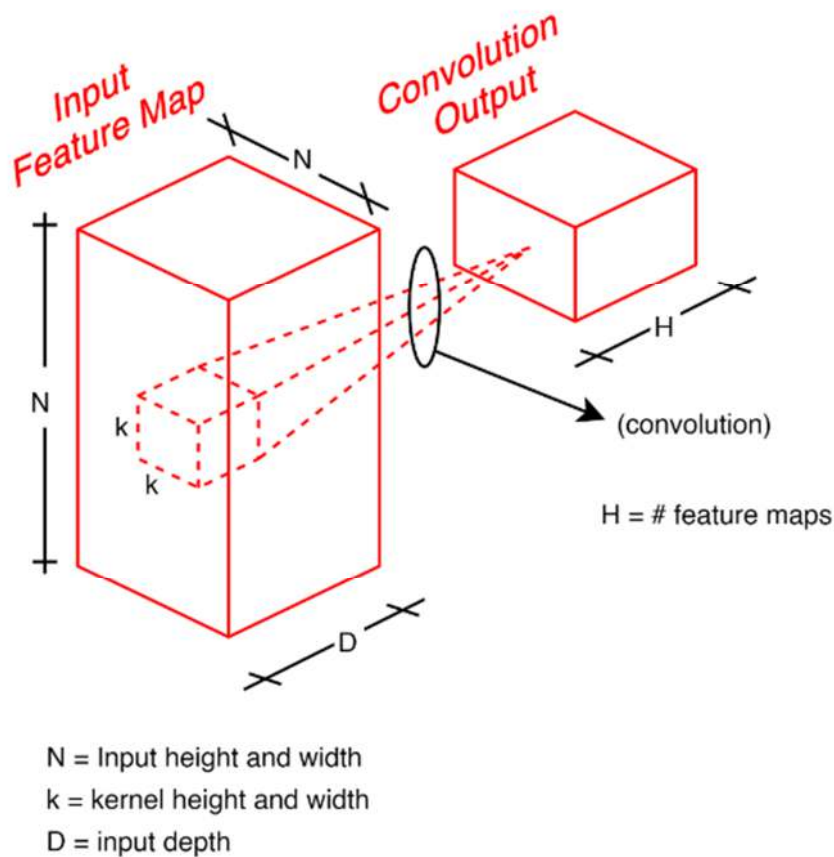


Figure 6.3. Convolutional process representation [93].

Figure 6.4 illustrates the filters and feature maps represented as a neuron in a convolutional layer. The same color links are applied in Figure 6.4 limited to

always having the same weight. This can be achieved by initializing all the connections within a group with the same weights and by always averaging a group's weight updates before applying them at the end of each backpropagation iteration. This filter produces the output layer of the function map. A neuron is triggered in the feature map where a filter is identified at the respective place in the prior layer to contribute to its activities.

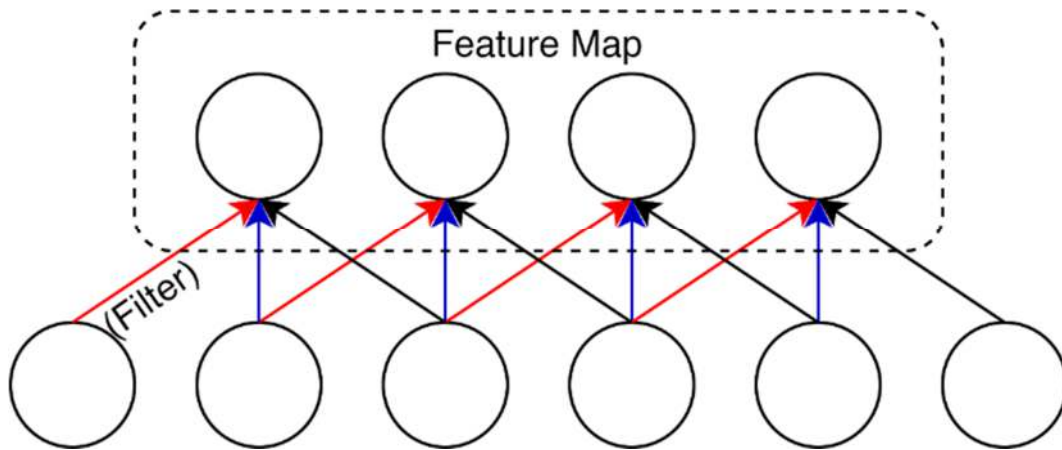


Figure 6.4. Filters and maps represented as neurons in a convolutional layer [93].

6.3 Anomalies in Industrial Medium-Voltage Power System Networks

An event in the electrical system, such as ground fault, phase fault, start or cease of electrical machines, and network topology changes have their own symptoms. These symptoms are categorized based on the electrical parameters, i.e., frequency, current flow, and voltage. As an illustration, during an SC fault, the closest source feeder relay to the fault location will experience a drop voltage, followed by an increasing current flow and frequency rate at the source side. Meanwhile, in the MS event, the feeder may sense a dip voltage, surge current, and frequency drop. The two events are clearly different even though the symptoms of the voltage and current are similar.

In the fault conditions, the CB is required to trip, whereas during the MS event, it is prohibited to trip. However, due to an improper setting, a record of CB trip is found during the MS event. This case happens quite often in most petrochemical or oil and gas companies [41]. The root causes for such a condition are because multi-function relays are installed with a default setting and the in-rush condition is not considered. As a containment action, engineers usually broaden or

disable the setting to anticipate the drop voltage or surge current during the MS event. This action comes with a risk, wherein a relay may not trip when the SC occurs during the start process. To validate this hypothesis, time series data are gathered using a commercial software called ETAP in a transient stability domain.

To set the simulation, the sequence of event is divided into three domains: PRE-event, ON-event, and POST-event [48].

To visualize the time domains, Figure 6.5 presents the voltage, frequency, and current measurements of a feeder that suffers an SC condition at $t = +1$ s.

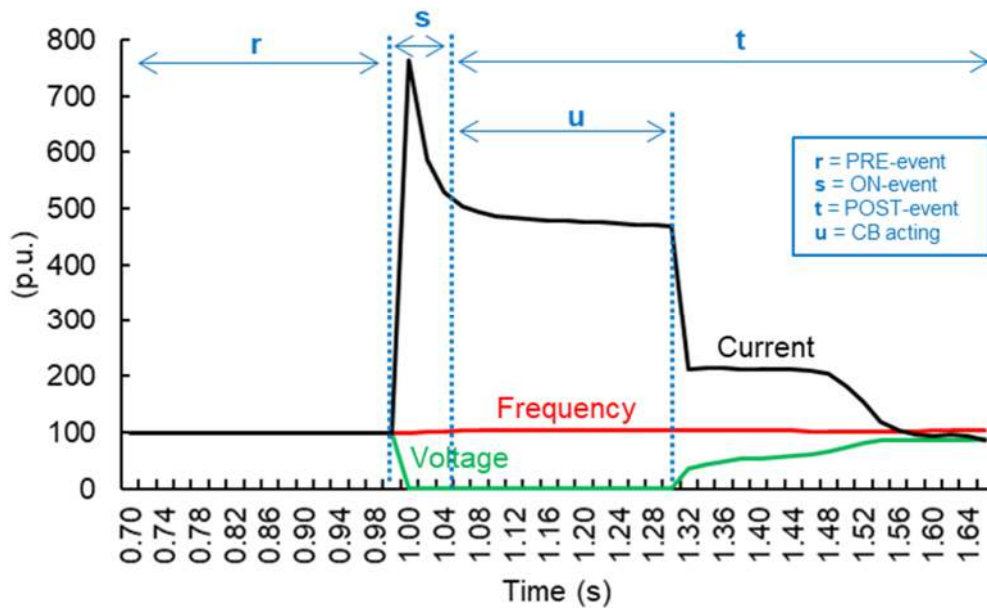


Figure 6.5. Sequence of events in the power system in terms of the voltage, frequency, and current flows.

As shown in Figure 6.5, the PRE-event is the state where there is no switching condition. That is, this domain happens before $t = 1$ s and might be stated as a normal or basis condition. Meanwhile, the ON-event is the state just after the switching. In this domain, the event happens without any controller reacting to overcome the events. The ON-event occurs at $t = +1$ s until any reactions or following events occur. Accordingly, the IPA must take action or decide during this time-domain. The POST-event is any event that happens with regard to the previous events. It could be an opening of a CB with the intention to clear the fault. However, in this POST-event, the system might go unstable or be stable. This condition most likely depends on the length of time required for the CB to react.

6.4 Proposed IPA Architecture and Working Principles

6.4.1 Relay Architecture

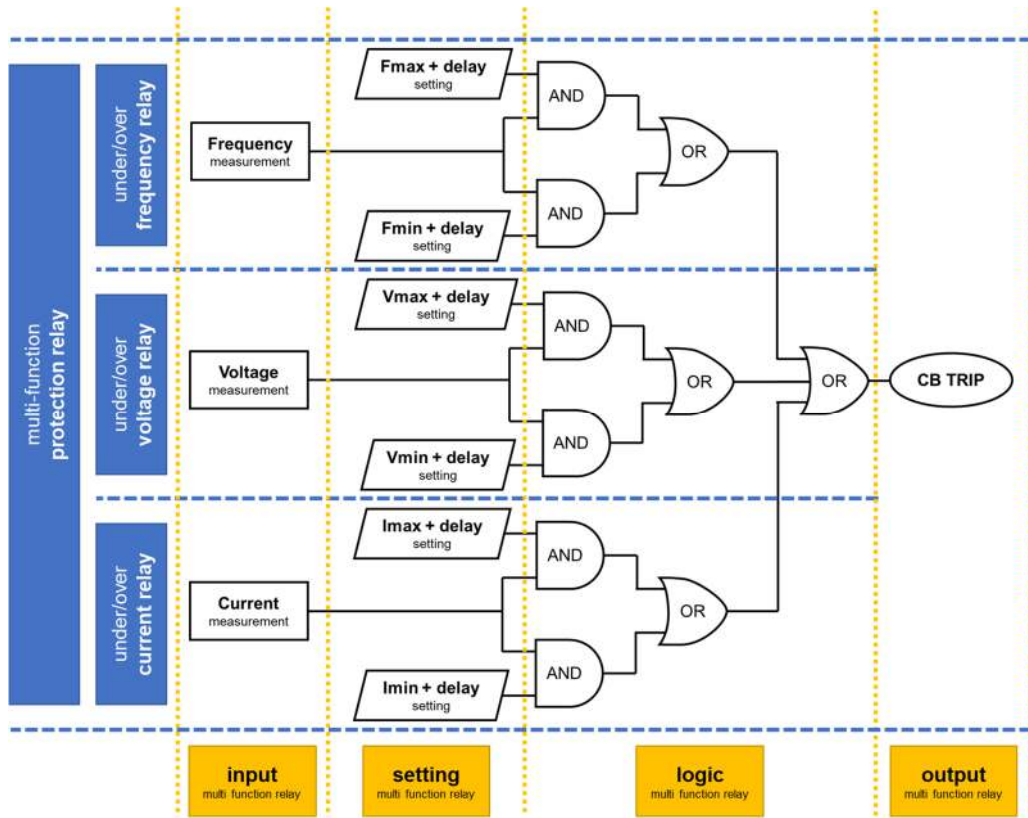
The state of the art of the multi-parameter IPA is framed in a relay with the ability to determine whether it senses a fault condition or not. Figure 6.6 shows the architecture comparison between the conventional relay (Figure 6.6.a) and proposed IPA (Figure 6.6.b). The IPA is activated based on a classifier and determinant at the end of the monitoring and logic process.

6.4.2 Working Principles

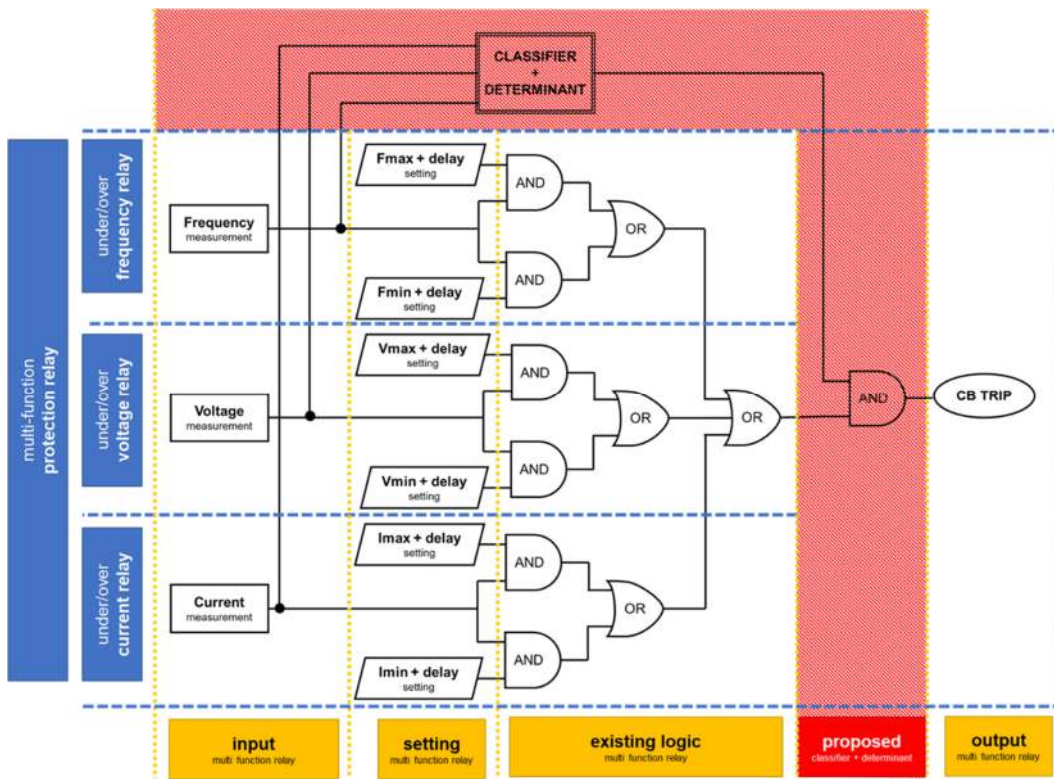
IPA is developed from the conventional relay. The conventional relay's working principle is depicted on Figure 6.7.a. The proposed method works in parallel with the conventional method to enhance the trip decision while mentioning the symptoms from the classifier, as shown in Figure 6.7.b.

In a conventional relay, the analog reading is converted into a digital logic with a specific threshold of the electrical parameters, such as V, f, and I. If one of the thresholds is violated, then the timer will start counting until a specific delay time is predetermined. Then, after the electrical threshold and time delay are passed, then the relay will send the command to trip the CB. This veracity inspired the improvement of conventional relays.

In the proposed IPA, an additional process is appended in parallel with a purpose of classifying symptoms based on analog readings. If the symptom is a part of the fault condition and the threshold and time delay of the relay are passed, then the relay is allowed to send a signal trip to the CB. Based on this idea, it is expected that the proposed IPA can minimize the fault trip caused by the spike of V, f, and I, which are not categorized as a fault condition.



(a)



(b)

Figure 6.6. State of the art: Comparison of the block diagram on the (a) existing available relay on the market and (b) the proposed IPA.

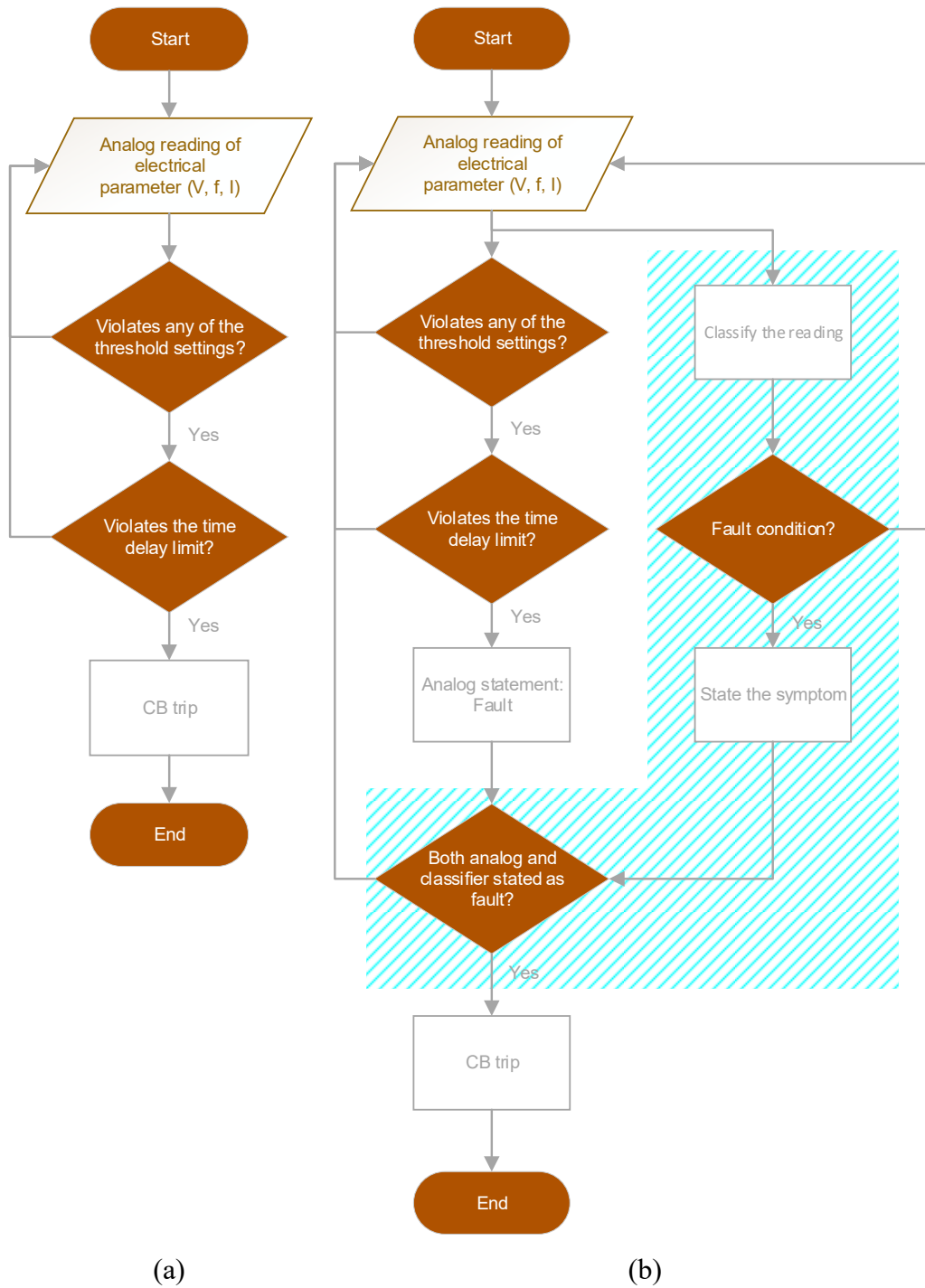


Figure 6.7. Working principle flowchart of (a) the conventional relay and (b) proposed IPA.

6.5 Simulation Performance

6.5.1 Testing Bench

A simple power system consists of two generators, where one of them is considered a DG. The main transfer bus of this system is an 11 kV that is connected into four different feeders. Every feeder on this system is equipped with a relay that can observe the voltage (V), frequency (f), and current flow (I) in rms. The relay IDs are A–F, as shown in the SLD (Figure 6.8).

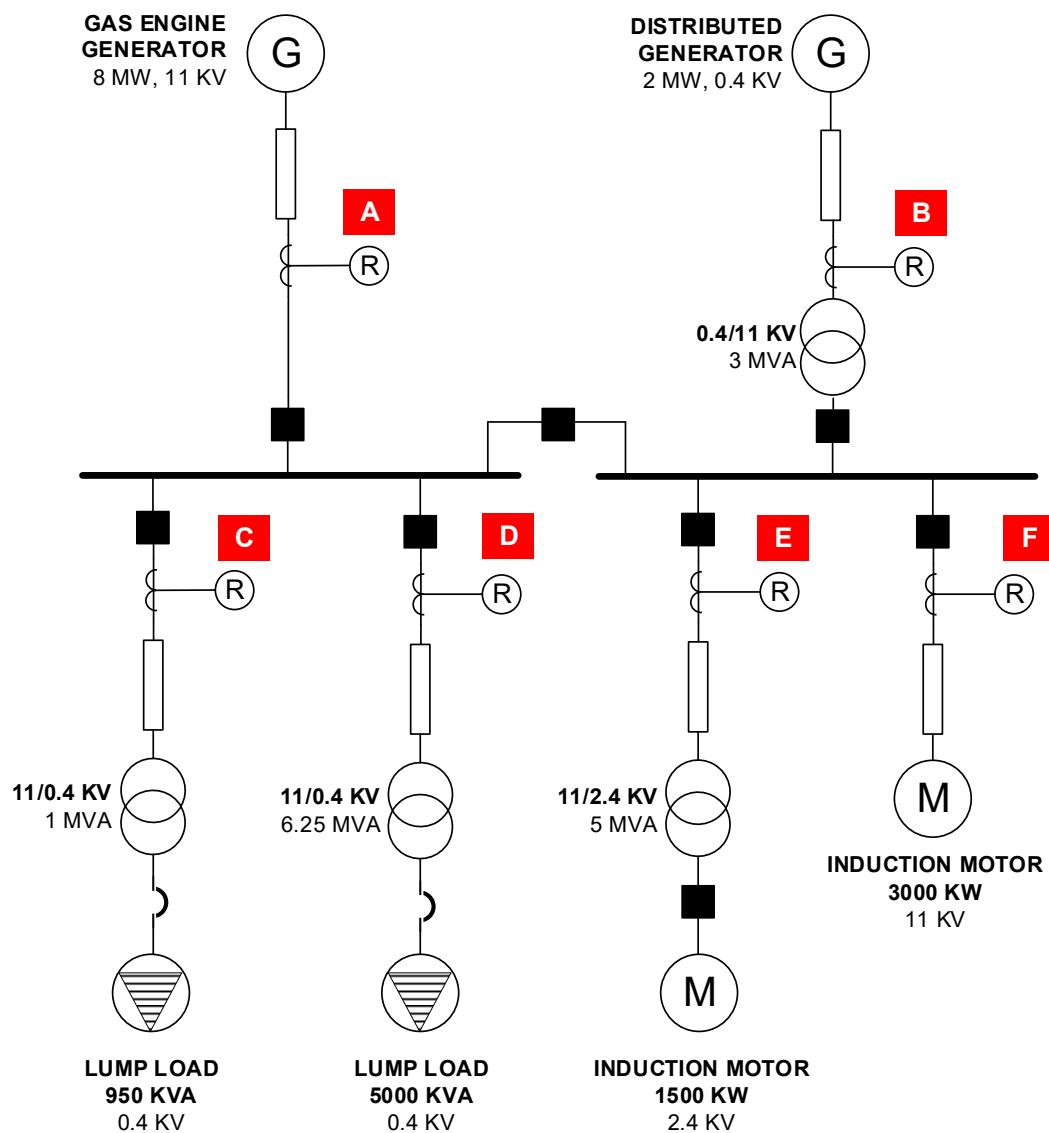


Figure 6.8. SLD used for the simulation and data gathering.

Several loads are connected to the main bus of 11 kV. However, this study is focused on the 11 kV events only. The following situations are taken into consideration:

1. Normal condition
2. Three-phase symmetrical (LLL) fault of phase a–b–c at 11 kV
3. Line-to-line (LL) fault of phase a–b at 11 kV
4. Line-to-ground (LG) fault of phase a–b at 11 kV
5. Event of DG outage
6. DOL MS of a 3000 kW induction machine

These six situations will be simulated under several circumstances, such as DG penetration and total load connection.

6.5.2 Data Collection

As stated in Section 6.3, the most crucial part in electrical circumstances is the ON-event. Therefore, by considering that the relay sampling is one cycle (equal to 20 ms for a 50 Hz system) and the relay must react within five cycles, the data consist of five samplings, which are constructed by the PRE-event and ON-event, as shown in Figure 6.9.

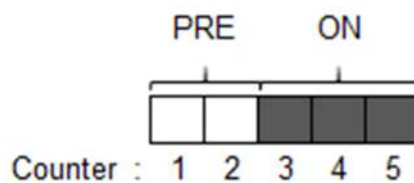


Figure 6.9. Visualization of the data required to be trained in CNN.

Assuming there are five rows of data to be recognized by the CNN. Then, the first two data consist of the PRE-event data or the normal (basis) condition. When the event occurs, a deviation occurs between the PRE- and ON-events. Using the SLD, as shown in Figure 6.8, the whole relay on the system is assumed to measure the current, voltage, and frequency. Each phase on every feeder is measured in terms of the voltage and current flows in rms, whereas the frequency

is measured only in a single phase. The illustration of the data measurement is shown in Figure 6.10.

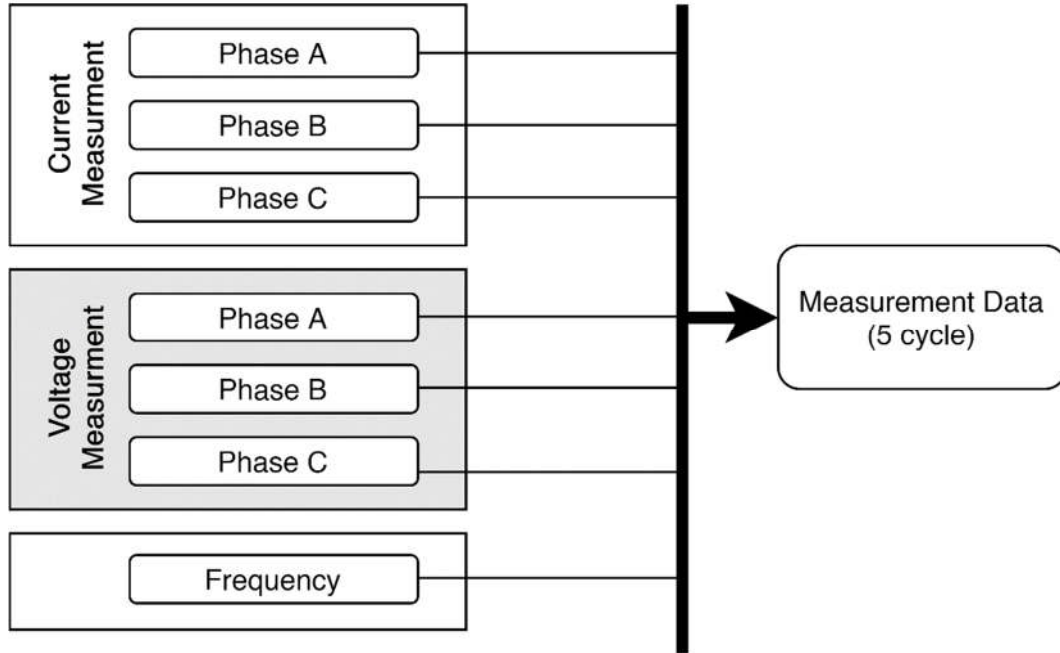
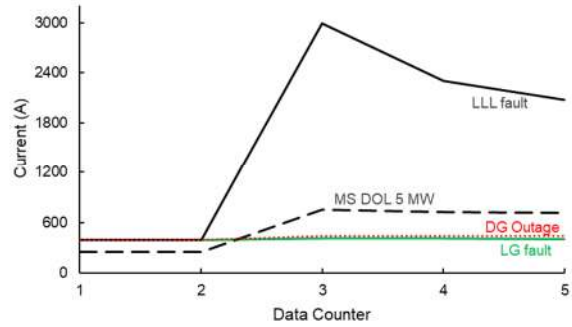
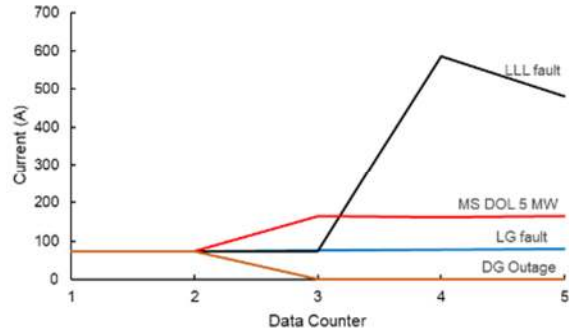


Figure 6.10. Practical measurement data from the simulation.

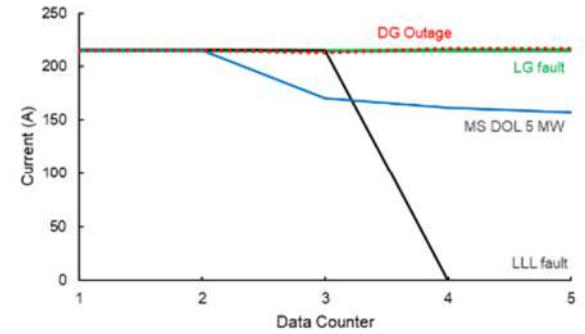
Generally, there are two types of feeders, as shown in Figure 6.8. The upper side of the 11 kV bus is called a source feeder, whereas the lower side is the load feeder. Figure 6.11 shows the illustration of the current reading for the whole relay with a variety of conditions, as stated in Section 6.3. Moreover, Figure 6.12 shows the illustration of the voltage and frequency readings in accordance with the data counter. In total, 193 symptoms are constructed based on the combination of the power system operations and events.



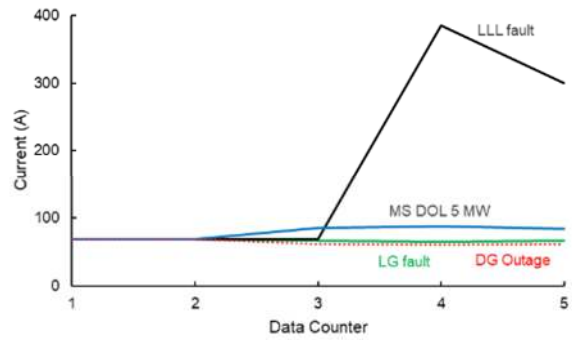
(a) Current reading on Relay A



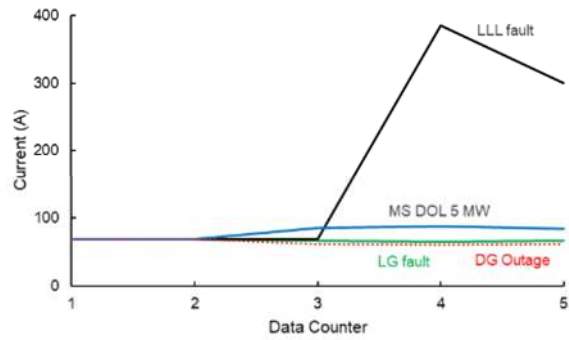
(b) Current reading on Relay B



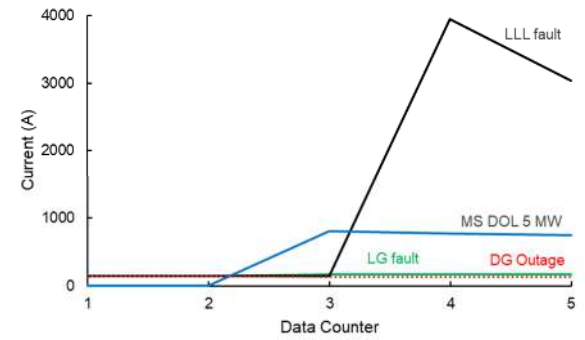
(c) Current reading on Relay C



(d) Current reading on relay D

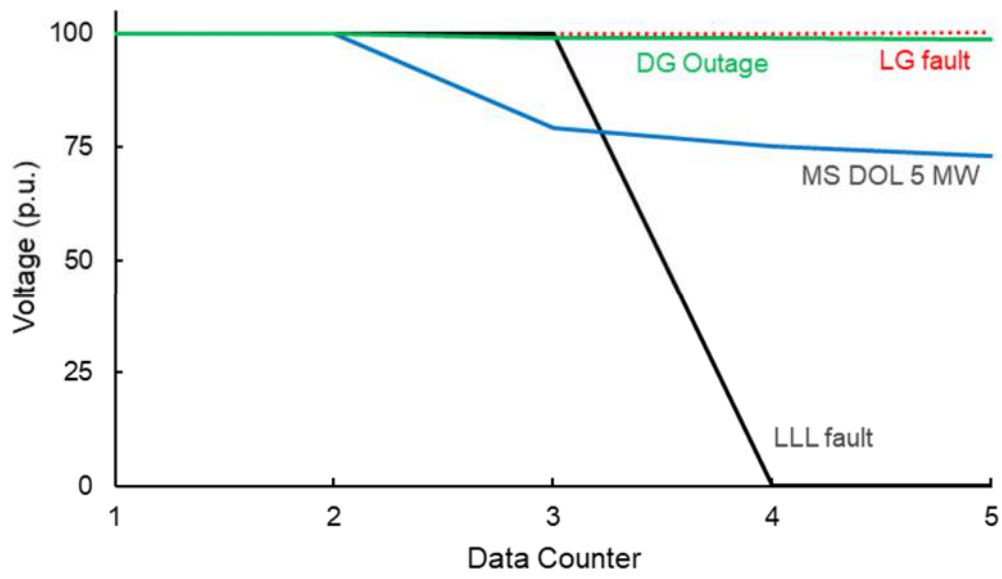


(e) Current reading on Relay E

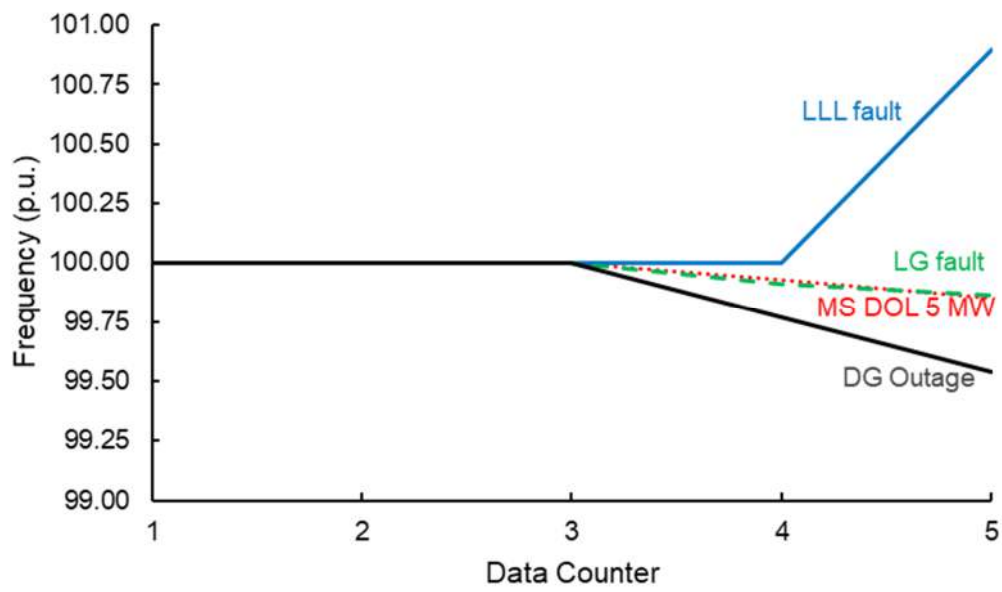


(f) Current reading on Relay F

Figure 6.11. Current reading on each relay with varying events in the 11 kV bus: LG fault, LLL fault, DG outage, and MS.



(a)



(b)

Figure 6.12. Voltage (a) and frequency (b) readings on each relay with varying events in the 11 kV bus: LG fault, LLL fault, DG outage, and MS.

6.5.3 Parameter Analysis per Events: Current Trends

Relays A and B can be grouped under the source feeder relay. As shown in Figure 6.11.a and Figure 6.11.b, there is a tremendous current spike when the LLL fault occurs. The other current surge occurs when there is an MS event. When DG outage is performed, the minor current increase is recorded in Relay A, whereas the current in Relay B reaches zero. When the LG fault happens, Relays A and B only sense a tiny deviation in terms of the current reading.

Relays C and D operate as a feeder-type relay. The immense current drop occurs when the LLL fault happens due to the source feeding to the load during the fault. A small current decrement happens during the MS event. During the DG outage and LG fault, no current variation occurs on the feeder line.

Relays E and F belong to an induction machine that operates on 2.4 and 11 kV. During the LLL fault, both relays sense a huge current spike as the motor acts as a generator that feeds the current to the fault location. A current spike also occurs during the MS event.

6.5.4 Parameter Analysis per Event: Voltage and Frequency Trends

Because all the relays are connected in parallel to the 11 kV bus, the voltage reading of all the six relays must be the same. Figure 6.12.a shows that the voltage collapse immensely happens during the LLL fault. A voltage collapse condition also happens during the MS event, but not as severe as the LLL fault. In the event of a DG outage, the voltage reading shows if there is no deviation compared to the PRE-event condition. Nonetheless, there is a minor increment of voltage during the LG fault.

Similar to the voltage measurement, the frequency reading only needs a one-perspective measurement because the system is fully synchronized. Figure 6.12.b shows that the major frequency collapse happens during the DG outage. A minor frequency collapse also happens when there are MS and LG fault. Meanwhile, during an LLL fault, the frequency dramatically increases.

6.5.5 Implementation of CNNs

The network input of a 135×35 matrix is considered a single-data channel. The first layer, C1, conducts four input conversions with 2×2 kernels, creating four

function maps of size 133×33 . The second layer, C2, executes 2×2 kernels. The information is rescaled to suit the Keras sequential model's 3D input criteria. For a simple univariate model, the input form is 35-time stages with one feature. In the convolutional layer, the sequence is not divided into several subsequences, but rather 32-time stages. Six neurons in the thick layer generate six outputs.

One of the most popular recurring neural network (RNN) models is LSTM. Figure 6.13 shows the schematic of LSTM. The notation σ implies as a sigmoid feature. There are three basic gates on LSTM: 1) an input, 2) an output, and 3) forget gates. The procedure operation among the three doors allows LSTM to fix long-term dependencies, which is not learned by particular RNNs.

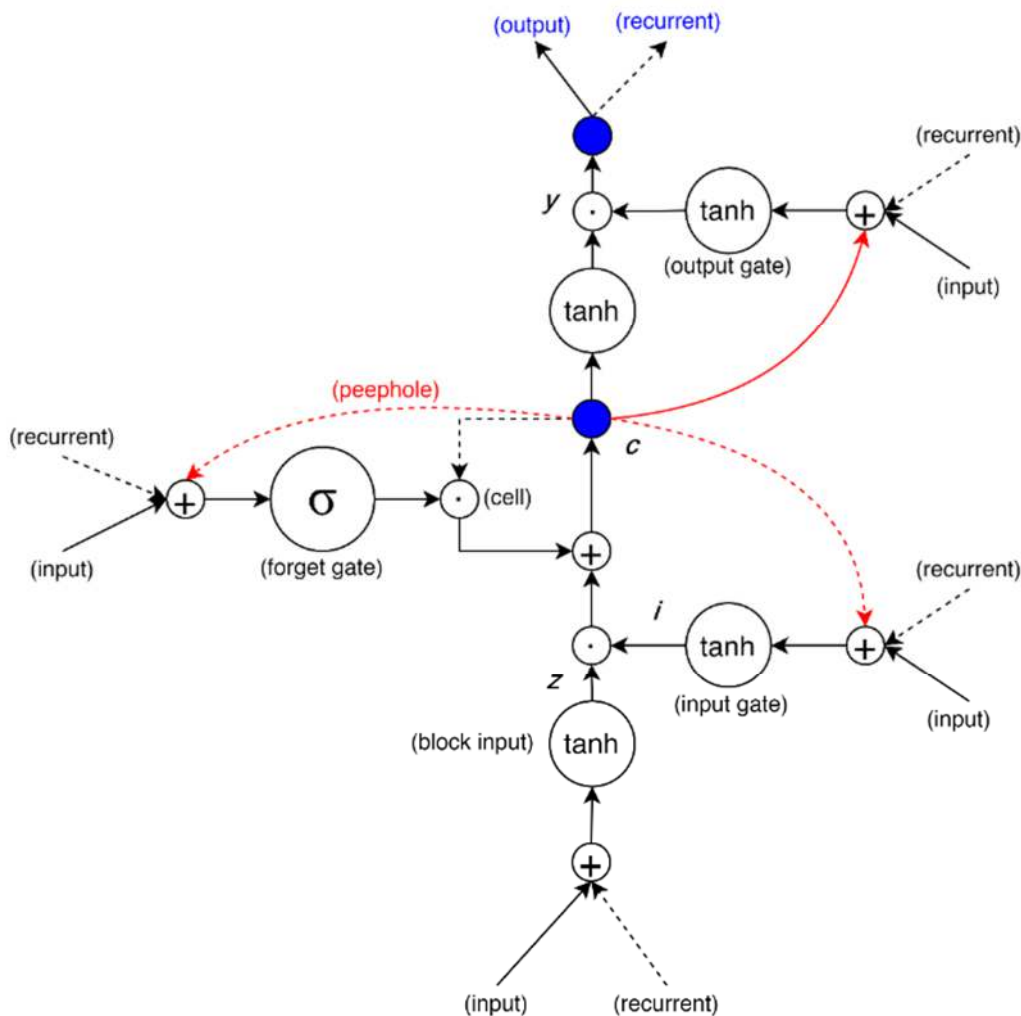


Figure 6.13. LSTM block.

In Keras, CNN and LSTM can be defined for training. A CNN–LSTM can be described by bringing the first layer of CNN layers, and the second layer is composed of LSTM layers with a dense layer at the output layer. This architecture should be considered when defining two sub-models, i.e., the CNN model for feature extraction and the LSTM model for feature analysis over time phases. Figure 6.14 depicts the illustration of the feeding process from the CNN to LSTM, and the architecture based on CNN is summarized in Table 6.1. CNN-based architecture. Figure 6.15 shows the Keras sequential model.

Table 6.1. CNN-based architecture

Layer	Kernel/Pooling Window	Layer Size
Input	-	1@135x35
LSTM (C1)	[32@2X2]	32@133X33
LSTM (C2)	[32@2x2]	32@122X31
LSTM (C3)	[32@2X2]	32@110X9
Dense (P2)	[6@2X2]	6@58
Full out (F1)	-	58

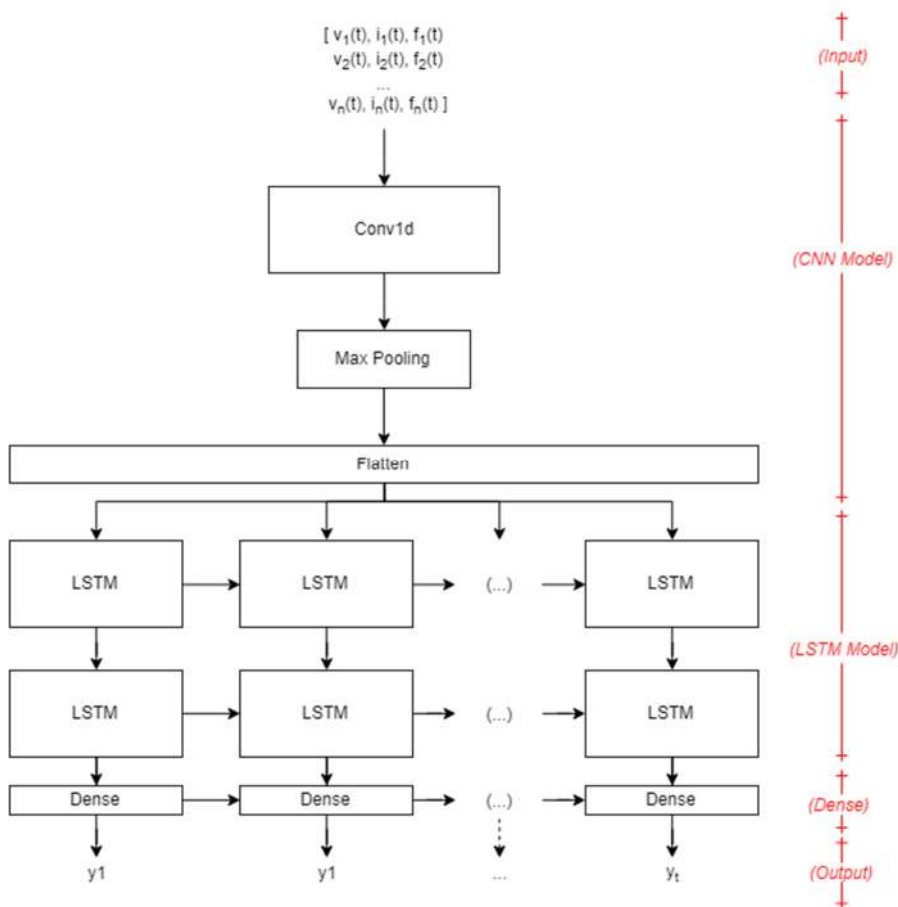


Figure 6.14. Feeding process to LSTM layers.

```

from keras.layers import (
    Activation, Flatten, Dropout, LSTM,
    Dense,

model.add(LSTM(32, return_sequences=True,
               input_shape=(35, 1)))
model.add(LSTM(32, return_sequences=True))
model.add(LSTM(32))
model.add(Dense(6, activation='softmax'))

model.compile(loss='categorical_crossentropy', optimizer='adam', metrics=['acc'])
model.summary()

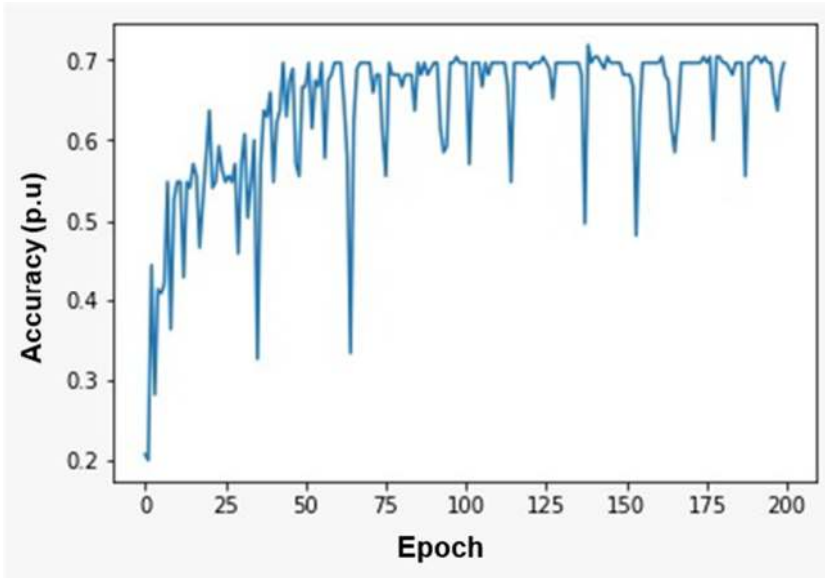
```

Figure 6.15. Keras sequential model.

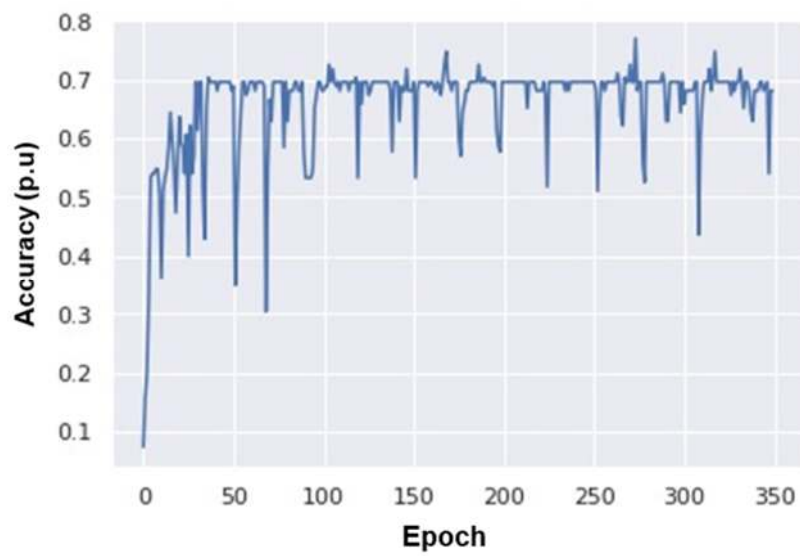
6.6 Results and Discussion

Figure 6.16 shows the experimental results of the proposed CNN to recognize the symptoms of power system operations. The model with 200 epochs could reach 69% accuracy, as shown in Figure 6.16.a.

When the epoch is increased to 350, there is an accuracy improvement that reaches 79% at epoch 275, as depicted in Figure 6.16.b. This result is later confirmed by the heatmap of the dataset of features 1–35 (x-axis) with the value of each feature per rows (y-axis), as shown in Figure 6.17. The results clearly indicate that the CNN and LSTM can not only generalize but also memorize the pattern. Furthermore, the CNN and LSTM may be helpful in supervising power system operations.



(a)



(b)

Figure 6.16. Trial results of the CNN in recognizing the symptoms of power system operations: (a) 200 epochs and (b) 275 epochs.

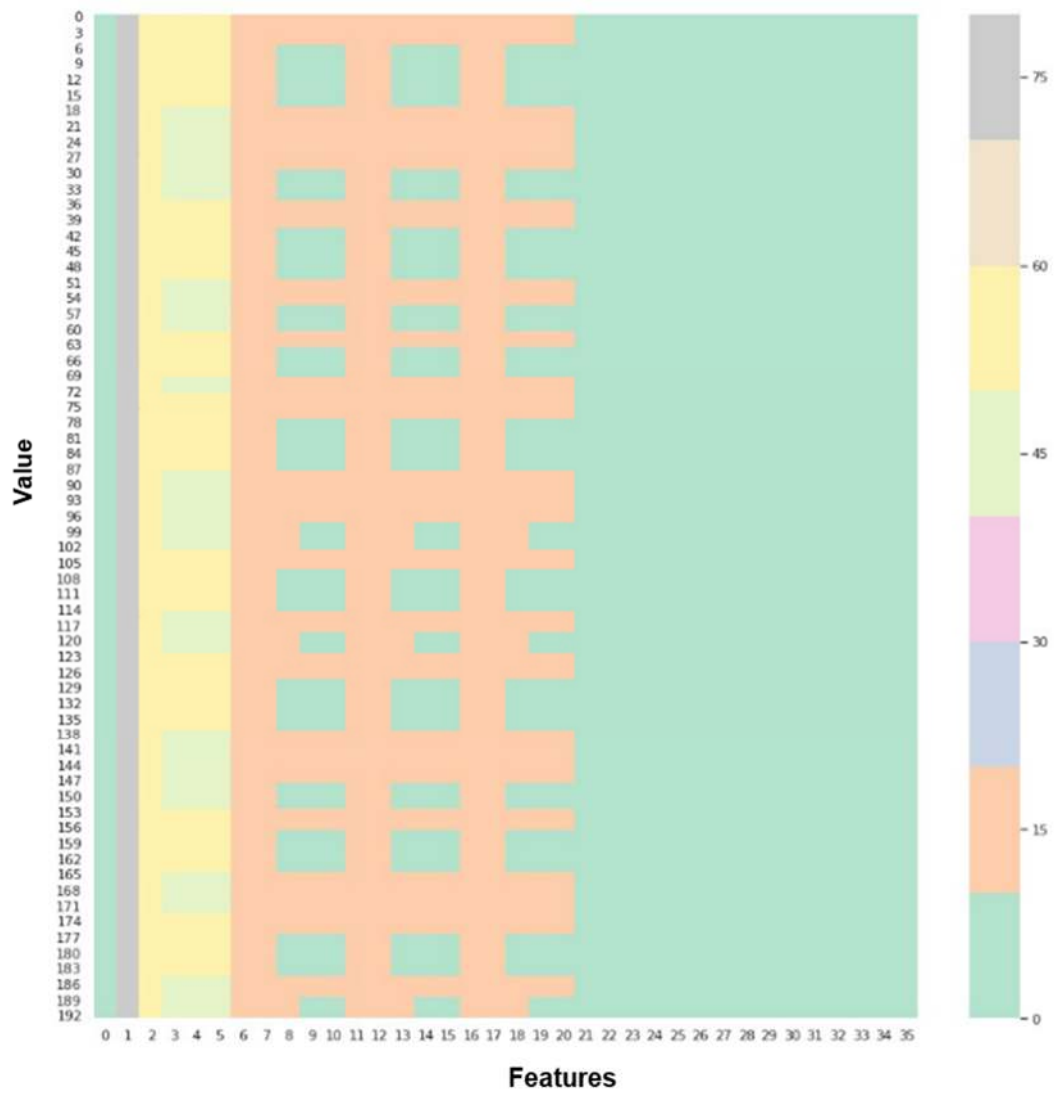


Figure 6.17. Heatmap dataset.

CHAPTER 7

CONCLUSIONS

This chapter summarizes the major findings and recommendations presented in this dissertation. Then, it discusses the implications of this study, including the theory of utilizing adequate and diversified resources to increase the overall efficiency.

7.1 Concluding Remarks

In this dissertation, investigations are performed to identify the possible causes of a problem with the power system network that involves an incorrect setting of the protection relay. Changes in the operation principle and network topology due to the power system maneuver affect the coordination function of the protection system.

To obtain the adequate setting for protection relays, a recognition of the protected equipment (e.g., induction machines, transformers, and generators) is required. If the protection relay fails to recognize the equipment being protected, then false trips due to relays might occur and lead to economic loss.

The time–current relation (i.e., damage curve, thermal limit, and starting in-rush current) of the protected equipment can be used as a constraint during the relay setting optimization process to avoid a false trip by the protection relay. In some cases, the utilization of the inverse-time function (ANSI 51) cannot reach the minimum tripping time. Thus, the combination of the inverse-time (ANSI 51) and definite-time (ANSI 50) functions is required to make the relay more sensitive and accurate.

The inclusion of RESs, which are distributed in a power system network, reduces the power system’s reliability if the enhancement of the protection system (i.e., applying multiple setting scenarios and improving the capability to detect and mitigate possible fault scenarios) is not followed. Moreover, under some circumstances, such as high penetration of IBR in a distribution network, the relay may fail to detect SC faults due to the low fault contribution from the IBR. To overcome this issue, a 3D voltage–current–time model is introduced with an expectation to increase the protection relay capability in estimating fault location in

a distribution system. Furthermore, along with the capability of estimating the fault location, the coordination function can be improved to determine the primary and backup protections for each fault location. The sensitivity of protection relays under distribution networks with high IBR penetration can be improved by aiding the voltage function in the overcurrent-based protection. Moreover, power system events can be categorized into symptoms, which later can be classified with the help of AI. The ability of protection relays to classify power system events can be used as an additional determiner before sending a tripping signal to the CB.

7.2 Suggestions for Future Research

The future studies for the topic discussed in this dissertation can be generally enhanced by following some recommendations:

1. Further experiments using the point-on-wave rather than RMS-based simulation software to attain more precise data can be conducted, which will be useful in the observation.
2. Observations on the voltage angle parameter under some power system events (e.g., SCs, power swings, and power outages) can uncover a new approach to classify the symptoms of power system events. Accordingly, the symptoms can be used as inputs to the AI for classification and identification purposes.
3. To accurately observe relay responses on multi-parameter readings, simulations using the hardware-in-loop module are recommended.
4. The creation of a protection relay prototype shall comply with the IEC 61850 protocol.
5. Real-time fault analyses can be conducted to observe parameters related to the fault mitigation and detection.
6. The computation or processing time in relays can be improved by employing advanced methods or techniques.

REFERENCES

- [1] K. Schwab, *The Fourth Industrial Revolution*. Penguin UK, 2017.
- [2] NERC, “State of Reliability 2018.” North American Electric Reliability Corporation (NERC), Jun. 2018. [Online]. Available: https://www.nerc.com/pa/rapa/pa/performance%20analysis%20dl/nerc_2018_sor_06202018_final.pdf
- [3] “IEEE Recommended Practice for Industrial and Commercial Power Systems Analysis (Brown Book),” *IEEE Std 399-1997*, pp. 1–488, Aug. 1998, doi: 10.1109/IEEESTD.1998.88568.
- [4] “IEEE Recommended Practice for Protection and Coordination of Industrial and Commercial Power Systems (IEEE Buff Book),” *IEEE Std 242-2001 (Revision of IEEE Std 242-1986) [IEEE Buff Book]*, pp. 1–710, Dec. 2001, doi: 10.1109/IEEESTD.2001.93369.
- [5] “IEEE Recommended Practice for the Design of Reliable Industrial and Commercial Power Systems,” *IEEE Std 493-2007 (Revision of IEEE Std 493-1997) - Redline*, pp. 1–426, Jun. 2007.
- [6] “IEEE Recommended Practice for Bus and Switchgear Protection in Industrial and Commercial Power Systems,” *IEEE Std 3004.11-2019*, pp. 1–63, Oct. 2019, doi: 10.1109/IEEESTD.2019.8870292.
- [7] “IEC International Standard for Measuring relays and protection equipment – Part 151: Functional requirements for over/under current protection,” *IEC 60255-151*, pp. 1–68, Aug. 2009.
- [8] A. Gupta and D. Bhattacharya, “Generator Differential Relay Trip on an Offshore Platform: Copyright Material IEEE, Paper No. PCIC-2018-09,” in *2018 IEEE Petroleum and Chemical Industry Technical Conference (PCIC)*, Sep. 2018, pp. 73–82. doi: 10.1109/PCIC31437.2018.9080472.
- [9] V. Gevorgian, E. Muljadi, Y. Luo, M. Mohanpurkar, R. Hovsapien, and V. Koritarov, “Supercapacitor to provide ancillary services,” in *2017 IEEE Energy Conversion Congress and Exposition (ECCE)*, Oct. 2017, pp. 1030–1036. doi: 10.1109/ECCE.2017.8095900.
- [10] H. Mortazavi, H. Mehrjerdi, M. Saad, S. Lefebvre, D. Asber, and L. Lenoir, “A Monitoring Technique for Reversed Power Flow Detection With High PV Penetration Level,” *IEEE Transactions on Smart Grid*, vol. 6, no. 5, pp. 2221–2232, Sep. 2015, doi: 10.1109/TSG.2015.2397887.
- [11] M. Hasheminamin, V. G. Agelidis, V. Salehi, R. Teodorescu, and B. Hredzak, “Index-Based Assessment of Voltage Rise and Reverse Power Flow Phenomena in a Distribution Feeder Under High PV Penetration,” *IEEE Journal of Photovoltaics*, vol. 5, no. 4, pp. 1158–1168, Jul. 2015, doi: 10.1109/JPHOTOV.2015.2417753.
- [12] J. Kim, E. Muljadi, V. Gevorgian, and A. F. Hoke, “Dynamic Capabilities of an Energy Storage-Embedded DFIG System,” *IEEE Transactions on*

- Industry Applications*, vol. 55, no. 4, pp. 4124–4134, Jul. 2019, doi: 10.1109/TIA.2019.2904932.
- [13] X. Liang and C. Andalib -Bin- Karim, “Harmonics and Mitigation Techniques Through Advanced Control in Grid-Connected Renewable Energy Sources: A Review,” *IEEE Transactions on Industry Applications*, vol. 54, no. 4, pp. 3100–3111, Jul. 2018, doi: 10.1109/TIA.2018.2823680.
- [14] E. Muljadi, N. Samaan, V. Gevorgian, J. Li, and S. Pasupulati, “Different Factors Affecting Short Circuit Behavior of a Wind Power Plant,” *IEEE Transactions on Industry Applications*, vol. 49, no. 1, pp. 284–292, Jan. 2013, doi: 10.1109/TIA.2012.2228831.
- [15] A. Hooshyar and R. Iravani, “Microgrid Protection,” *Proceedings of the IEEE*, vol. 105, no. 7, pp. 1332–1353, Jul. 2017, doi: 10.1109/JPROC.2017.2669342.
- [16] A. J. Urdaneta, R. Nadira, and L. G. Perez Jimenez, “Optimal coordination of directional overcurrent relays in interconnected power systems,” *IEEE Transactions on Power Delivery*, vol. 3, no. 3, pp. 903–911, Jul. 1988, doi: 10.1109/61.193867.
- [17] “Computer representation of overcurrent relay characteristics,” *IEEE Transactions on Power Delivery*, vol. 4, no. 3, pp. 1659–1667, Jul. 1989, doi: 10.1109/61.32656.
- [18] C. S. Mardegan and R. Rifaat, “Considerations in Applying IEEE Recommended Practice for Protection Coordination in Industrial and Commercial Power Systems—Part I,” *IEEE Transactions on Industry Applications*, vol. 52, no. 5, pp. 3705–3713, Sep. 2016, doi: 10.1109/TIA.2016.2563405.
- [19] J. D. Pico, D. Celeita, and G. Ramos, “Protection Coordination Analysis Under a Real-Time Architecture for Industrial Distribution Systems Based on the Std IEEE 242-2001,” *IEEE Transactions on Industry Applications*, vol. 52, no. 4, pp. 2826–2833, Jul. 2016, doi: 10.1109/TIA.2016.2538739.
- [20] A. Tjahjono *et al.*, “Adaptive modified firefly algorithm for optimal coordination of overcurrent relays,” *Transmission Distribution IET Generation*, vol. 11, no. 10, pp. 2575–2585, 2017, doi: 10.1049/iet-gtd.2016.1563.
- [21] R. M. Chabanloo and N. Mohammadzadeh, “A fast numerical method for optimal coordination of overcurrent relays in the presence of transient fault current,” *Transmission Distribution IET Generation*, vol. 12, no. 2, pp. 472–481, 2018, doi: 10.1049/iet-gtd.2017.0055.
- [22] P. A. Gaynor, A. Abu Zaid, M. Hazmi, and T. Gari, “Protective Relay Coordination Study at a Petrochemical Complex,” in *2019 IEEE Petroleum and Chemical Industry Committee Conference (PCIC)*, Sep. 2019, pp. 359–368. doi: 10.1109/PCIC30934.2019.9074540.
- [23] N. El-Naily, S. M. Saad, T. Hussein, and F. A. Mohamed, “A novel constraint and non-standard characteristics for optimal over-current relays

- coordination to enhance microgrid protection scheme,” *Transmission Distribution IET Generation*, vol. 13, no. 6, pp. 780–793, 2019, doi: 10.1049/iet-gtd.2018.5021.
- [24] S. Saad M., “A new constraint considering maximum PSM of industrial over-current relays to enhance the performance of the optimization techniques for microgrid protection schemes - ScienceDirect,” *Sustainable Cities and Society*, vol. 44, pp. 445–457, Jan. 2019, doi: <https://doi.org/10.1016/j.scs.2018.09.030>.
- [25] M. Ghotbi Maleki, R. Mohammadi Chabanloo, and M. Farrokhifar, “Accurate coordination method based on the dynamic model of overcurrent relay for industrial power networks taking contribution of induction motors into account,” *Transmission Distribution IET Generation*, vol. 14, no. 4, pp. 645–655, 2020, doi: 10.1049/iet-gtd.2019.0325.
- [26] R. C. Dugan and T. E. McDermott, “Operating conflicts for distributed generation on distribution systems,” in *2001 Rural Electric Power Conference. Papers Presented at the 45th Annual Conference (Cat. No.01CH37214)*, Apr. 2001, p. A3/1-A3/6. doi: 10.1109/REPCON.2001.949511.
- [27] T. Ackermann, G. Andersson, and L. Söder, “Distributed generation: a definition,” *Electric Power Systems Research*, vol. 57, no. 3, pp. 195–204, 2001, doi: [https://doi.org/10.1016/S0378-7796\(01\)00101-8](https://doi.org/10.1016/S0378-7796(01)00101-8).
- [28] M. Dewadasa, A. Ghosh, G. Ledwich, and M. Wishart, “Fault isolation in distributed generation connected distribution networks,” *IET Generation, Transmission Distribution*, vol. 5, no. 10, pp. 1053–1061, Oct. 2011, doi: 10.1049/iet-gtd.2010.0735.
- [29] A. Ukil, B. Deck, and V. H. Shah, “Current-Only Directional Overcurrent Protection for Distribution Automation: Challenges and Solutions,” *IEEE Transactions on Smart Grid*, vol. 3, no. 4, pp. 1687–1694, Dec. 2012, doi: 10.1109/TSG.2012.2208127.
- [30] A. Al-Riyami, K. Burt, G. Manhangwe, P. Pretlove, and S. Georgiopoulos, “An investigation into alternatives to directional overcurrent protection on grid transformers to improve the network capacity to accommodate reverse power flow,” in *12th IET International Conference on Developments in Power System Protection (DPSP 2014)*, Mar. 2014, pp. 1–6. doi: 10.1049/cp.2014.0159.
- [31] F. B. Costa, A. Monti, and S. C. Paiva, “Overcurrent Protection in Distribution Systems With Distributed Generation Based on the Real-Time Boundary Wavelet Transform,” *IEEE Transactions on Power Delivery*, vol. 32, no. 1, pp. 462–473, Feb. 2017, doi: 10.1109/TPWRD.2015.2509460.
- [32] M. G. Maleki, R. M. Chabanloo, and H. Javadi, “Method to resolve false trip of non-directional overcurrent relays in radial networks equipped with distributed generators,” *Transmission Distribution IET Generation*, vol. 13, no. 4, pp. 485–494, 2019, doi: 10.1049/iet-gtd.2018.5610.

- [33] A. A. Balyith, H. M. Sharaf, M. Shaaban, E. F. El-Saadany, and H. H. Zeineldin, "Non-Communication Based Time-Current-Voltage Dual Setting Directional Overcurrent Protection for Radial Distribution Systems With DG," *IEEE Access*, vol. 8, pp. 190572–190581, 2020, doi: 10.1109/ACCESS.2020.3029818.
- [34] L. Jenkins, H. P. Khincha, S. Shivakumar, and P. K. Dash, "An application of functional dependencies to the topological analysis of protection schemes," *IEEE Transactions on Power Delivery*, vol. 7, no. 1, pp. 77–83, Jan. 1992, doi: 10.1109/61.108892.
- [35] M. Abdi-Khorsand and V. Vittal, "Modeling Protection Systems in Time-Domain Simulations: A New Method to Detect Mis-Operating Relays for Unstable Power Swings," *IEEE Transactions on Power Systems*, vol. 32, no. 4, pp. 2790–2798, Jul. 2017, doi: 10.1109/TPWRS.2016.2628726.
- [36] D. F. C. Rodriguez, J. D. P. Osorio, and G. Ramos, "Virtual Relay Design for Feeder Protection Testing With Online Simulation," *IEEE Transactions on Industry Applications*, vol. 54, no. 1, pp. 143–149, Jan. 2018, doi: 10.1109/TIA.2017.2741918.
- [37] H. F. Albinali and A. P. S. Meliopoulos, "Resilient Protection System Through Centralized Substation Protection," *IEEE Transactions on Power Delivery*, vol. 33, no. 3, pp. 1418–1427, Jun. 2018, doi: 10.1109/TPWRD.2017.2789318.
- [38] C. A. Castillo, A. Conde, and E. Fernandez, "Mitigation of DOCR miscoordination through distance relays and non-standard overcurrent curves," *Electric Power Systems Research*, vol. 163, pp. 242–251, Oct. 2018, doi: 10.1016/j.epsr.2018.06.012.
- [39] S. Mitra and P. Chattopadhyay, "Design and implementation of flexible Numerical Overcurrent Relay on FPGA," *International Journal of Electrical Power & Energy Systems*, vol. 104, pp. 797–806, Jan. 2019, doi: 10.1016/j.ijepes.2018.07.022.
- [40] S. A. Saleh, C. Richard, X. F. St. Onge, J. Meng, and E. Castillo-Guerra, "Comparing the Performance of Protection Coordination and Digital Modular Protection for Grid-Connected Battery Storage Systems," *IEEE Transactions on Industry Applications*, vol. 55, no. 3, pp. 2440–2454, May 2019, doi: 10.1109/TIA.2018.2886891.
- [41] R. M. Vincentius, A. W. Nugraha, P. S. Talitha, P. Margo, P. Ardyono, and H. P. Mauridhi, "Recognition of Electric Machines Boundary as The Constraint of Over Current Relay Coordination in Real Industrial Application with Serial Firefly Algorithm Optimization," in *2019 IEEE 12th International Symposium on Diagnostics for Electrical Machines, Power Electronics and Drives (SDEMPED)*, Aug. 2019, pp. 153–159. doi: 10.1109/DEMPED.2019.8864828.
- [42] N. A. Wibowo, V. R. Mahindara, A. Priyadi, M. Pujiantara, and M. H. Purnomo, "Optimization of Overcurrent Relay Operation Using Artificial Intelligent on Radial Topology with Load Constraint," in *2018 International*

- Seminar on Intelligent Technology and Its Applications (ISITIA)*, Aug. 2018, pp. 205–208. doi: 10.1109/ISITIA.2018.8711089.
- [43] V. R. Mahindara, M. G. Istiqlal, M. Pujiantara, D. A. Asfani, A. Priyadi, and M. H. Purnomo, “Obtaining The Setting of Inverse-Curve Overcurrent Relay using Serial Computing Modified Particle Swarm Optimization in Real System Applications,” in *2018 International Seminar on Intelligent Technology and Its Applications (ISITIA)*, Aug. 2018, pp. 187–192. doi: 10.1109/ISITIA.2018.8710868.
- [44] V. R. Mahindara, D. F. C. Rodriguez, M. Pujiantara, A. Priyadi, M. H. Purnomo, and E. Muljadi, “Practical Challenges of Inverse and Definite-Time Overcurrent Protection Coordination in Modern Industrial and Commercial Power Distribution System,” *IEEE Transactions on Industry Applications*, vol. 57, no. 1, pp. 187–197, Jan. 2021, doi: 10.1109/TIA.2020.3030564.
- [45] V. R. Mahindara, D. F. C. Rodriguez, M. Pujiantara, A. Priyadi, M. H. Purnomo, and E. Muljadi, “Modern Concerns and Challenges of Overcurrent Protection Coordination in Distribution Systems,” presented at the 2020 IEEE/IAS 56th Industrial and Commercial Power Systems Technical Conference (I&CPS), Virtual Conference, Apr. 2020.
- [46] V. R. Mahindara, A. Priyadi, M. Pujiantara, M. H. Purnomo, A. Y. Saber, and E. Muljadi, “Protection Coordination Challenges for Microgrid Distribution Network with High Penetration Inverter-Based Resources,” in *2020 IEEE Energy Conversion Congress and Exposition (ECCE)*, Oct. 2020, pp. 1618–1622. doi: 10.1109/ECCE44975.2020.9235817.
- [47] V. R. Mahindara, D. F. C. Rodriguez, M. Pujiantara, A. Priyadi, E. Muljadi, and M. H. Purnomo, “Voltage Function in Directional Over-Current Protection to Enhance the Sensitivity and Coordination Problem in Microgrid with High Penetration of Inverter-Based Resources,” *International Journal of Intelligent Engineering and Systems*, vol. 14, no. 3, pp. 516–527, Jun. 2021, doi: 10.22266/ijies2021.0630.43.
- [48] F. W. Rahmat, M. Pujiantara, V. Lystianingrum, V. R. Mahindara, and T. P. Sari, “Self Classification of Multifunction Relay Based on Neural Network for Industrial Scale,” in *2020 International Seminar on Intelligent Technology and Its Applications (ISITIA)*, Jul. 2020, pp. 13–18. doi: 10.1109/ISITIA49792.2020.9163719.
- [49] N. A. Wibowo, V. R. Mahindara, A. Priyadi, M. Pujiantara, and M. H. Purnomo, “Optimization of Overcurrent Relay Operation Using Artificial Intelligent on Radial Topology with Load Constraint,” in *2018 International Seminar on Intelligent Technology and Its Applications (ISITIA)*, Aug. 2018, pp. 205–208. doi: 10.1109/ISITIA.2018.8711089.
- [50] M. Pujiantara, V. R. Mahindara, B. Fachrurriza, A. Priyadi, and M. H. Purnomo, “The Design of RBMP Technique to Limit The Fault Current and Voltage Dip in Medium Voltage Electrical System Application,” in *2019 International Seminar on Intelligent Technology and Its Applications (ISITIA)*, Aug. 2019, pp. 159–164. doi: 10.1109/ISITIA.2019.8937291.

- [51] NERC, “NERC Misoperation by Cause Code (Q2 2012-Q3 2016),” *North American Electric Reliability Corporation (NERC)*.
<https://www.nerc.com/pa/RAPA/Pages/Misoperations.aspx> (accessed Oct. 18, 2018).
- [52] “IEEE Recommended Practice for Motor Protection in Industrial and Commercial Power Systems,” *IEEE Std 3004.8-2016*, pp. 1–163, May 2017, doi: 10.1109/IEEEESTD.2017.7930540.
- [53] “IEEE Guide for AC Motor Protection,” *IEEE Std C37.96-2012 (Revision of IEEE Std C37.96-2000)*, pp. 1–160, Feb. 2013, doi: 10.1109/IEEEESTD.2013.6468048.
- [54] “IEC 60076-7 Power transformers - Part 7: Loading guide for mineral-oil-immersed power transformers,” *International Electrotechnical Commission (IEC)*, vol. IEC 60076-7, Jan. 2018, [Online]. Available: <https://webstore.iec.ch/publication/34351>
- [55] “IEEE Guide for Liquid-Immersed Transformers Through-Fault-Current Duration,” *IEEE Std C57.109-2018 (Revision of IEEE Std C57.109-1993)*, pp. 1–24, Oct. 2018, doi: 10.1109/IEEEESTD.2018.8486931.
- [56] “IEEE Guide for AC Generator Protection,” *IEEE Std C37.102-2006 (Revision of IEEE Std C37.102-1995)*, pp. 1–177, 2006, doi: 10.1109/IEEEESTD.2006.320495.
- [57] N. E. Nilsson and J. Mercurio, “Synchronous generator capability curve testing and evaluation,” *IEEE Transactions on Power Delivery*, vol. 9, no. 1, pp. 414–424, Jan. 1994, doi: 10.1109/61.277713.
- [58] “ETAP | Electrical Power System Analysis Software | Power Management System.” <https://etap.com/> (accessed Jun. 28, 2020).
- [59] “SKM Systems Analysis, Inc. - Power System Software and Arc Flash Hazard Analysis and Design Solutions.” <http://www.skm.com/captor.html> (accessed Jan. 18, 2019).
- [60] “Siemens Time Current Curve (TCC) Software - Power Distribution - Siemens.” <https://w3.usa.siemens.com/powerdistribution/us/en/time-current-curve-software/pages/time-current-curve-software.aspx> (accessed Jan. 18, 2019).
- [61] O. Arreola Soria, A. Conde Enríquez, and L. A. Trujillo Guajardo, “Overcurrent relay with unconventional curves and its application in industrial power systems,” *Electric Power Systems Research*, vol. 110, pp. 113–121, May 2014, doi: 10.1016/j.epsr.2013.12.012.
- [62] J. C. Das, *Short-Circuits in AC and DC Systems: ANSI, IEEE, and IEC Standards*, vol. 1. CRC Press, 2017.
- [63] “IEEE Standard for Inverse-Time Characteristics Equations for Overcurrent Relays,” *IEEE Std C37.112-2018 (Revision of IEEE Std C37.112-1996)*, pp. 1–25, Feb. 2019, doi: 10.1109/IEEEESTD.2019.8635630.
- [64] X.-S. Yang, *Nature-Inspired Metaheuristic Algorithms: Second Edition*. Luniver Press, 2010.

- [65] X.-S. Yang and X. He, “Firefly Algorithm: Recent Advances and Applications,” *IJSI*, vol. 1, no. 1, pp. 36–50, Aug. 2013, doi: 10.1504/IJSI.2013.055801.
- [66] *Sepam™ Series 20 Protective Relays: User Manual*, Instruction Bulletin 63230-216-208C1. Schneider Electric, 2017.
- [67] R. C. Dugan, T. S. Key, and G. J. Ball, “Distributed resources standards,” *IEEE Industry Applications Magazine*, vol. 12, no. 1, pp. 27–34, Jan. 2006, doi: 10.1109/MIA.2006.1578562.
- [68] IEEE Committee Report, “Computer representation of overcurrent relay characteristics,” *IEEE Transactions on Power Delivery*, vol. 4, no. 3, pp. 1659–1667, Jul. 1989, doi: 10.1109/61.32656.
- [69] Beheshtaein, S., R. Cuzner, M. Savaghebi, and J. M. Guerrero, “Review on microgrids protection - IET Journals & Magazine,” *IET Generation, Transmission & Distribution*, vol. 13, no. 6, pp. 743–759, Mar. 2019.
- [70] A. Darabi, M. Bagheri, and G. B. Gharehpetian, “Highly sensitive microgrid protection using overcurrent relays with a novel relay characteristic,” *IET Renewable Power Generation*, vol. 14, no. 7, pp. 1201–1209, 2020, doi: 10.1049/iet-rpg.2019.0793.
- [71] M. N. Alam, R. Gokaraju, and S. Chakrabarti, “Protection coordination for networked microgrids using single and dual setting overcurrent relays,” *IET Generation, Transmission & Distribution*, vol. 14, no. 14, pp. 2818–2828, Jul. 2020, doi: 10.1049/iet-gtd.2019.0557.
- [72] C. S. Mardegan and R. Rifaat, “Considerations in applying IEEE Recommended Practice for Protection Coordination in Industrial and Commercial Power Systems - Part I,” in *2015 IEEE/IAS 51st Industrial Commercial Power Systems Technical Conference (I&CPS)*, May 2015, pp. 1–10. doi: 10.1109/ICPS.2015.7266442.
- [73] M. H. Samimi, A. Mahari, M. A. Farahnakian, and H. Mohseni, “The Rogowski Coil Principles and Applications: A Review,” *IEEE Sensors Journal*, vol. 15, no. 2, pp. 651–658, Feb. 2015, doi: 10.1109/JSEN.2014.2362940.
- [74] V. Mahindara and D. Celeita, “ETAP file of IEEE 242-2001 Protection Coordination Single-line Diagram.” IEEE Dataport, 2020. [Online]. Available: <http://dx.doi.org/10.21227/zc7t-sn76>
- [75] E. Muljadi and V. Gevorgian, “Short-circuit modeling of a wind power plant,” in *2011 IEEE Power and Energy Society General Meeting*, Jul. 2011, pp. 1–9. doi: 10.1109/PES.2011.6039068.
- [76] T. S. Aghdam, H. K. Karegar, and H. H. Zeineldin, “Optimal Coordination of Double-Inverse Overcurrent Relays for Stable Operation of DGs,” *IEEE Transactions on Industrial Informatics*, vol. 15, no. 1, pp. 183–192, Jan. 2019, doi: 10.1109/TII.2018.2808264.
- [77] “1547-2018 - IEEE Standard for Interconnection and Interoperability of Distributed Energy Resources with Associated Electric Power Systems

Interfaces - IEEE Standard,” *IEEE Std 1547-2018*, Feb. 2018, Accessed: Oct. 29, 2019. [Online]. Available: <https://ieeexplore.ieee.org/document/8332112>

- [78] “IEEE Guide for Smart Grid Interoperability of Energy Technology and Information Technology Operation with the Electric Power System (EPS), End-Use Applications, and Loads,” *IEEE Std 2030-2011*, pp. 1–126, Sep. 2011, doi: 10.1109/IEEESTD.2011.6018239.
- [79] R. Seguin, J. Woyak, D. Costyk, J. Hambrick, and B. Mather, “High-Penetration PV Integration Handbook for Distribution Engineers,” National Renewable Energy Laboratory, Technical Report NREL/TP-5D00-63114, Jan. 2016.
- [80] “IEEE Recommended Practice for Protection and Coordination of Industrial and Commercial Power Systems (IEEE Buff Book),” *IEEE Std 242-2001 (Revision of IEEE Std 242-1986) [IEEE Buff Book]*, pp. 1–710, Dec. 2001, doi: 10.1109/IEEESTD.2001.93369.
- [81] A. R. Haron, A. Mohamed, and H. Shareef, “Coordination of Overcurrent, Directional and Differential Relays for the Protection of Microgrid System,” *Procedia Technology*, vol. 11, pp. 366–373, Jan. 2013, doi: 10.1016/j.protcy.2013.12.204.
- [82] M. Singh, “Protection coordination in distribution systems with and without distributed energy resources- a review,” *Protection and Control of Modern Power Systems*, vol. 2, no. 1, p. 27, Jul. 2017, doi: 10.1186/s41601-017-0061-1.
- [83] C. Marnay, C. Abbey, G. Joos, and WG C6.22, *Microgrids 1 Engineering, Economics, & Experience*, vol. TB 635. CIGRE, 2015.
- [84] H. Gu, R. Yan, T. K. Saha, and E. Muljadi, “System Strength and Inertia Constrained Optimal Generator Dispatch under High Renewable Penetration,” *IEEE Transactions on Sustainable Energy*, pp. 1–1, 2019, doi: 10.1109/TSTE.2019.2957568.
- [85] V. Gurevich, *Electric Relays Principles and Applications*, First. FL, USA: CRC Press Taylor & Francis Group, 2006.
- [86] J. M. Gers and E. J. Holmes, *Protection of Electricity Distribution Networks*, Third. London, United Kingdom: The Institution of Engineering and Technology, 2011.
- [87] J. P. Holguin, D. C. Rodriguez, and G. Ramos, “Reverse Power Flow (RPF) Detection and Impact on Protection Coordination of Distribution Systems,” *IEEE Transactions on Industry Applications*, vol. 56, no. 3, pp. 2393–2401, May 2020, doi: 10.1109/TIA.2020.2969640.
- [88] A. Prasad, J. Belwin Edward, and K. Ravi, “A review on fault classification methodologies in power transmission systems: Part—I,” *Journal of Electrical Systems and Information Technology*, vol. 5, no. 1, pp. 48–60, May 2018, doi: 10.1016/j.jesit.2017.01.004.

- [89] A. Prasad, J. Belwin Edward, and K. Ravi, "A review on fault classification methodologies in power transmission systems: Part-II," *Journal of Electrical Systems and Information Technology*, vol. 5, no. 1, pp. 61–67, May 2018, doi: 10.1016/j.jesit.2016.10.003.
- [90] Y. LeCun, Y. Bengio, and G. Hinton, "Deep learning," *Nature*, vol. 521, no. 7553, pp. 436–444, May 2015, doi: 10.1038/nature14539.
- [91] H. Chiroma *et al.*, "Progress on Artificial Neural Networks for Big Data Analytics: A Survey," *IEEE Access*, vol. 7, pp. 70535–70551, 2019, doi: 10.1109/ACCESS.2018.2880694.
- [92] "Fundamentals of Deep Learning [Book]." <https://www.oreilly.com/library/view/fundamentals-of-deep/9781491925607/> (accessed Jul. 25, 2019).
- [93] K. Ovtcharov, O. Ruwase, J. Kim, J. Fowers, K. Strauss, and E. S. Chung, "Toward accelerating deep learning at scale using specialized hardware in the datacenter," in *2015 IEEE Hot Chips 27 Symposium (HCS)*, Aug. 2015, pp. 1–38. doi: 10.1109/HOTCHIPS.2015.7477459.

This page is left intentionally blank.

APPENDIX 1. IEEE 242-2001 TEST CASE

Some technical information regarding the system setup, according to Figure 3.3, is provided as follows:

1. Power grid:
 - a. Voltage level : 138 Kv
 - b. Short circuit capacity : 5000 MVA_{sc}
 - c. R - Impedance component : [+], [-], and [0] = 0.24807 %
 - d. X - Impedance component : [+], [-], and [0] = 1.98456 %
 - e. X/R ratio : 8
2. Transformer (Main Tx)
 - a. Voltage level : 138/13.8 kV
 - b. Power rating : 30 MVA
 - c. Z - Impedance component : [+] and [0] = 9%
 - d. X/R ratio : 23.7
3. Transformer (4160SS Tx)
 - a. Voltage level : 13.8/4.16 kV
 - b. Power rating : 10 MVA
 - c. Z - Impedance component : [+] and [0] = 6.5%
 - d. X/R ratio : 15.5
4. Transformer (480SS Tx)
 - a. Voltage level : 13.8/0.48 kV
 - b. Power rating : 1 MVA
 - c. Z - Impedance component : [+] and [0] = 5.75%
 - d. X/R ratio : 5.79
5. Motor (Mtr A)
 - a. Nameplate information : 900 HP, 4.16 kV, FLA: 110 A,
60 Hz, 4 poles, 1715 RPM,
(4.74% slip), PF: 92.33 %,
Eff: 95.38 %, NEMA Design A
 - b. Impedance information : %LRC = 600, LRA = 660,
LR kVA/HP = 5.08, %PF = 16,
X/R = 6.169, T'' = 0.2 sec,

Sequence Z: $X'' = 16.452$;
 $X_o = 18.462$; $X_2 = 18.462\%$;
 $X''/R = 23.364$, ANSI Short Circuit
Z calculated using the Std. MF

6. Motor (Mtr B)

- a. Nameplate information : 75 HP, 0.48 kV, FLA: 92 A, 60 Hz,
4 poles, 1715 RPM, (4.71% slip),
PF: 91.35 %, Eff: 80.04 %,

NEMA Design A,
NEMA Code Letter G,
(4.74% slip), PF: 92.33,
Eff: 95.38 %, NEMA Design A
- b. Impedance information : %LRC = 600, LRA = 552,
LR kVA/HP = 6.12, %PF = 33.06,
 $X/R = 2.855$, $T'' = 0.2$ sec,
Sequence Z: $X'' = 15.729$; $X_o = 20$;
 $X_2 = 20\%$; $X''/R = 6.745$,
ANSI Short Circuit Z calculated
using the Std. MF

7. Distribution line (Cable 5)

- a. Size : 750 kcmil
- b. Length and tolerance : 100 ft, 1 %
- c. R- impedance component :
 - i. [+] : 0.0203 ohm/1000-ft
 - ii. [0] : 0.03248 ohm/1000-ft
- d. X- impedance component :
 - i. [+] : 0.0332 ohm/1000-ft
 - ii. [0] : 0.08466 ohm/1000-ft
- e. X/R ratio :
 - i. [+] : 1.635
 - ii. [0] : 2.607

8. Distribution line (Cable 5, between 13.8 F3 and 13.8 F2)

- a. Size : 750 kcmil
- b. Length and tolerance : 100 ft, 1 %
- c. R- impedance component :
 - i. [+] : 0.0203 ohm/1000-ft
 - ii. [0] : 0.03248 ohm/1000-ft
- d. X- impedance component :
 - i. [+] : 0.0332 ohm/1000-ft
 - ii. [0] : 0.08466 ohm/1000-ft
- e. X/R ratio :
 - i. [+] : 1.635
 - ii. [0] : 2.607

9. Distribution line (Cable 4, between 0.48 F2 and 0.48 F1)

- a. Size : 4/0 AWG
- b. Length and tolerance : 100 ft, 1 %
- c. R- impedance component :
 - i. [+] : 0.0633 ohm/1000-ft
 - ii. [0] : 0.10058 ohm/1000-ft
- d. X- impedance component :
 - i. [+] : 0.0332 ohm/1000-ft
 - ii. [0] : 0.08433 ohm/1000-ft
- e. X/R ratio :
 - i. [+] : 0.524
 - ii. [0] : 0.838

10. Distribution line (Cable 3, between 0.48 F1 and 0.48 F0-1)

- a. Size : 1 AWG
- b. Length and tolerance : 100 ft, 1 %
- c. R- impedance component :
 - i. [+] : 0.16 ohm/1000-ft
 - ii. [0] : 0.25424 ohm/1000-ft
- d. X- impedance component :
 - i. [+] : 0.038 ohm/1000-ft
 - ii. [0] : 0.09652 ohm/1000-ft

- e. X/R ratio :
 - i. [+] : 0.237
 - ii. [0] : 0.38

11. Distribution line (Cable 2, between 13.8 F3 and 13.8 F1)

- a. Size : 750 kcmil
- b. Length and tolerance : 100 ft, 1 %
- c. R- impedance component :
 - i. [+] : 0.0203 ohm/1000-ft
 - ii. [0] : 0.03248 ohm/1000-ft
- d. X- impedance component :
 - i. [+] : 0.0332 ohm/1000-ft
 - ii. [0] : 0.08466 ohm/1000-ft
- e. X/R ratio :
 - i. [+] : 1.635
 - ii. [0] : 2.607

12. Distribution line (Cable 1, between 4.16 F1 and 4.16 F0-1)

- a. Size : 2 AWG
- b. Length and tolerance : 100 ft, 1 %
- c. R- impedance component :
 - i. [+] : 0.202 ohm/1000-ft
 - ii. [0] : 0.3232 ohm/1000-ft
- d. X- impedance component :
 - i. [+] : 0.0457 ohm/1000-ft
 - ii. [0] : 0.11653 ohm/1000-ft
- e. X/R ratio :
 - i. [+] : 0.226
 - ii. [0] : 0.361

APPENDIX 2. CURRICULUM VITAE

Personal Information

Full Name : Vincentius Raki Mahindara
Place, Date of Birth : Bontang, Indonesia, March 27, 1994
Nationality : Indonesia
Contact : +62 822 3360 8125
vrmahindara@gmail.com, raki@ieee.org
Apartment Sukolilo Dian Regency #2202
Jl. Sukolilo Kasih I/19, Keputih, Sukolilo
Surabaya, Jawa Timur, Indonesia
60111



Education Background

Graduate program

Doktor (Dr.); equivalent with Philosophy of Doctor (Ph.D)

On-going since June 2018 (expected to graduate in mid-2021)
Department of Electrical Engineering (Power System Engineering)
Faculty of Intelligence Electrical and Informatics Technology
Institut Teknologi Sepuluh Nopember, Surabaya, Indonesia
Emphasis: Protection system and stability issue

Undergraduate program

Sarjana Teknik (ST.); equivalent with Bachelor of Engineering (B. Eng)

Graduated with Honors (Cum Laude) in 2016
Department of Electrical Engineering (Power System Engineering)
Faculty of Industrial Technology
Institut Teknologi Sepuluh Nopember, Surabaya, Indonesia
Final Project: “Time Dial Setting Optimization of Over Current Relay using Adaptive Modified Firefly Algorithm in PT. Pupuk Kaltim”

Professional Experience

1. Visiting Researcher: Protection System on Microgrid, Auburn University, Alabama, United States of America.
October 2019-March 2020
Conducting the research with the emphasis on power system protection for microgrid distribution network penetrated by renewable energy resources.
2. Research Associate: Power System Protection and Stability, Institut Teknologi Sepuluh Nopember, Indonesia.
October 2017-presents
Conducting the research and working on various industrial projects related to power system analysis, protection system, fault analysis, and transient stability.
3. Product Specialist: Altivar Variable Speed Drive, Schneider Electric.
February-October 2017
Expertise for Variable Speed Drive (VSD) called 'Altivar Product' and managing the

development from a manufacturer perspective. Product range: Altivar ATV930, Altivar ATV630, Toshiba VFAS3.

4. Product Specialist: Zelio Control and Timer Relay, Schneider Electric, September 2016-October 2017
Role as an engineer who focuses on Relay product (including control and timer relay) and responsible for piloting any evolution related to the product and quality. Product range: Zelio Low Voltage Relay.
5. Coordinator of Electrical Measurements Practicum, Laboratorium Instrumentasi Pengukuran dan Identifikasi Sistem Tenaga (LIPIST), ITS Surabaya. February 2015-February 2016
Managing the lab work and train teaching assistants
6. Internship Engineer, PT. Pertamina EP Asset 5-Field Sangasanga June-October 2014
Assist the electrical supervisor to manage the oil and gas exploration plant within the scope of the electrical power system under Reliability Availability Maintenance (RAM) Department.
7. Assistant Laboratory, Laboratorium Instrumentasi Pengukuran dan Identifikasi Sistem Tenaga (LIPIST), ITS Surabaya May 2014-September 2016
Support the lab research, contribute as a trainer at practicum or lab work, and becoming the technician for calibrating electrical measurement equipment using Fluke-5500A

Publications

1. M Basu, VR Mahindara, J Kim, RM Nelms, E Muljadi, “Comparison of Active and Reactive Power Oscillation Damping with PV plants”, IEEE Transactions on Industry Applications, 2021
2. VR Mahindara, D Celeita, M Pujiantara, A Priyadi, MH Purnomo, E Muljadi, “Voltage Function in Directional Over-Current Protection to Enhance the Sensitivity and Coordination Problem in Microgrid with High Penetration of Inverter-Based Resources”, International Journal of Intelligent Engineering and System, 2021
3. M Basu, VR Mahindara, J Kim, E Muljadi, “Effect of high penetrated reactive power support based Inverter-Based-Resources on the power stability of microgrid distribution system during faults”, International Conference, IEEE IAS Annual Meeting, 2020
4. VR Mahindara, D Celeita, M Pujiantara, A Priyadi, MH Purnomo, E Muljadi, “Practical Challenges of Inverse and Definite-Time Overcurrent Protection Coordination in Modern Industrial and Commercial Power Distribution System”, IEEE Transactions on Industry Applications, 2020
5. VR Mahindara, M Pujiantara, A Priyadi, MH Purnomo, AY Saber, E Muljadi, “Protection Coordination Challenges for Microgrid Distribution Network with High Penetration Inverter-Based Resources”, International Conference, IEEE ECCE, 2020
6. P Chhun, A Priyadi, M Pujiantara, VR Mahindara, “Optimal Coordination of OCR with TCC Selection for Radial Industrial System Using Firefly Algorithm”, International Conference, ISITIA, 2020

7. K Chheng, A Priyadi, M Pujiantara, VR Mahindara, “The Coordination of Dual Setting DOCR for Ring System Using Adaptive Modified Firefly Algorithm”, International Conference, ISITIA, 2020
8. RF Wijanarko, M Pujiantara, V Listyaningrum, VR Mahindara, TP Sari, “Self-Classification of Multifunction Relay Based on Neural Network for Industrial Scale”, International Conference, ISITIA, 2020
9. VR Mahindara, D Celeita, M Pujiantara, A Priyadi, MH Purnomo, E Muljadi, “Modern Concerns and Challenges of Over-Current Protection Coordination in Distribution System”, International Conference, 56th IEEE I&CPS, 2020
10. A Priyadi, M Pujiantara, TP Sari, RF Wijanarko, VR Mahindara, Adi P, Ira S, “The Design of Kalimantan Transmission System Interconnection in Electrical Stability Perspective”, International Conference, ICT-PEP, 2019
11. MH Purnomo, VR Mahindara, RF Wijanarko, AB Gumelar, “The Role of Deep Learning in Computation for Power System Operations”, International Conference, ICESTI, 2019
12. M Pujiantara, VR Mahindara, B Fachrurriza, A Priyadi, MH Purnomo, “The Design of RBMP Technique to Limit the Fault Current and Voltage Dip in Medium Voltage Electrical System Application”, International Conference, ISITIA, 2019
13. VR Mahindara, NA Wibowo, TP Sari, A Priyadi, M Pujiantara, MH Purnomo, “Recognition of Electric Machines Boundary as The Constraint of Over Current Relay Coordination in Real Industrial Application with Serial Firefly Algorithm Optimization”, International Conference, SDEMPED, 2019
14. MH Purnomo, VR Mahindara, “Smart Economy: Sistem Tenaga Listrik Cerdas sebagai Penunjang Pertumbuhan Ekonomi di Indonesia”, Book Chapter on: “Smart City-Konsep, Model dan Teknologi”, AISINDO, ISBN: 978-602-74309-4-5, 2019
15. M Pujiantara, VR Mahindara, TP Sari, “*Study of Overcurrent Relay Coordination Using Non-Standard Tripping Characteristic Method in 150 kV and 20 kV Network of PT. PLN (LTD) APJ Gilimanuk*”, International Conference, CENIM, 2018
16. M Pujiantara, VR Mahindara, TP Sari, “Coordination of Electricity Protection System in Samarinda Airport”, International Conference, ICPERE, 2018
17. M Pujiantara, VR Mahindara, A Indrasaputra, TP Sari, DC Riawan, “The Automation of Time Dial Setting Calculation and Inverse Type Curve Selection for Over Current Relay Based on Numerical Computation in Real Industrial Electrical System”, International Conference, ICPERE, 2018
18. MH Purnomo, Q Aini, EI Setiawan, VR Mahindara, “Green Computing: Opportunity of Using Breadth Fixed Gossip Algorithm for Optimizing Power Supply Route in Power Plant”, International Conference, ICITACEE, 2018
19. VR Mahindara, MG Istiqlal, M Pujiantara, DA Asfani, A Priyadi, MH Purnomo, “Obtaining the Setting of Inverse-Curve Overcurrent Relay using Serial Computing Modified Particle Swarm Optimization in Real System Applications”, International Conference, ISITIA, 2018
20. NA Wibowo, VR Mahindara, A Priyadi, M Pujiantara, MH Purnomo, “Optimization of Overcurrent Relay Operation Using Artificial Intelligent on Radial Topology with Load Constraint”, International Conference, ISITIA, 2018

21. VR Mahindhara, M Pujiantara, A Priyadi, “Optimasi Time Dial Setting (TDS) Relay Arus Lebih Menggunakan Adaptive Modified Firefly Algorithm Pada Sistem Kelistrikan PT. Pupuk Kalimantan Timur”, Jurnal Teknik ITS, 2016

Patents

1. M Pujiantara, VR Mahindhara, A Priyadi, MH Purnomo, A Tjahjono, V Lystianingrum, “Metode Penentuan Parameter Sistem Proteksi Aliran Daya dan Visualisasi Time-Power-Curve untuk Jaringan Tenaga Listrik dengan Pertimbangan Penetrasi Pembangkit Listrik Energi Baru Terbarukan”, P00202002682 (Indonesia)

Awards and Recognitions

1. Scholarship awardee, Ernst Mach-Grant – ASEA-UNINET Sandwich Scholarship at TU Graz, Austria, 2020 (postponed due to pandemic situation).
2. Grant fellowships, COVID-19 Projects, IEEE Special Interest Group on Humanitarian Technology (IEEE SIGHT), 2020
3. Awardee of EIP (Enhancing International Publication) program scholarship for visiting world class university, Kementrian Riset dan Pendidikan Tinggi (DIKTI), Indonesia, 2019-2020
4. Awardee of PMDSU (Program Magister dan Doktoran untuk Sarjana Unggul) Scholarship for Master and Doctoral Degree, Kementrian Riset dan Pendidikan Tinggi (DIKTI), Indonesia, 2017-2021
5. Interviewees at Big Bang Show Kompas TV, Inspiring inventor show about Vampire Power Eliminator (VPE), 2016
6. 2nd Winner of Blue Technology Festival, Prototype Research, Telkom University, Bandung, 2016
7. 3rd Winner of Aeroexpo ITB (Aerospace Engineering), Research Innovation, Institut Teknologi Bandung, 2015
8. 1st Winner of National Research and Paper Competition, Research Innovation, Universitas Negeri Padang, 2015
9. 3rd Winner of Environment Technology Innovation, Research Innovation, Environmental Engineering ITS Surabaya, 2015
10. 2nd Winner of English Debate Competition, Electrical Engineering Department, ITS Surabaya, 2015
11. Best Idea for Air Transportation, Young Engineer and Scientist Summit, ITS Surabaya, 2014

Keynote and Trainer Experience

1. Keynote speaker, May 2021
Webinar IEEE Industrial Electronics Society (IES) Indonesia Section
Strategy for publishing in reputable peer-reviewed journal
2. Keynote speaker, June 2020
Webinar FORTEI (Forum Pendidikan Tinggi Teknik Elektro Indonesia)
Advance Power System Protection for Distributed Generation
3. Keynote speaker, September 2019
IEEE Student Branch, Institut Teknologi Sepuluh Nopember (ITS)
IEEE Connect: Digital Transformation
4. Trainer, December 2018
Politeknik Elektronika Negeri Surabaya (PENS), Surabaya
Mentor on training about power system analysis using Digsilent, Power Factory
5. Trainer, November 2018
PT. Waskita Karya (Head Office), Jakarta
Mentor of training about design and installation of power system in industrial EPC
6. Trainer, February 2018
Laboratorium Instrumentasi Pengukuran dan Identifikasi Sistem Tenaga (LIPIST),
Electrical Engineering Dept, ITS Surabaya
Training about basic electrical protection system and design using ETAP
7. Workshop Mentor: Protection Coordination, August 2016
Laboratorium Instrumentasi Pengukuran dan Identifikasi Sistem Tenaga (LIPIST),
Electrical Engineering Dept, ITS Surabaya
Give a training about basic electrical protection system and design using ETAP

Organizational Experience

1. Member of IEEE Power and Energy Society, 2019-present
2. Student Member of IEEE, 2016-present
3. Coordinator of Design, Website and Documentation, International Seminar on Intelligent Technology and Its Application (ISITIA), Lombok, ITS Surabaya, 2016
4. Coordinator of Website and Documentation. Electrical Engineering Event, ITS Surabaya, 2015
5. Head of Technical Division, ITS TV Campus Television, ITS Surabaya, 2014
6. Head of News Division, ITS TV Campus Television, ITS Surabaya, 2013

Project Based-Consulting Experience (Limited to last 5 years)

1. Protection System Engineer, April 2021
Multiguna Technologies Sdn. Bhd.
Evaluating the Protection Coordination of Belingus Power Station 11 kV, Brunei Darussalam
2. Power System Engineer, February-March 2021
PT. Pertamina Refinery Unit IV, Cilacap

- Designing medium voltage automatic transfer switch (MV-ATS) for 13.8 kV substation of refinery and petrochemical plant*
3. Power System Engineer, January-April 2021
PT. Pertamina Refinery Unit VII, Kasim, Sorong, Papua
Power system design for Kasim refinery plant development and the creation of FEED document for new gas turbine generator.
 4. Power System Engineer, January-March 2021
PT. Gresik Power Indonesia (Linde Group)
Medium voltage power system analysis and coordination protection study to evaluate the blackout event
 5. Power System Engineer, January-March 2021
PT. Petrokimia Gresik
Protection coordination study and transient stability analysis to design the defend scheme of Petrochemical plant
 6. Power System Engineer, November-December 2020
PT. Indocement
Power system analysis for dust filter conversion from electrostatic precipitator to fabric bag filter in Plant 11 Indocement, Citeurup
 7. Power System Engineer, October-December 2020
PT. Pertamina Refinery Unit III, Plaju, Palembang
Load shedding analysis for oil refinery plant with total load up to 25 MW.
 8. Lead Engineer, September-November 2020
PT. Pelindo III, Surabaya
Detailed engineering design for enhancing the reliability performance of Terminal Teluk Lamong by installing a 16 MVA 20 kV insulation transformer
 9. Lead Engineer, August-September 2020
PT. Terminal Petikemas Surabaya (TPS)
Electrical detailed engineering design for reefer rack construction in PT. TPS Container Yard
 10. Lead Engineer, July-August 2020
PT. Pertamina Exploration and Production, Asset 4, Field Cepu
Load shedding analysis and internal gas turbine generator protection review for Central Processing Plant (CPP) Gundih
 11. Assistant Engineer, June-September 2020
PT. Pertamina Refinery Unit VI, Balongan, Indramayu
Assessment of internal lightning protection to mitigate the risk of personnel hazard and instrument system failure.
 12. Project Engineer, May-June 2020
PT. Lamong Energi Indonesia
Technical assessment for the electrical distribution network of Terminal Teluk Lamong
 13. Project Engineer, April-June 2020
PT. Lamong Energi Indonesia
Technical and detailed engineering design for the electrical network of Berkah Manyar Sejahtera (BMS) port
 14. Project Engineer, April-July 2020
PT. Pertamina Refinery Unit II, Dumai

Study of interconnection oil and gas refinery plant to the 150 kV network grid and creation of detailed engineering design with an estimated bill of quantity for tendering purpose

15. Project Engineer, April-June 2020
PT. Lamong Energi Indonesia
Technical and detailed engineering design for medium voltage electrical network of Tanjung Perak seaport
16. Protection Engineer, March-May 2020
PT. Pertamina Refinery Unit V, Balikpapan
Assessment of relay protection coordination, transient stability, dynamic motor acceleration, load shedding and voltage sag for the electrical system of refinery plant.
17. Protection Engineer, March-May 2020
PT. Solusi Bangun Indonesia
Relay protection review for TQ 2 Cement Plant of Solusi Bangun Indonesia, Tuban
18. Project Engineer, December 2019-June 2020
PT. PLN (Persero), Sumatera Selatan, Jambi, and Bengkulu.
Master plan study of network expansion in the area of Jambi, Muara Bungo, Lahat, and Bengkulu based using 20 kV distribution line on year period 2020-2030
19. Protection Engineer, October-December 2019
PT. Pupuk Indonesia Energi
Internal generator protection review for Gas Turbine Generator GGCP PIE at Petrokimia Gresik
20. Project Engineer, July-August 2019
PT. Pertamina Exploration and Production, Asset 4, Field Cepu
Electrical assessment for main power distribution network of Kawengan, Ledok, Semanggi, and Nglobo
21. Protection Engineer, June-August 2019
PT. PJB UBJOM PLTU Tenayan
Electrical system protection review of Steam Turbine Generator 2x110 MW after catastrophic blackout
22. Project Engineer, May-September 2019
PT. Terminal Petikemas Surabaya (TPS)
Detailed engineering design for electrification of ERTG (Electrified Rubber Tired Gantry) crane with medium voltage distribution network
23. Project Engineer, March-July 2019
PT. Pertamina Refinery Unit V, Balikpapan
Study of interconnection oil and gas refinery plant 33 kV to the network grid and creation of detailed engineering design and estimated bill of quantity for tendering purpose
24. Project Engineer, February-June 2019
PT. Pertamina Refinery Unit IV, Cilacap
Study of interconnection oil and gas refinery plant 13.8 kV to the network grid and creation of detailed engineering design and estimated bill of quantity for tendering purpose
25. Protection Engineer, January 2019
PT. Gresik Power Indonesia (Linde Group), Gresik

The analysis of 11 MW steam turbine generator blackout due to short circuit during start-up procedure

26. Project Engineer, December 2018
PT. Kaltim Daya Mandiri (KDM) & PT. Pupuk Kaltim, Bontang
Master plan development of electrical system with total load 120 MW and evaluating the impact of installation gas engine generator to the system
27. Project Engineer, December 2018
PT. Pertamina Exploration and Production, Asset 4, Field Cepu
Relay protection review in central processing unit crude oil "Gundih" substation
28. Assistant Engineer, October 2018
PT. PLN (Persero) Kantor Pusat, Divisi Perencanaan Sistem
Master plan study of electricity market from Indonesia to Sabah, Malaysia
29. Project Engineer, July-September 2018
PT. PLN (Persero) Kantor Pusat, Divisi Regional Sumatera
Selection of generator type and unit size with total capacity 200 MW for peak-load in Lampung area
30. Project Engineer, May-July 2018
PT. Pupuk Kujang, Cikampek
Stability study regarding the impact of new load configuration and designing the installation procedure of new emergency backup generator
31. Project Engineer, November 2017-May 2018
PT. PLN (Persero) Kantor Pusat, Divisi Perencanaan Sistem
Master plan study of Kalimantan Island 500 kV transmission line on year period 2017-2050
32. Project Engineer, October-December 2017
PT. Energi Pelabuhan Indonesia (EPI)
Feasibility study to electrify the sea-port in PT. Pelindo 2, Indonesia
33. Assistant Project Engineer, 2016
PT. Pembangunan Jawa Bali (PJB) UP. Paiton 1&2
Evaluating the generator protection system and giving recommendation about existing electrical protection for generator utilities
34. Assistant Project Engineer, 2016
PT. Kaltim Daya Mandiri (KDM) & PT. Pupuk Kaltim, Bontang
Evaluation of electrical system, including analyze power flow, short circuit, transient stability and protection designing